Copyright Statement

MITOCHONDRIAL INVOLVEMENT IN PANCREATIC BETA CELL GLUCOLIPOTOXICITY

by

JONATHAN PAUL BARLOW

A thesis submitted to Plymouth University in partial fulfillment of the requirements for the degree of

DOCTOR OF PHILOSOPHY

Department of Biomedical and Healthcare Sciences

March 2015

Abstract

High circulating glucose and non-esterified free fatty acid (NEFA) levels can cause pancreatic β-cell failure. The molecular mechanisms of this β-cell glucolipotoxicity are yet to be established conclusively. In this thesis by exploring mitochondrial energy metabolism in INS-1E insulinoma cells and isolated pancreatic islets, a role of mitochondria in pancreatic β-cell glucolipotoxicity is uncovered. It is reported that prolonged palmitate exposure at high glucose attenuates glucose-stimulated mitochondrial respiration which is coupled to ADP phosphorylation. These mitochondrial defects coincide with an increased level of mitochondrial reactive oxygen species (ROS), impaired glucose-stimulated insulin secretion (GSIS) and decreased cell viability. Palmitoleate, on the other hand, does not affect mitochondrial ROS levels or cell viability and protects against the adverse effects of palmitate on these phenotypes. Interestingly, palmitoleate does not significantly protect against mitochondrial respiratory or insulin secretion defects and in pancreatic islets tends to limit these functions on its own. Furthermore, strong evidence suggests that glucolipotoxic-induced ROS are of a mitochondrial origin and these ROS are somehow linked with NEFA-induced loss in cell viability. To explore the mechanism of glucolipotxic-induced mitochondrial ROS and associated cell loss, uncoupling protein-2 (UCP2) protein levels and activity were probed in NEFA exposed INS-1E cells. It is concluded that UCP2 neither mediates palmitate-induced mitochondrial ROS production and the related cell loss, nor protects against these deleterious effects. Instead, UCP2 dampens palmitoleate protection against palmitate toxicity. Collectively, these data shed important new light on the area of glucolipotoxicity in pancreatic β-cells and provide novel insights into the pathogenesis of Type 2 diabetes.

Table of Contents

List of Figures

Chapter 1

Chapter 2

Chapter 5

Acknowledgements

I would like to start by thanking my director of studies, Dr Charles Affourtit, who has been instrumental in the progression of my PhD. With his expert scientific knowledge and continuous support throughout the last three years, he has provided me with a great foundation for a future career in academia. I would like to extend my thanks to Dr Verena Hirschberg Jensen, Dr Raid Nisr, Professor Noel Morgan, Dr Martin Jastroch, Dr Ruchi Jain and Daniel Lamp for their continuous technical help and in depth scientific discussions that have all helped to inform the experimental chapters in this thesis. I would also like to thank my long-term partner Lois Tucker and family for their continuous encouragement throughout this process. Finally it is important to thank Plymouth University and the Medical Research Council for the funding that has supported this work.

Author's Declaration

At no time during the registration for the degree of Doctor of Philosophy has the author been registered for any other University award without prior agreement of the Graduate Committee.

Work submitted for this research degree at Plymouth University has not formed part of any other degree either at Plymouth University or at another institution.

This study was financed with the aid of a studentship from the Plymouth University Peninsula School of Medicine and School of Biological and Healthcare Sciences.

Word count of main body of thesis: 45,247

Signed: 

Date: 31/03/2015

List of Abbreviations

ADP	Adenosine Diphosphate
ATP	Adenosine Triphosphate
BCA	Bicinchoninic Acid
BSA	Bovine Serum Albumin
C2C12 myoblasts	Immortalized cell line of mouse skeletal myoblasts
CMRL	Connaught Medical Research Laboratories Medium
CoA	Coenzyme A
CPT-1	Carnitine Palmitoyltransferase 1
DAPI	4',6-diamidino-2-phenylindole
DHE	Hydroethidine
DMEM	Dulbecco's Modified Eagles Medium
DNA	Deoxyribonucleic Acid
DPBS	Dulbecco's Phosphate-buffered Saline
dsDNA	Double Stranded Deoxyribonucleic Acid
ECL	Enhanced Chemiluminescence
EDTA	Ethylenediaminetetraacetic Acid
ELISA	Enzyme-Linked Immunosorbent Assay

ER	Endoplasmic Reticulum
FBS	Fetal Bovine Serum
GLUT	Glucose Transporter
GPR120	G Protein-Coupled Receptor 120
GPR40	G Protein-Coupled Receptor 40
GSIS	Glucose-Stimulated Insulin Secretion
H_2O_2	Hydrogen Peroxide
Hepes	4-(2-hydroxyethyl)-1-piperazineethanesulfonic Acid
hUCP2	Human Recombinant UCP2
IgG	Immunoglobulin G
INS-1E	Clone of Parental Insulinoma Cells
IRS-2	Insulin Receptor Substrate 2
K^{ATP}	ATP-sensitive Pottassium Channels
KRH	Krebs-Ringer HEPES Buffer
KSIS	Potassium-Stimulated Insulin Secretion
MDR	Multi-drug Resistance
MitoSOX	Hydroethidine conjugated to triphenylphosphonium

mRNA	Messenger RNA
NADPH	Nicotinamide Adenine Dinucleotide Phosphate
NEFA	Non-Esterified Fatty Acids
NEFAu	Non-Esterified Unbound Fatty Acids
$O_2^{\cdot -}$	Superoxide
PBS	Phosphate-buffered Saline
PDH	Pyruvate Dehydrogenase
PFA	Paraformaldehyde
PMF	Protonmotive Force
RFU	Relative Fluorescent Units
RIPA	Radiommunoprecipitation Assay Buffer
RNA	Ribonucleic Acid
RNAi	RNA interference
ROS	Reactive Oxygen Species
RPMI	Roswell Park Memorial Institute Medium
SDS	Sodium Dodecyl Sulphate
SEM	Standard Error of the Mean

siRNA	Small Interfering Ribonucleic Acid
SOD	Superoxide Dismutase
SREBP-1c	Sterol Regulatory Element-Binding Protein 1c
TAG	Triacylglyceride
TBS	Tris-buffered Saline
TBST	Tris-buffered Saline with Tween-20
TCA	Tricarboxylic Acid Cycle
TMB	3,3’,5,5’-Tetramethylbenzidine
UCP2	Uncoupling Protein-2
UCPs	Uncoupling proteins
β-cells	Pancreatic Beta Cells

Chapter 1

INTRODUCTION AND LITERATURE REVIEW

Permission to include parts of the following book chapter as part of this literature review: Barlow, J., Hirschburg, V. and Affourtit, C. On the role of mitochondria in pancreatic beta cells. In Research on Diabetes. ISBN: 978-14777555-01-9 was granted by iConceptPress Ltd.

1.1 Introduction

The pathogenesis of Type 2 diabetes is characterized both by insulin resistance of peripheral organs and by disruption of pancreatic beta (β) cell function [1]. In healthy subjects, pancreatic β-cells secrete insulin in response to increasing levels of blood glucose, which is a signal for tissues such as skeletal muscle and the liver to increase their uptake and storage of glucose [2]. The maintenance of blood glucose homeostasis involves multiple organs, which is frequently disturbed in diabetic subjects, such that blood glucose concentration is chronically elevated [3]. Work over the past decade has suggested a dominant role of adipose tissue as a regulator in both lipid and glucose homeostasis [4]. More specifically, adipose dysfunction that occurs in many cases of obesity leads to impairment of triglyceride storage and increased lipolysis [5]. Collectively, these abnormalities contribute to elevated levels of circulating non-esterified fatty acids (NEFA) [6] along with increased lipid stores in skeletal muscle and liver tissues [4]. Hyperlipideamia has been linked with insulin insensitivity in these compartments [7], which is initially overcome by a prolonged stimulation of insulin secretion [4]. However, persistent insulin resistance together with enhanced insulin secretion eventually leads to pancreatic β-cell dysfunction [1]. As a consequence of this β-cell dysfunction, a hyperglycemic state develops, which defines Type 2 diabetes [8]. Importantly, the exact mechanisms of how obesity leads to impaired insulin action and

secretion is still a subject of ongoing debate, yet experimental evidence indicates a strong relationship with the high level of NEFAs that circulate in the obese state [9,10], a phenomenon more commonly referred to as lipotoxicity [11].

Pancreatic β-cell lipotoxicity is difficult to understand due to the dual effect that NEFAs exert on cellular function, which is both time and glucose-dependent [12]. For example, NEFAs potentiate glucose-stimulated insulin secretion (GSIS) after an acute exposure [13], but impair GSIS after a chronic exposure [14,15]. Moreover, even a long-term exposure is not necessarily harmful to β-cells, as any toxic effect of NEFAs seems to be dependent on a high glucose level – a phenomenon referred to as glucolipotoxicity [16]. β-cell glucolipotoxicity is a complicated event that represents the combined deleterious effects of supra-physiological glucose and NEFA levels on β-cell function and survival [12]. Furthermore, not all NEFAs are equal, as the toxicity of a fatty acid is dependent on both the carbon chain number and the degree of saturation of the molecule [17]. For example, saturated NEFAs with carbon chains larger than C_{16} such as palmitate ($C_{16:0}$) and stearate ($C_{18:0}$) are potently toxic to β-cells, whilst their unsaturated counterparts palmitoleate ($C_{16:1}$) and oleate ($C_{18:1}$) appear to be well tolerated and in some cases may even protect against adverse effects of saturated molecules [17]. Generally though, it is well accepted that chronic NEFA exposure leads to impaired pancreatic β-cell function [10] and, consequently, Type 2 diabetes [9]. However the underlying mechanisms of

glucolipotoxicity are yet to be established [18]. The following literature review will address the current knowledge and understanding of pancreatic β-cell glucolipotoxicity and highlight areas that require further investigation that has informed the experimental work of this thesis.

1.2 Literature Review

1.2.1 Type 2 diabetes and obesity

The global incidence of diabetes mellitus is increasing rapidly, which is associated with an ageing population, widespread urbanization and general lifestyle changes [19]. Over the last three decades the number of people with diabetes has more than doubled giving rise to an estimated 382 million patients worldwide of which a vast majority suffer from Type 2 diabetes [20]. The etiology of Type 2 diabetes is not fully understood, but it is clear that the development of this metabolic disorder is multifactorial: people's genetic and environmental backgrounds are both critical risk factors and the disease involves the dysfunction of multiple organs [21]. Obesity is one of the more firmly established risk factors for Type 2 diabetes [22]. Although it is not yet known precisely how obesity and Type 2 diabetes are linked mechanistically, and despite the occurrence of differences between individuals, it is evident that these two pandemic conditions are associated [23]. Indeed, obesity is a key disorder in the Metabolic Syndrome, a combination of metabolic disturbances

that collectively increase the risk of developing Type 2 diabetes and cardiovascular disease [24].

The pathogenesis of Type 2 diabetes is characterised both by insulin resistance of peripheral organs and by disruption of pancreatic β-cell function [24]. In healthy subjects, pancreatic β-cells release insulin in response to rising blood glucose levels, which is a signal for tissues such as skeletal muscle and the liver to take up and store glucose, respectively [25]. Multiple organs are thus responsible for the maintenance of blood glucose homeostasis, which is disturbed in diabetic subjects such that the glucose concentration is chronically elevated [21]. Nutrient surplus in obesity causes insulin insensitivity [9,26] that may be compensated initially by increased insulin secretion. Persistent insulin resistance, however, leads to pancreatic β-cell dysfunction in many cases and, as a consequence of insufficient insulin secretion, to the hyperglycemic state that defines Type 2 diabetes [8]. How exactly obesity results in deficient insulin action and secretion is subject of ongoing research but the causal links likely involve excess availability of dietary nutrients as well as the action of inflammatory molecules [27]. High levels of plasma circulating free fatty acids [9,10], in combination with an elevated glucose concentration, have for example been suggested to impair pancreatic β-cell function by a phenomenon referred to as glucolipotoxicity [12,28]. The mechanisms that are responsible for this toxic effect of nutrient excess on β-cells are incompletely understood at present.

The remainder of this review will introduce the reader into the insulin secretory function of pancreatic β-cells and provide an overview of the recent advances in the field of pancreatic β-cell glucolipotoxicity.

1.2.2 Glucose-stimulated insulin secretion by pancreatic β-cells

1.2.2.1 Triggering and amplifying pathways

Pancreatic β-cells increase their oxidative catabolism of glucose in response to an increased blood glucose concentration [2,29]. The glycolytic breakdown of glucose allows pyruvate to feed into the mitochondria stimulating an increase in the tricarboxylic acid (TCA) cycle [30,31]. As a result of enhanced TCA cycle activity, electrons are transferred to the respiratory chain, eventually reducing molecular oxygen to water. This electron transport leads to proton export from the mitochondrial matrix across the inner membrane generating a proton gradient, which is referred to as the protonmotive force (pmf) [31]. ATP is generated by dissipation of the pmf via the re-entry of protons into the mitochondrial matrix through the ATP synthase [31]. Consequently, ATP is sythesised from ADP and inorganic phosphate and translocates to the cell cytosol via the adenine nucleotide translocator, increasing the cytosolic ATP/ ADP ratio [31]. The increase in the ATP/ADP ratio leads to closure of ATP-sensitive potassium channels, depolarization of the plasma membrane, opening of voltage-gated calcium channels, influx of calcium and eventual exocytosis of insulin-containing granules (Figure 1.1). This order of events has been well

established and is often referred to as the 'triggering' GSIS pathway [32]. It is becoming increasingly clear, however, that additional insulin secretory mechanisms occur that augment the insulin secretion response to glucose, these mechanisms are known as 'amplifying' GSIS pathways and comprise both hormonal and metabolic processes (Figure 1.1) [33].

GSIS is a biphasic event: 1st phase insulin release lasts only a few minutes, whilst a 2nd prolonged phase sustains insulin secretion to deal with post-prandial nutrient loads. Two models have been proposed to explain the biphasic nature of GSIS. The first model refers to the heterogeneity of insulin-containing granules, such that some vesicles are primed for immediate release, whilst others need mobilization and activation, causing delayed release [34]. The second model assumes a homogenous pool of insulin granules and attributes the biphasic GSIS pattern to temporal differences in the generation of triggering and amplifying signals that regulate exocytosis [33]. The current view in this respect is that a triggering Ca^{2+} signal is essential for both GSIS phases, but the amplifying signals play a more prominent role in phase 2 than in phase 1.

The amplitude and duration of GSIS may be augmented by mechanisms that involve either hormones or metabolic intermediates (Figure 1.1). Although GSIS amplification is less well understood at present than GSIS triggering, it is important to appreciate that amplifying signals are not able to initiate insulin

secretion as they can only enhance the effect of an existing triggering signal. Hormones such as glucagon-like peptide 1 and neurotransmitters such as acetylcholine mainly potentiate nutrient-induced insulin secretion by amplifying the action of Ca^{2+} on exocytosis [33]. The precise mechanism through which metabolic amplifiers augment GSIS is yet to be established, but their molecular nature is slowly emerging as metabolic amplification depends on the generation of short-chain fatty acyl-CoA esters [35,36]. Metabolic GSIS potentiation may involve fatty acid biosynthesis [37], and thus the formation of

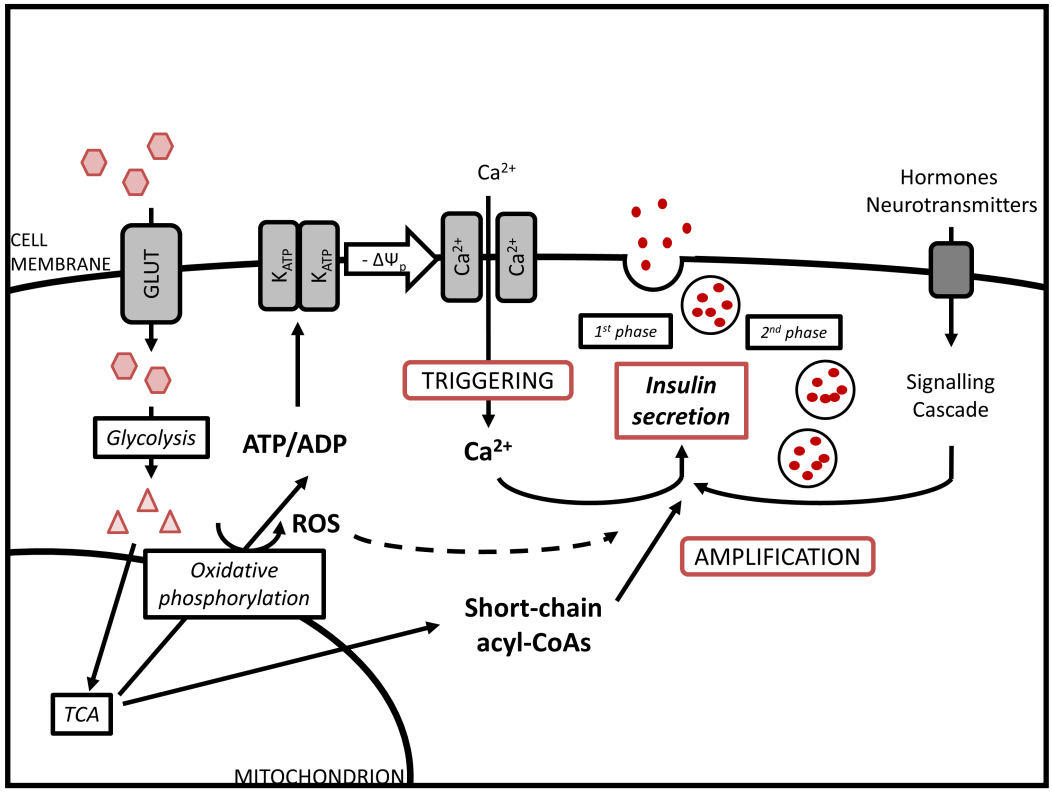

Figure 1.1 — Glucose-stimulated insulin secretion (GSIS) by pancreatic β-cells

Glucose (⬡) is taken up by β-cells via glucose transporter (GLUT) and stimulates insulin secretion as its glycolytic breakdown product (△) increases the rate of tricarboxylic (TCA) cycle turnover and oxidative phosphorylation. The resultant rise in the ATP/ADP ratio triggers closure of ATP-sensitive potassium channels (K^{ATP}), collapse of the plasma membrane potential (ΔΨp), calcium influx and exocytosis of insulin-containing granules. This triggering GSIS pathway can be amplified via hormonal and metabolic processes. Mitochondria-derived reactive oxygen species (ROS) stimulate insulin release through unknown mechanisms. Derived from [1].

long-chain fatty acyl-CoA esters from their short-chain counterparts, but such involvement is still a matter of debate [38].

1.2.2.2 Mitochondria derived triggering and amplifying signals

A glucose-induced rise in the cytosolic ATP/ADP ratio is central to the canonical GSIS model (Figure 1.1). It has indeed been established firmly that the ATP/ ADP poise increases in response to glucose [39-41]. The production of ATP in β-cells is predominantly derived from mitochondrial oxidative phosphorylation as β-cells exhibit an exceptionally low lactate dehydrogenase level [42] and, therefore, do not run glycolysis anaerobically to any significant extent. Oxidative phosphorylation is a mitochondrial process by which energy liberated from the oxidation of carbon substrates is conserved as ATP [43]. Mitochondria thus play an essential role in GSIS as they provide a key signal for the triggering pathway [30]. The relative importance of mitochondrial oxidative phosphorylation during GSIS is supported by the observations that (i) acute over-expression of lactate dehydrogenase, which lowers mitochondrial pyruvate oxidation, impairs GSIS [44], and that (ii) inhibiting mitochondrial Na^{+}/Ca^{2+} exchange, which stimulates mitochondrial metabolism, potentiates GSIS [45].

Not only is mitochondrial metabolism pivotal for the triggering GSIS pathway, it is also crucially important for GSIS amplification [35]. Cytosolic short-chain fatty acyl-CoA esters are key players in the GSIS amplifying pathway (Figure

1.2) and their formation is secondary to the export of carbon skeletons from the mitochondrial matrix [35]. These acyl-CoA esters can be generated from different carbon precursors [36], which are formed themselves via separate mechanisms that are likely species-specific [46]. Importantly, generation of all relevant carbon skeletons involves activity of the tricarboxylic acid (TCA) cycle [36], which puts mitochondria at the core of metabolic GSIS amplification.

Another potential role for mitochondria in GSIS is demonstrated by the discovery that reactive oxygen species (ROS) are key insulin secretion signals [47,48]. Indeed the origin of these signaling ROS in β-cells have not been

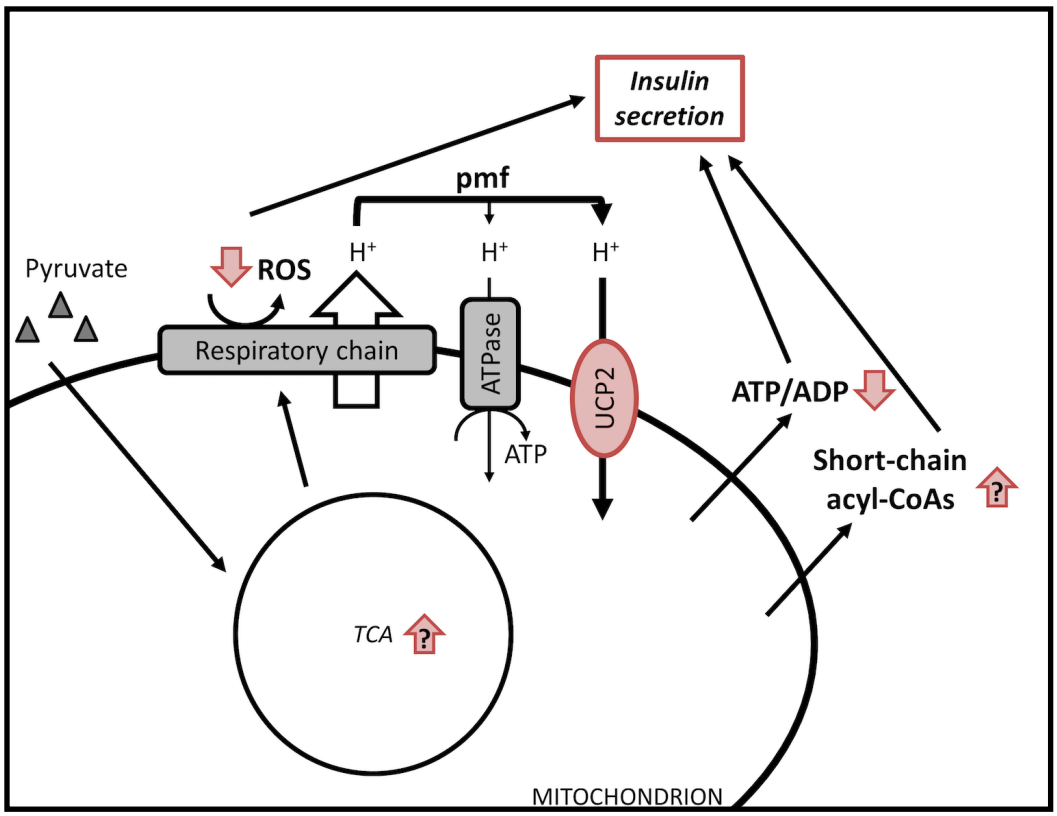

Figure 1.2 — The coupling efficiency of oxidative phosphorylation modulates formation of GSIS signals

ATP, reactive oxygen species (ROS) and tricarboxylic acid (TCA) cycle-derived short-chain fatty acyl-CoA esters are signals that link glucose catabolism to insulin secretion. UCP2 partially dissipates the mitochondrial protonmotive force (pmf) and regulates the production of at least some of these mitochondrial GSIS signals (see text for full detail). Derived from [1].

determined conclusively [49], but emerging evidence suggests that at least some of them arise from mitochondria [50]. Mitochondrial ROS production reflects a leak of electrons from the mitochondrial respiratory chain by which not all electrons are used to fully reduce molecular oxygen to water at respiratory complex IV (Figure 1.2). As a consequence of this, the escaped electrons partially reduce oxygen to superoxide, which can occur at multiple sites in the mitochondria [51-54]. In the presence of high glucose, fatty acids also directly contribute to GSIS amplification by increasing mitochondrial glucose oxidation [13], however the underlying mechanisms of this potentiation are incompletely understood.

1.2.3 Glucolipotoxicity of pancreatic β-cells

The biochemical mechanisms linking obesity and Type 2 diabetes have become increasingly appreciated over the past decade. Generally, it is well accepted that when insulin resistance develops in response to environmental factors such as obesity, pancreatic β-cells fail to adequately compensate for the increased insulin demand and cellular dysfunction arises [8]. Although the mechanisms of pancreatic β-cell dysfunction are unclear at present, the high level of free fatty acids that circulate in the obese state are a major risk factor in Type 2 diabetes [9,10]. Importantly, it is the chronic exposure of non-esterified fatty acids (NEFAs) that leads to the lipotoxicity of pancreatic β-cells and although

the underlying mechanisms of this process are yet to be established unequivocally [18], pancreatic β-cell lipotoxicity has been explored in detail.

Lipotoxicity is a complicated process due to the differential effects that NEFAs exert on cellular function. For example, GSIS is augmented by NEFAs acutely, perhaps via a mechanism similar to metabolic GSIS amplification, but impaired chronically. Interestingly, not all NEFAs exert harmful effects, since the effect of free fatty acids on β-cell viability depends on double bond configuration: saturated NEFAs are toxic to β-cells but non-saturated species appear well tolerated by β-cells and in some cases protect against adverse effects of their saturated counterparts [55]. Importantly, even a chronic exposure to NEFAs is not necessarily harmful to β-cells as any deleterious action of fatty acids tends to only occur in the presence of elevated glucose levels [18]. Such a permissive role of glucose in the lipotoxic process has led to the concept of glucolipotoxicity, which is defined as the synergy between levels of both glucose and NEFAs to cause tissue dysfunction [56]. Pancreatic β-cell glucolipotoxicity is thus a phenomenon that represents the combined deleterious effects of supra-physiological glucose and NEFA levels on β-cell function and survival [18].

1.2.3.1 Glucose permissibility of lipotoxicity

The permissive action of glucose on the detrimental consequences of chronic NEFA exposure stems from the effect of glucose on fatty acid metabolism [16].

The first evidence of glucose and lipid metabolic pathways converging in a glycerolipid/free fatty acid cycle, transpired many decades ago by the Randle cycle. For example, when glucose concentrations are low, long chain fatty acids are transported into the mitochondria for β oxidation via carnitine-palmitoyl transferase-1 (CPT-1). In contrast, when both glucose and fatty acid levels are high, the oxidation of glucose is favorable, leading to the formation of cataplorotic intermediates such as citrate, which are exported out of the mitochondria into the cell cytosol [18]. In combination with coenzyme A, exported citrate is used to form acetyl-CoA, which is then carboxylated to malonyl-CoA, and since fatty acid synthetase activity is lower than that of acetyl-CoA carboxylase in the β-cell [57], the predominant role of malonyl-CoA is to inhibit CPT-1 [16]. Consequently, long-chain fatty acid β oxidation is significantly decreased, leading to the accumulation of cytosolic long-chain acyl CoA esters, which have been associated with β-cell dysfunction [58]. Although the esterification of fatty acids into triacylglyceride (TAG) and lipid synthesis have been considered as the mechanisms of glucolipotoxicity, the specific lipid derivatives responsible for fatty acid-induced β-cell failure and survival remain elusive. Given that TAG is a relatively safe form of lipid storage in humans, it is unclear how exactly TAG leads to the deleterious effects in β-cell glucolipotoxicity. Related, mono-unsaturated fatty acids are also able to protect

against the harmful actions of their saturated counterparts by promoting esterification of toxic intermediates into neutral lipids [59,60].

Alternatively, lipotoxic effects have been attributed to the generation of lipid-derived cytosolic signals that in turn adversely affect β-cell function. Such cytosolic signals are derived from either the esterification pathway or from *de novo* synthesis of ceramide [61,62]. Palmitate derived ceramide has been linked with palmitate-induced effects on insulin gene expression [63]. However, it is unclear if ceramide is important for the NEFA impairment of GSIS, since cell-permeable analogs of ceramide are unable to replicate palmitate-induced GSIS defects in pancreatic islets [61]. Based on this evidence it is unlikely that ceramide alone is accountable for the loss of pancreatic β-cell function and survival, suggesting multiple mechanisms of glucolipotoxicity in Type 2 diabetes.

1.2.4 Fatty acid-induced glucose-stimulated insulin secretion defects

The chronic exposure of clonal pancreatic β-cells [64], and both rodent [14,65] and human [66] isolated pancreatic islets to NEFAs significantly dampens GSIS. Potential mechanisms of this dysfunction have been investigated, including mitochondrial dysfunction, regulation of UCP2 and diminished insulin granule exocytosis.

1.2.4.1 Mitochondrial dysfunction

As described previously, GSIS of pancreatic β-cells is dependent on an increase in the ATP/ADP ratio, which is determined in β-cells by substrate-coupled respiration [2]. The effects of NEFAs on pancreatic β-cell bioenergetics are scarce and although recent reports suggest that palmitate impairs aspects of mitochondrial function [14,64], it is unclear how such palmitate-induced defects link with GSIS. For example, it has been reported that palmitate-induced GSIS defects are due to decreased glucose oxidation by the attenuation of pyruvate dehydrogenase activity (PDH) [67]. The mechanism of this attenuation has been linked to increased fatty acid β oxidation by mechanisms that result in the inhibition of critical enzymes needed for glucose metabolism [68]. However, the glucose permissibility of lipotoxicity (discussed in section 1.2.3.1) disagrees with this view, which suggests that fatty acid β oxidation is attenuated under conditions that cause pancreatic β-cell dysfunction [18]. Clearly the involvement of mitochondria in pancreatic β-cell glucolipotoxicity is not well understood.

1.2.4.2 Uncoupling protein-2

Although the fundamental mechanisms responsible for glucolipotoxic-induced defects in β-cell mitochondrial function are currently unknown, the assumption that inefficient oxidative phosphorylation attenuates GSIS opened up the possibility that UCP2 might play a role in pancreatic β-cell glucoliptoxicity [29].

The role of UCP2 in glucolipotoxicity derived from experiments that showed UCP2 overexpression lowers the coupling efficiency of oxidative phosphorylation in INS-1E cells. Consequently, it was thought that UCP2 dampens GSIS by lowering the ATP/ADP ratio in β-cells [69]. Due to this pathological effect of UCP2 it was proposed as a suitable target in the therapy of Type 2 diabetes. This therapeutic prospect helps to explain the considerable research interest in the β-cell UCP2 area [29,70-74]. Despite the vast number of papers published with reference to UCP2, this field still suffers from many unresolved controversies. It is for example by no means generally accepted that the novel UCPs do in fact uncouple oxidative phosphorylation as their name implies [75-77] and molecular functions separate from dissipation of the pmf have also been suggested [78-80]. Similarly, the physiological function of UCP2 in β-cells is topic of current dispute as studies with various genetically modified murine models have yielded inconsistent phenotypes. The original global *Ucp2*-knockout mouse exhibits improved glucose tolerance and GSIS [81] [82]. When this *Ucp2*-deficient mouse is backcrossed on different genetic backgrounds, however, glucose tolerance is no longer improved [83] and GSIS is in fact impaired [82]. Pancreatic islets isolated from β-cell-specific *Ucp2*-knockout mice also exhibit enhanced GSIS, but interestingly, appear to be glucose intolerant, which is most probably due to their increased alpha cell mass and glucagon secretion [84]. Not surprisingly, the discrepant outcomes of animal experiments

have provoked rather different proposals for the function of UCP2 in β-cells, which range from a pathological role in the development of Type 2 diabetes [29] to a protective role in the physiological management of oxidative stress [73].

In spite of the unresolved physiological and molecular function of UCP2, its role in glucolipotoxicity has still been investigated [84-86]. After the expression of UCP2 was discovered in islet β-cells [87], subsequent experiments investigating the overexpression of UCP2 in pancreatic islets implicated its involvement in dysregulated GSIS [88]. The negative impact of elevated UCP2 on β-cell function was then shown to coincide with palmitate-induced defects in GSIS [85]. Collectively, these findings provided evidence suggesting a possible role of UCP2 in glucolipotoxic-induced β-cell dysfunction. The involvement of UCP2 in glucolipotoxicity has now been investigated in detail using both isolated pancreatic islets and clonal β-cells. In murine models lacking the Ucp2 gene, the insulin secretory capacity and glucose responsiveness of pancreatic islets is significantly improved after high fat feeding [85]. In agreement with [85], the knockdown of islet UCP2 by about 60% also significantly improves GSIS [71]. These early studies, therefore, support a pathological model of UCP2 in pancreatic β-cells. In contrast, other studies provide evidence to support a protective function of UCP2, since chronic absence of UCP2 causes oxidative stress and impaired GSIS in pancreatic islets [82]. Therefore it is also suggested that a major physiological function of UCP2 is to attenuate mitochondrial ROS

production [73]. In the context of glucolipotoxicity, it is therefore possible that UCP2 levels are attenuated by NEFAs leading to the generation of harmful ROS and consequent apoptosis [89]. The ongoing debate about the physiological function of UCP2 is partly explained by the fact that whole islet studies are confounded due to the expression of UCP2 in other islet cells [90]. Thereby it is hard to causally link UCP2 effects in whole islets to specific cellular functions.

The interpretational difficulties associated with whole animal experiments can be overcome by using cellular models. Importantly, experiments in cell models have obvious drawbacks and should be treated with caution when forming physiological inferences. Nevertheless, work with INS-1E insulinoma cells, one of the most widely used β-cell models, has provided direct support for a role of UCP2 in pancreatic β-cells [91]. The contribution of UCP2 in β-cells has been attributed to GSIS mechanisms by modulating the generation of mitochondrial signals [50,91]. Furthermore, in INS-1E cells exposed to NEFAs, the expression level of UCP2 mRNA is increased in line with GSIS defects [92], suggesting a possible involvement of UCP2 in pancreatic β-cell glucolipotoxicity. Importantly however, UCP2 protein mRNA levels are not always translated to protein and the activity of UCP2 has not been firmly established in β-cell glucoliptoxicity. Thereby a role of UCP2 involvement in pancreatic β-cell glucoliptoxicity is yet to be determined conclusively.

1.2.4.3 Insulin exocytosis

It is also possible that NEFAs suppress insulin secretion by modulating changes in one or more late phases of insulin exocytosis. In palmitate treated islets, the expression of granuphillin, a protein which has a key role in the docking of insulin secretory granules to the plasma membrane, is increased as a result of enhanced regulation of the sterol regulatory element-binding protein 1c (SREBP-1c) [93]. In consequence, insulin secretion is inhibited in response to fuel and non-fuel stimuli [93]. Moreover, it has been demonstrated that prolonged exposure of islets to either oleate or palmitate strongly inhibits both glucose and potassium stimulated insulin secretion without altering cell capacitance or Ca^{2+} signaling [94]. Therefore it is possible that NEFAs suppress insulin secretion at a very late stage of insulin exocytosis by interfering with the emptying of secretory granules, causing a switch from full fusion to incomplete fusion events. Furthermore, prolonged palmitate exposure can limit insulin secretion by changing Ca^{2+} concentration microdomains so that the influx of Ca^{2+} into islet β-cells is lowered [95]. This occurs in such a way that palmitate causes disassembly between tight complexes of Ca^{2+} channels, weakening Ca^{2+} concentration microdomains that are critical for insulin exocytosis [95]. Under normal conditions, adequate exocytosis of insulin, which is triggered by localised Ca^{2+}, only occurs when there is a close proximity between the Ca^{2+} channels and the secretory granules themselves. After palmitate treatment,

however, these events are modified, such that increased Ca^{2+} does not reach sufficiently high concentrations close to the secretory granule to produce exocytosis [95]. Thereby the mechanisms responsible for NEFA-induced impairment of insulin secretion might, at least in part, lie at the level of the exocytotic machinery. Consequently, NEFAs might also impair insulin secretion in response to other secretagogues distinct from glucose.

1.2.5 Fatty acids and β-cell viability

In addition to the functional deterioration of pancreatic β-cells, glucolipotoxic conditions have adverse effects on β-cell survival [18]. The propensity of NEFAs to induce negative effects on β-cell viability are complicated due to the differential effects that NEFAs exert on target tissues within the body. The exposure of β-cells to excessively high levels of almost any NEFA (irrespective of its structural features) leads to loss of cell viability, suggesting that almost all fatty acid species possess an intrinsic toxicity under certain conditions [59,96]. However, in glucolipotoxicity the situation is much more complex, since studies with isolated human islets, primary murine β-cells and various clonal β-cell lines demonstrate that the degree of NEFA toxicity is dependent on a variety of different factors including i) the degree of saturation [55], ii) the number of carbon atoms present in the molecule [97], iii) the exposure time [96], and iv) the glucose concentration [18].

It is therefore now generally accepted that certain long-chain saturated fatty acids such as palmitate (C_{16}) or stearate (C_{18}) are powerfully cytotoxic, whereas shorter chain saturated molecules such as myristate (C_{14}) or laurate (C_{12}) and long-chain unsaturated species like palmitoleate ($C_{16:1}$) or oleate ($C^{18:1}$) are far less destructive to β-cells [55,98]. Furthermore, there are additional pronounced differences between saturated and unsaturated fatty acids, since mono-unsaturated fatty acids like palmitoleate and oleate exhibit a tendency to maintain cell viability under conditions which might otherwise be cytotoxic [17,99,100]. Moreover, even long-chain saturated molecules might not be harmful to β-cells, as the effects of long-chain saturated fatty acids on β-cell viability and GSIS are both time and glucose dependent [18]. For example, after a short-term exposure, saturated fatty acids tend to potentiate insulin secretion [101], while chronic treatment is associated with attenuated insulin secretion and loss of cell viability [96]. To complicate things even further, even a chronic exposure to long-chain saturated molecules might not be detrimental to β-cell health, since the glucose concentration influences the ability of fatty acids to be actively toxic [16].

1.2.5.1 Possible mediators of fatty acid-induced loss of β-cell viability

In regard to NEFA-induced β-cell death, several mechanisms have been proposed, including ceramide formation, endoplasmic reticulum (ER) stress and reactive oxygen species (ROS) [18]. In particular, in pancreatic β-cells,

palmitate-derived ceramide [63] and treatment of β-cells with ceramide analogues leads to a loss in cell viability and abnormal mitochondrial activity [102,103]. Furthermore, pharmacological inhibition of ceramide *de novo* synthesis attenuates palmitate-induced cytotoxicity in rodent [102,104] and human islets [62,99]. In support for a role of ceramide in palmitate-induced loss of β-cell viability, ceramide levels are unchanged when treated with non-toxic shorter-chain fatty acids such as myristate [59]. The lack of ceramide formation in cells exposed to myristate provides a possible explanation for the differential specificity of shorter and long-chain saturated fatty acids as mediators of β-cell death. Discrepant with these findings, in pure populations of pancreatic β-cells, pharmacological inhibition of ceramide was unsuccessful in ameliorating palmitate-induced apoptosis [17,105]. Therefore it is possible that ceramide is associated with glucolipotoxic-induced cell death under certain conditions, but is unlikely to account for the complete toxic response of long-chain saturated species.

Another possible mediator of glucolipotoxic-induced β-cell death is the ER stress response [59]. ER stress is primarily a protective response designed to minimise cell damage by inhibiting protein synthesis in the face of unfavorable situations (reviewed in [106]). Excessive or prolonged ER stress however, is ultimately detrimental by triggering cell suicide, usually in the form of apoptosis as way to deal with dysfunctional cells [106]. In pancreatic β-cells,

exposure to palmitate induces protein alterations which are consistent with long-term ER stress [107], therefore ER stress is a contributory factor in NEFA-induced apoptosis in β-cells [107-110]. A particular gene that may be associated with a state of ER stress is the increased expression of the transcription factor SREBP-1c [111]. Overexpression of SREBP-1c has been linked with increased TAG content and reduced β-cell survival and function in pancreatic islets [112]. SREBP-1c is also elevated in isolated β-cells exposed to NEFAs [59]. In INS-1 cells, however, the negative impact of elevated SREBP-1c is alleviated by the knockdown of UCP2, which occurs independently from changes in intracellular TAG content [113]. Consequently, exacerbated TAG content is an unlikely cause for ER stress mediated β-cell destruction. Alternatively, it has been suggested that elevated SREBP-1c is associated with decreased transcription of insulin receptor substrate-2 (IRS-2) [111], which plays a key role in the regulation of critical survival pathways in β-cells [114]. IRS-2 is also involved in pro-apoptotic pathways that lead to enhanced cell death [105] so it is difficult to believe that suppression of IRS-2 is responsible for ER stress-mediated cell death. Sustained expression of SREBP- 1c - perhaps due to elevated ER stress may prove to be involved in the cause of NEFA-induced cell death, but its specific actions in pancreatic β-cells requires further exploration.

A role of mitochondria in NEFA-induced cell death has also gained significant interest over the past decade. It has been reported that glucolipotoxicity leads to

loss of mitochondrial membrane potential and consequently the release of cytochrome c, implicating a role for the mitochondrial apoptotic pathway in cytotoxicity [99,104,115]. Cytochrome c is normally bound to cardiolipin in the inner face of the lipid bilayer of the mitochondrial inner membrane, however, in the face of elevated saturated NEFAs, possibly by increased ROS [51], cardiolipin is altered in such a way that its affinity for cytochrome c is markedly reduced [116,117]. Concomitantly, cytochrome c dissociates from cardiolipin and exits the mitochondrion initiating a signaling cascade that ultimately leads to apoptotic cell death through the activation of caspases. In agreement for a role of mitochondria in glucolipotoxic related β-cell death, NEFA-induced apoptosis in pancreatic islets is accompanied by a marked alteration in the expression level of critical mitochondrial proteins that are important for pro-apoptotic and anti-apoptotic signaling in cells [56,62,99,115,118].

1.2.5.2 Cytoprotection by long-chain mono-unsaturated fatty acids

The cytoprotective properties of long-chain mono-unsaturated fatty acids were discovered about a decade ago [17,99]. Initially palmitate-induced β-cell death was shown to be significantly attenuated by co-exposure with palmitoleate ($C_{16:1}$) or oleate ($C_{18:1}$) [17,99,104,119]. This evidence demonstrates that it is possible to alter the way in which cells respond to saturated NEFAs by simply exposing them in the presence or absence of long-chain mono-unsaturated species. Importantly, it is worth note that cytoprotection is a distinct

characteristic of unsaturated molecules, as similar effects are not seen if toxic saturated fatty acids like palmitate are co-exposed with 'non-toxic' saturate species like myristate [98]. Moreover a reduction in the chain length from ($C_{16:1}$ to $C_{14:1}$ [myristoleate]) of mono-unsaturated is associated with a noticeable decrease in anti-apoptotic activity [120]. Thereby long-chain mono-unsaturates have a distinct feature that promotes cell viability in situations that might otherwise be cytotoxic [100]. Interestingly, cytoprotection is not limited to NEFA-induced toxicity, since palmitoleate also protects against the loss in cell viability in response to pro-inflammatory cytokines and serum deprivation [96]. Therefore the anti-apoptotic function of long-chain mono-unsaturated fatty acids is more general and not limited simply to its capacity to overcome the cytotoxic actions of saturated fatty acids.

The underlying mechanisms of cytoprotection are yet to be determined conclusively. It is known however, that treatment of β-cells with metabolically inert long-chain mono-unsaturates do not lead to a loss in cell viability [98]. More importantly, such molecules also retain their anti-apoptotic properties of their unmodified counterparts [96,120], suggesting that the metabolism of long-chain mono-unsaturates are not necessary for their cytoprotective activity. This concept is bought into focus in studies showing an identical potency between palmitoleate and methyl-palmitoleate [98]. Indeed methyl-palmitoleate might be de-methylated during incubation releasing free palmitoleate that then

provides the cytoprotective effect. However differences between methyl-palmitoleate and normal palmitoleate to alter β-cell phospholipid disposition or TAG content provides evidence against this [96]. Furthermore, the pharmacological inhibition of fatty acid β oxidation has no consequence on the cytoprotective actions of long-chain mono-unsaturated fatty acids [17]. It is therefore suggested that structural, rather than metabolic, determinants are most important for the cytoprotective actions of mono-unsaturated fatty acids.

The concept that the structural features of long-chain monounsaturated fatty acids are crucial for their anti-apoptotic actions, prompts the consideration of G-protein-coupled receptors in cytoprotection {Ichimura:2014hp}. In β-cells G-protein-coupled receptor 40 (GPR40) is abundantly expressed [121], and has been attributed to the acute and chronic effects of NEFAs on GSIS [122]. In the context of cytoprotection, GPR40 is activated by medium/long chain fatty acids, which is not specific to mono-unsaturated species [123]. GPR40 is also not activated by methyl palmitoleate [123]. Consequently, it is implausible to conclude that the cytoprotective actions of mono-unsaturates are associated with the activation of GPR40. Another free fatty acid receptor that has received interest over the last 5 years is GPR120 [124]. GPR120 is however mainly activated by polyunsaturated omega-6 and omega-3 fatty acids such as docosahexaenoic acid ($C_{22:6}$) and linolenic ($C_{18:3}$) at physiological concentrations {Ichimura:2014hp}. Moreover GPR120 has been implicated as a functional

omega-3 free fatty acid receptor that mediates anti-diabetic effects through the suppression of macrophage-induced tissue inflammation {Ichimura:2014hp}. GPR120 therefore plays an important anti-inflammatory role in β-cells which is unlikely related to the cytoprotective actions of long-chain mono-unsaturated species.

Alternatively, the actions of cytoprotection might involve other cell-surface receptors that allow mono-unsaturates to operate very quickly to elicit their anti-apoptotic mechanism. One line of evidence that has attracted considerable interest is the effect of mono-unsaturated fatty acids on the activity of caspase enzymes [100]. For example, in palmitate exposed β-cells, palmitoleate can rapidly attenuate caspase 3 activity [120]. Since caspase 3 is an essential effector enzyme in apoptosis [104,123], attenuation by long-chain mono-unsaturates could be the target for their cytoprotective responses. Importantly, the activation of caspase 3, which is increased dramatically in β-cells treated with long-chain saturated fatty acids, is prevented by the addition of palmitoleate [98]. When palmitate and palmitoleate are added simultaneously, caspase 3 activity is no longer detected, suggesting that the pro-apoptotic action of palmitate is completely prevented by palmitoleate [98]. The precise mechanisms of this signaling remain to be established, however it is unlikely that palmitoleate acts directly to inhibit caspase 3 but rather, mediates its effects indirectly via other pathways, since palmitoleate only causes a modest

reduction in caspase 3 activity against cell death mediated by mechanisms that are distinct from those induced by saturated fatty acids [120].

1.2.6 Fatty acids and reactive oxygen species

In the context of glucolipotoxicity it is likely that ROS are associated with NEFA-induced β-cell dysfunction and loss in viability [125-128], although the exact source of these ROS are currently unclear [128]. In pancreatic β-cells, the generation of ROS predominantly arise in either the mitochondria (reviewed in [51]) or by activation of cytoplasmic NADPH oxidase (reviewed in [49]).

1.2.6.1 Mitochondrial oxidative stress

Mitochondria are an important source of ROS in mammalian cells [129-134], in particular, in β-cells, mitochondrial ROS are key signals for the amplification of GSIS [50]. However under conditions that result in excessive ROS formation, ROS can lead to many complications that contribute to hyperglycemia and consequently Type 2 diabetes (Figure 1.3). In mitochondria, superoxide ($O_2^{\cdot-}$) is produced by a one-electron reduction of oxygen [51]. The production of $O_2^{\cdot-}$ in mitochondria predominantly arises at respiratory complexes I and/or III [51,135], although it is important to note that other sites of mitochondrial ROS production have also been identified [53,54]. In almost all living cells, the generation of $O_2^{\cdot-}$ is rapidly dismutated to H_2O_2 and then back into molecular oxygen and water by superoxide dismutase (SOD) and catalase, respectively [51]. However, in pancreatic β-cells the expression levels of antioxidant

enzymes are much lower compared to other tissues [136,137], making β-cells prime targets for oxidative stress [125-127,138,139]. Hence, elevated $O_2^{\cdot-}$ production due to increased flux through the respiratory chain in β-cells faced with supra-physiological glucose and NEFA levels are likely candidates for the deterioration of pancreatic β-cells in Type 2 diabetes.

The mechanisms responsible for the deleterious effects of combined glucose and NEFAs on pancreatic β-cell $O_2^{\cdot-}$ remain to be elucidated, but several studies have provided insight in this area. For example, UCP2 plays a pivotal role in $O_2^{\cdot-}$ formation in β-cells, by its ability to control the ATP/ADP potential through the dissipation of the pmf [140]. Thus, when UCP2 activity is high, proton leak across the inner mitochondrial membrane is stimulated, dissipating the pmf and consequently lowering the reduction of O_2 to $O_2^{\cdot-}$ [141]. In contrast, several other studies disagree with such an uncoupling function of UCP2 [78-80]. Furthermore, as described previously, a pathological role of UCP2 has also been suggested in β-cells, whereby increased activity of UCP2 is linked with impaired insulin secretion and increased $O_2^{\cdot-}$ production [142-144]. Clearly, a role of UCP2 involvement in glucolipotoxic-induced mitochondrial ROS is unclear and warrants additional investigation.

1.2.6.2 Cytoplasmic oxidative stress

As mentioned previously, another possible source for the generation of ROS in β-cells involves the activation of a plasma membrane associated enzyme known

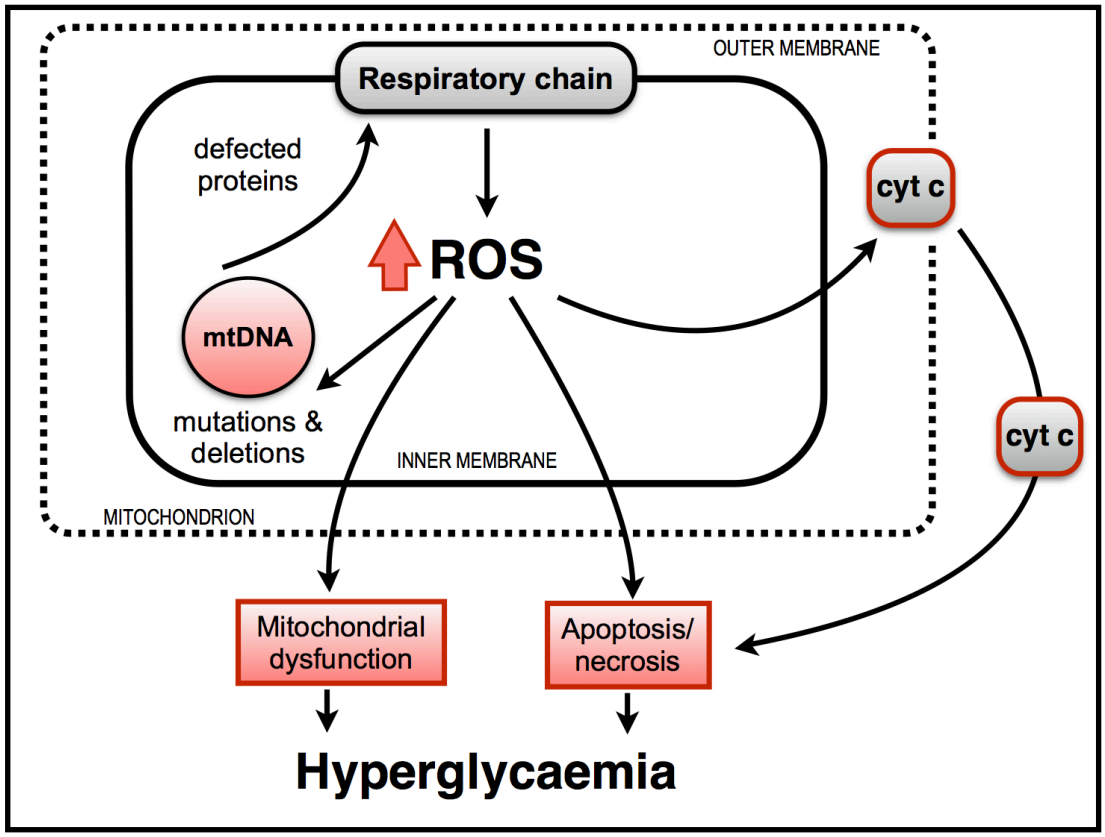

Figure 1.3 Consequences of mitochondrial ROS production in β-cells

Mitochondrial ROS production can lead to oxidative damage of mitochondrial DNA (mtDNA), proteins and membranes leading to the impairment of mitochondrial function. Furthermore, oxidative damage can lead to permeabilisation of the outer mitochondrial membrane, increasing the tendency of mitochondria to release intermembrane space proteins such as cytochrome c (cyt c) to the cytosol and thereby activating key apoptotic signaling cascades. Adapted from [51].

as NADPH oxidase (reviewed in ref [49]). NADPH oxidase activation is initiated in cells by the phosphorylation of several serine or threonine residues of the $p47^{phox}$ subunit, promoting the translocation of cytosolic subunits to the plasma membrane [49]. Upon activation, the enzyme complex catalyses a one-electron reduction of oxygen to generate $O_2^{\cdot-}$, using NADPH as the electron donor [128]. Following on from the discovery of an NADPH oxidase component in rat pancreatic islets [145] and BRIN BD11 clonal β-cells [146], considerable efforts were made to identify its possible role in pancreatic β-cell glucolipotoxicity. Importantly, cytoplasmic NADPH oxidase activity is elevated

in the β-cells of Type 2 diabetic animal models [128]. Furthermore, in combination with high glucose, prolonged exposure of pancreatic islet cells and clonal BRIN BD11 β-cells to palmitate have enhanced production and activity of cytoplasmic NADPH oxidase [128]. An elevated NADPH oxidase activity in these cells is also supported by augmented ROS generation [128]. Although the consequences of NADPH oxidase derived ROS have not been shown experimentally, it is indeed possible that these ROS are associated with pancreatic β-cell dysfunction and survival in glucolipotoxicity [49].

1.2.7 Conclusions

Investigating the effect of NEFAs in pancreatic β-cells and islets has developed the understanding of how different NEFAs act *in vitro* [14,64]. Studies using animal models of diabetes have also contributed to the understanding of the detrimental actions of NEFAs *in vivo* [65]. Collectively, these studies provide critical insights into pancreatic β-cell dysfunction and destruction in the development of Type 2 diabetes. It is now well established that chronic exposure of long-chain saturated NEFAs contribute to worsening of insulin resistance and impairment of pancreatic β-cell function [10,14,65] and survival [96], whilst long-chain mono-unsaturated fatty acids are not as harmful and might even protect against the adverse effects of their saturated counterparts [120]. However, despite considerable efforts, the relative importance and precise causal relationships of the multifarious effects of fatty acids on β-cell function

and survival are currently unknown [18]. Furthermore, the mechanism by which elevated long-chain saturated NEFAs dampen GSIS remains elusive and it is yet to be determined if long-chain mono-unsaturated fatty acids are able to protect against these effects [98]. Indeed, studies do exist to support a role of UCP2 in mediating NEFA-induced GSIS defects in β-cells, suggesting a possible role of mitochondria in this toxicity, but direct evidence to support a mitochondrial involvement is absent. The conflicting molecular function of UCP2 [75-79] also makes it difficult to draw a firm conclusion on the role of UCP2 in pancreatic β-cell glucolipotoxicity.

Based on the preceding literature review, the research in this thesis aims to investigate i) if NEFA exposure at high glucose impedes mitochondrial energy metabolism of pancreatic β-cells, ii) to identify if mitochondrial dysfunction is associated with NEFA-induced GSIS defects, iii) to determine if NEFA exposure is associated with loss of β-cell viability and increased ROS production, iv) to identify if monounsaturated fatty acids protect against cellular toxicity induced by saturated fatty acids, and v) to establish if glucolipotoxic-induced pancreatic β-cell dysfunction is in any way mediated or protected by UCP2.

Chapter 2

METHODS

Permission to include some of the methods from the following publication: Barlow, J., Hirschberg, V., Brand, M. D. and Affourtit, C. (2013) Measuring Mitochondrial Uncoupling Protein-2 Level and Activity in Insulinoma Cells. Methods in Enzymology. 528, 257–267 was granted by Elsevier.

2.1 Cell Culture

2.1.1 Rat INS-1E insulinoma cells

INS-1E insulinoma cells are a clone from the original parental INS-1 insulinoma pancreatic β-cell model and were a kind donation from Prof. Noel Morgan (University of Exeter, UK). INS-1E cells retain key characteristics of primary pancreatic β-cells and were therefore invaluable in the present study as a model for the *in vitro* investigation of mechanistic pathways in pancreatic β-cell glucolipotoxicity. INS-1E cells were grown and maintained in a humidified carbogen atmosphere (5% CO_2, 95% air) in RPMI-1640 medium (Sigma R0883) that contained 11 mM glucose and 2 g/L sodium bicarbonate - buffering the growth medium at pH 7.2 under carbogen. RPMI-1640 medium was supplemented with 5% (v/v) heat-inactivated fetal bovine serum (FBS, Sigma F9665), 10 mM Hepes, 1 mM sodium pyruvate, 2 mM glutamax, 50 μM β-mercaptoethanol, 100 U/ml penicillin, and 100 mg/ml streptomycin [147]. Note that Glutamax is a dipeptide of L-alanyl-L-glutamine which is more stable in aqueous solutions compared with L-glutamine alone [148], therefore Glutamax was preferred over the monopeptide, L-glutamine. The presence of glutamine in INS-1E cell culture medium and assay buffers was an absolute requirement to ensure full translation of UCP2 mRNA [149]. Cells were routinely cultured in 75 cm^2 canted neck BD Falcon™ flasks and passaged by trypsinisation. At 85–90% confluence, cells were washed twice with 10 ml Dulbecco's modified

phosphate-buffered saline (DPBS, Invitrogen 14190-185) after which 2 ml of 0.25% trypsin-EDTA (Invitrogen 15630-056) was pipetted equally across the monolayer and aspirated. Cells were detached by gentle agitation and resuspended in 10 ml fully supplemented RPMI-1640 culture medium. For maintenance of INS-1E cell cultures, cells were counted with an "Improved Neubauer" hemocytometer (Weber Scientific International Ltd) and seeded at 2.0 x 10^6 cells into new 75 cm^2 tissue culture flasks in a total volume of 15 ml culture medium. Medium was exchanged with heated (37 ^oC) RPMI-1640 culture medium every 2-3 days after seeding.

2.1.2 Mouse C2C12 myoblasts

C2C12 myoblasts were a kind donation from Dr Jane Carre (University College London, UK) and were grown in 75 cm^2 canted neck BD Falcon™ flasks under humidified carbogen conditions. Myoblasts were passaged by trypsinization at 70–80% confluence by the same method described in section 2.1.1 for INS-1E cells. However, it is important to highlight that C2C12 myoblasts were washed and grown in Dulbecco's modified eagles medium (DMEM) (Sigma, #D6546) supplemented with 25 mM glucose, 10% FBS, 100 U/ml penicillin, 100 mg/ml streptomycin and 4 mM glutamine after trypsinisation. Furthermore, C2C12 myoblasts were seeded at a density of 5 x 10^5 cells and passaged every 2-3 days after seeding.

2.2 Primary Islet Culture

All of the islet work carried out in this project was performed at the Helmholtz Zentrum Munich (HMGU) institute of Diabetes and Obesity in the mitochondrial biology laboratory directed by Dr Martin Jastroch. German animal welfare laws are strictly enforced at HMGU, and its animal facilities are clean, well-organized and properly maintained. All animal housing and handling were performed in accordance with the directive 2010/63/EU of 22nd November 2010 of the European Council on the protection of animals used for scientific purposes and its revisions, and with the laws governing the use of animals for research in Germany and Upper Bavaria.

2.2.1 Isolation of pancreatic mouse islets

Pancreatic islets of Langerhans secrete important hormones that are vital for maintaining blood glucose homeostasis and are, therefore, a key focus of diabetes research. The significance of purifying viable and functional islets from the pancreas is an intricate process which is necessary for the *in vitro* study of islet function or pancreatic β-cell physiology and pathology.

2.2.1.1 Preparation of liberase enzyme

One vial containing 5 mg of liberase (Roche, Cat No. 05401020001) was reconstituted into 200 µl of low glucose DMEM medium (GE Healthcare, SH30021.FS). The vial was kept on ice for 20-30 minutes with gentle circular

swirling. Aliquots of 50 µl were made in eppendorf microfuge tubes and stored at -20 °C. On the day of isolation 1 x aliquot of liberase was defrosted and diluted to 185 µg/ml in low glucose DMEM, and kept on ice.

2.2.1.2 Surgical procedure

Mice euthanised by CO_2 were sterilised with 70% ethanol and placed onto absorbent tissue paper. Using a pair of sterile pattern scissors the organs in the peritoneal cavity of the mouse were exposed by cutting from the lower abdomen and extending to the lateral portion of the diaphragm. Using a Bulldog clamp (Roboz, RS-7441), the common bile duct was clamped at the ampulla in the duodenum to facilitate perfusion of liberase into both the dorsal and ventral pancreas (Figure 2.1). After clamping, the common bile duct was located and cannulated with a 30 gauge 0.5 inch needle (Sigma, Z192341) secured to a 5 ml syringe. 2 ml of ice cold liberase solution was injected into the common bile duct to start the perfusion as shown in Figure 2.1. After successful perfusion, the pancreas was cut away from connecting tissues by removing the Bulldog clamp and carefully pulling the pancreas away from internal structures. After dissection, each pancreas was placed immediately into a 50 ml falcon tube and kept on ice. If perfusion of the pancreas was not successful, 2 ml of the enzyme solution was injected directly into the lobes of the ventral and dorsal parts of the pancreas before removal as described previously. To start the

digestion process, each pancreas was incubated in a 37 °C water bath for 14-15 minutes.

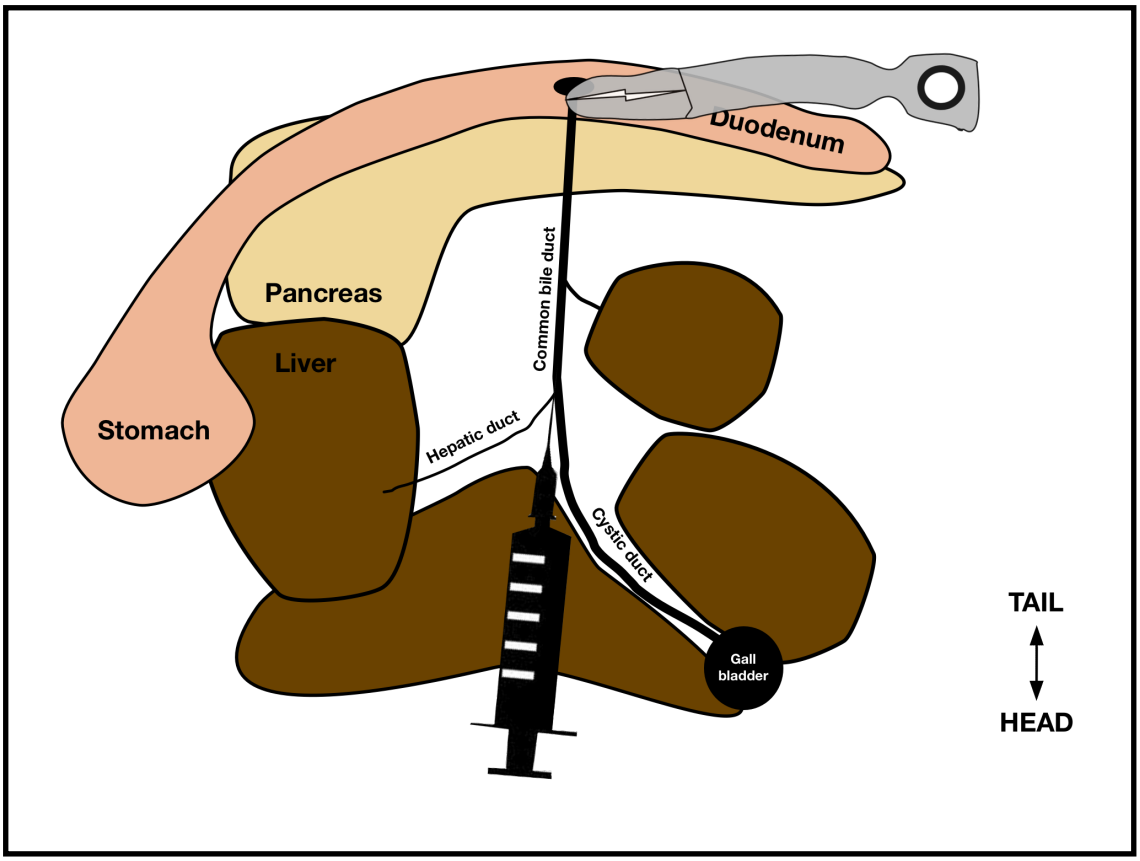

Figure 2.1 – Injection site and clamping of the common bile duct at the duodenum

2.2.1.3 Islet purification

Due to the abundance of digestive enzymes present throughout the exocrine pancreas, the purification of islets after isolation was a critical procedure to achieve the greatest islet yield. To purify the islets after digestion, the pancreata were removed immediately from the water bath, supplemented with 40 ml low glucose DMEM containing 10% heat inactivated FBS and shaken vigorously. Each 50 ml falcon tube was then centrifuged for 3 minutes at 900 rpm using a bench top centrifuge (Heraeus™ Multifuge™ X3 Centrifuge Series, Thermo

Scientific) and the supernatant was aspirated with any floating fat tissue. The remaining tissue pellet was resuspended in 20 ml low glucose DMEM by gentle swirling and passing through a tea strainer into new 50 ml falcon tubes. The falcon tubes were washed with another 20 ml low glucose DMEM and passed again through the cell strainer. Each sample was then centrifuged at 900 rpm (Heraeus™ Multifuge™ X3 Centrifuge Series, Thermo Scientific) for 3 minutes to pellet the islets and any remaining tissue. Following the second centrifugation step, the supernatant was aspirated and the tissue pellet was resuspended in 13 ml Histopaque®-1077 (Sigma, 10771). Carefully, 13 ml of low glucose DMEM was added on top of the Histopaque®-1077 creating a density gradient. The samples were centrifuged again at 900 rpm (Heraeus™ Multifuge™ X3 Centrifuge Series, Thermo Scientific) but for 35 minutes with the slowest acceleration (1) and deceleration (0). During the centrifugation step, the islets dissociated from the remaining exocrine tissue and migrated between the Histopaque®-1077 and DMEM layer. After centrifugation, the interphase layers containing the islets were collected and transferred into new 50 ml falcon tubes and centrifuged for a final time in a total volume of 50 ml DMEM at 1200 rpm (Heraeus™ Multifuge™ X3 Centrifuge Series, Thermo Scientific) for 5 minutes. After this, 35-40 ml of supernatant was aspirated leaving the islet pellet which was re-suspended in the remaining 15-10 ml of medium and transferred into a sterile petri-dish (FisherBrand, #12653575). Isolated islets

were inspected using a stereomicroscope (Nikon, SMZ1000) and purified further from any remaining exocrine tissue by 'hand picking' in volumes of 10 µl into a petri-dish containing 10 ml CMRL growth medium (Gibco, #21530027) containing 5.5 mM glucose and supplemented with 15 % serum, 50 U/ml penicillin, 50 µg/ml streptomycin, 50 µM β-mercaptoethanol, 17.8 mM NaHCO3, and 2 mM L-glutamine. To allow for the islets to equilibrate following the isolation procedure, they were left overnight in an humidified atmosphere at 37 °C with carbogen prior to any experimentation or treatment.

2.3 Fatty acids

NEFAs are one of the major energy sources for mammals, however to provide this energy, NEFAs must be transported through the blood to appropriate tissues. Therefore most NEFAs in the blood associate with serum albumin, facilitating transport of these relatively insoluble molecules [150]. Although most of the NEFA will bind to serum, a small amount will dissociate from the protein and be present in the aqueous phase, more commonly referred to as the unbound level of free fatty acid ($NEFA_u$). The interaction between NEFAs and albumin creates an equilibrium that buffers the level of $NEFA_u$, regulating the rate at which NEFAs are transported to target tissues. Moreover, it must not be disregarded that total serum concentrations of NEFAs are within the millimolar range but the actual effective $NEFA_u$ concentration and the binding affinities for NEFA-protein receptors are in the nanomolar range [151]. Because of the

insoluble nature of NEFAs they need to be applied with bovine serum albumin (BSA) *in vitro.* To achieve known concentrations of $NEFA_u$ it is important to determine specific molar ratios between NEFAs and BSA [151]. Many studies investigating the exogenous effect of NEFAs in insulinoma cells [97,146,152,153] or in pancreatic islets [14,146,154] tend to neglect this and refer only to the total NEFA concentration. In such studies it is therefore possible that the effective $NEFA_u$ concentration is not comparable with a physiological $NEFA_u$ concentration. Furthermore, many protocols designed for making NEFA:BSA conjugations include an unnecessary step that requires dissolving the pure fatty acid at high temperatures into a solvent [97,152,154,155], prior to conjugating with BSA. Evidence shown in Figure 2.2 highlights that by using such method (A) to create NEFA:BSA conjugations, the oxidation rate of the $NEFA_u$ by C2C12 myoblasts is suppressed significantly compared to a different method (B) that eliminates this step completely. Therefore, the BSA:NEFA conjugations used for this study were designed based on the protocol described in [153].

Specifically, essentially fatty acid-free BSA (Sigma A7030) was dissolved to 1.6 mM in medium containing 135 mM NaCl, 3.6 mM KCl, 10 mM Hepes (pH 7.4), and 0.5 mM $MgCl_2$. Palmitate (8 mM), palmitoleate (3.5 mM) or a combination of palmitate (5.5 mM) and palmitoleate (1 mM) were added as powder or liquid, respectively, and stirred continuously at 35-38 ^oC for 1 h or until all of the fatty acid had dissolved. Cooled BSA:NEFA conjugations were filter-

sterilised using a 0.22 μM filter attached to a 50 ml syringe (BD Biosciences) and were stable for 2 months when kept at 4 °C. Unless otherwise stated, the previously described BSA and NEFA concentrations were used because of published binding parameters [151] that predict the respective molar ratios should result in similar $NEFA_u$ levels of 20 nM, a concentration that correlates physiologically with an obese Type 2 diabetic subject [151].

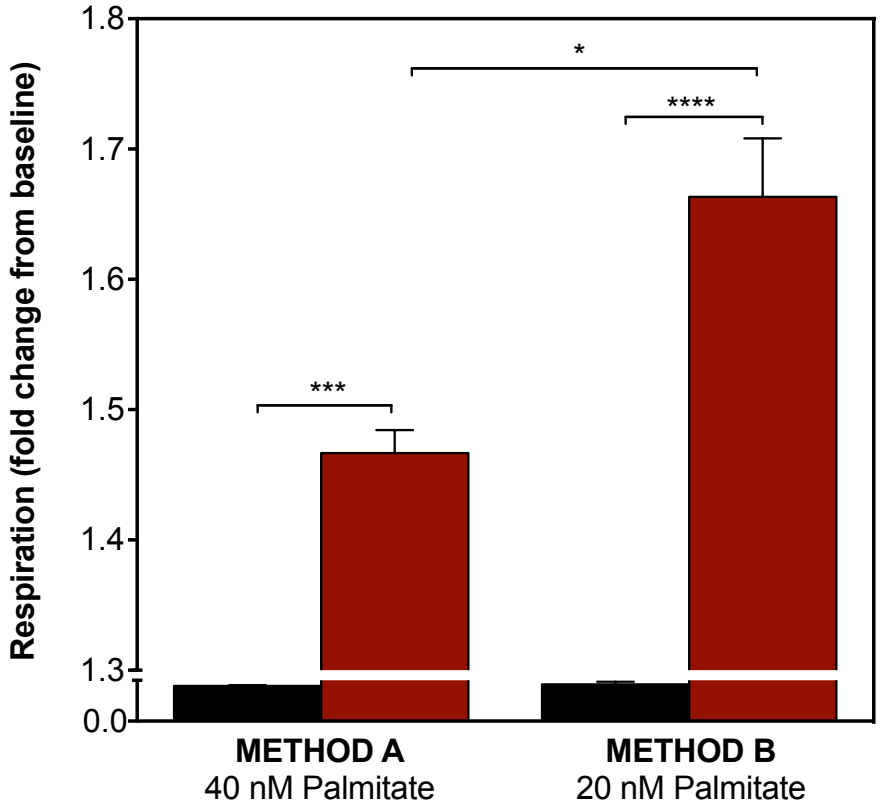

Figure 2.2 – The rate of palmitate oxidation by C2C12 myoblasts from two different fatty acid conjugation protocols

Myoblast cells were grown as described in section 2.1 and probed for respiratory activity in the presence of BSA conjugated to palmitate (red bars) or BSA alone (black bars) using Seahorse technology (see section 2.4). Data were normalised to basal oxygen uptake and non-mitochondrial respiratory rates were subtracted from all other activities. **Method A -** Palmitate:BSA conjugation was made based on the design that requires an initial step to dissolve the palmitate in ethanol prior to conjugating with BSA. **Method B -** Palmitate:BSA conjugation was made based on the design that adds the palmitate directly to a BSA solution. The different conjugations were estimated to contain 40 and 20 nM free palmitate for A and B respectively. Data represent the averaged fold stimulation in respiration ± SEM of 12-14 wells sampled from 3 independent XF24 plates. Statistical significance of mean differences between conditions were tested for by oneway ANOVA with Newman-Keuls Multiple Comparison posttest. *$p < 0.05$, ***$p < 0.001$ and ****$p < 0.0001$.

2.4 Mitochondrial Bioenergetics

Glucose-stimulated mitochondrial respiration and the coupling efficiency of oxidative phosphorylation – defined as the proportion of mitochondrial respiration used to make ATP – were measured in both intact INS-1E cells and isolated pancreatic islets. Parameters of mitochondrial bioenergetics were calculated from mitochondrial oxygen uptake rates using Seahorse extracellular flux (XF) technology [156]. Furthermore, absolute respiration rates were calculated after normalisation to cell number or DNA content for INS-1E cells and pancreatic islets, respectively.

2.4.1 Bioenergetics of INS-1E cells

INS-1E cells were trypsinised as described in section 2.1 and seeded onto XF24 cell culture microplates (Part #100777-004) at a density of 6 x 10^4 cells/well in 200 µl of RPMI culture medium. Seeded cells were incubated at 37 ^oC with carbogen and at 80-90% confluency were washed into 675 µl pre-warmed glucose-free Krebs-Ringer buffer (KRH) containing 135 mM NaCl, 3.6 mM KCl, 10 mM Hepes (pH 7.4), 0.5 mM $MgCl_2$, 1.5 mM $CaCl_2$, 0.5 mM NaH_2PO_4 and 2 mM L-glutamine. The cells were incubated in this buffer for 45 minutes at 37 ^oC under air and then transferred to a Seahorse XF24 extracellular flux analyser (maintained at 37 ^oC). After an initial 10-minute calibration, oxygen uptake rates were measured by a 3-4 loop cycle consisting of a 1-min mix, 2-min wait and 3-min measure to record cellular basal respiration (Figure 2.3A). After

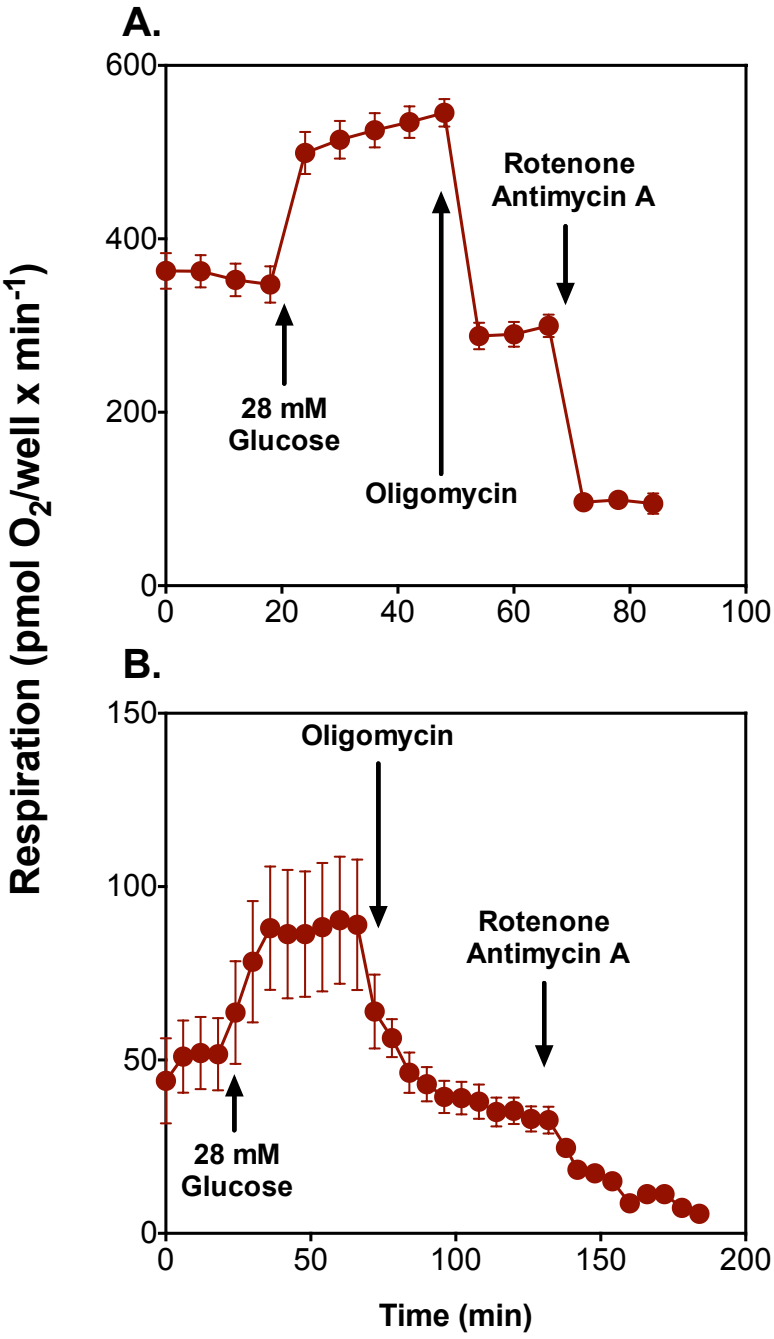

Figure 2.3 – Oxygen uptake rates of INS-1E cells and pancreatic islets exposed to 28 mM glucose using extracellular flux technology

(**A**) INS-1E cells were seeded on XF24 plates at 6 x 10^4 cells per well and grown for 48 hr in supplemented RPMI (see section 2.1.1). Cells were washed into a glucose-free Krebs-Ringer buffer and then incubated in a Seahorse XF24 extracellular flux analyser. The basal oxygen consumption rate was measured 4x after which the glucose concentration was raised to 28 mM. After 5 further measurements, 1 µg/ml oligomycin and a mix of 1 µM rotenone and 2 µM antimycin A were added sequentially to inhibit the mitochondrial ATP synthase and to determine the non-mitochondrial respiratory rate, respectively. Data represent averaged oxygen uptake rates ± SEM from 3 wells of a single XF24 microplate. (**B**) Pancreatic islets were seeded on XF24 capture plates at 20-30 islets per well in modified DMEM and then incubated in a Seahorse XF24 extracellular flux analyser. The basal oxygen consumption rate was measured 4x after which the glucose concentration was raised to 28 mM. After 8 further measurements, 10 µg/ml oligomycin and a mix of 2 µM rotenone and 2 µM antimycin A were added sequentially to inhibit the mitochondrial ATP synthase and to determine the non-mitochondrial respiratory rate, respectively. Data represent averaged oxygen uptake rates ± SEM of 3 wells of a single XF24 microplate.

measuring basal respiration, glucose was added by pneumatic injection and glucose-stimulated oxygen uptake rates were monitored for 5 further loops consisting of a 1-min mix, 2-min wait and 3-min measure (Figure 2.3A). After this point, 1 μg/ml oligomycin and a mixture of 2 μM rotenone and 2 μM antimycin A were added sequentially to, respectively, inhibit the mitochondrial ATP synthase or complex I and III of the electron transport chain to determine non-mitochondrial respiration (Figure 2.3A).

2.4.2 Bioenergetics of pancreatic islets

Pancreatic islets were isolated as described in section 2.2 and transferred to an XF24 islet capture microplate (Seahorse Bioscience #101122-100). Specifically, 20-30 islets were 'hand-picked' in 10 μl incubation medium and transferred into the depression chamber of each well of an XF24 capture microplate containing 490 μl modified DMEM containing 0.8 mM $MgSO_4$, 1.8 mM $CaCl_2$, 143 mM NaCl, 5.4 mM KCl, 0.91 mM NaH_2PO_4, 5.5 mM glucose and 2 mM Glutamax (Seahorse Bioscience #100965-000). To capture the islets into the depression chamber, a pre-wetted screen was firmly inserted into each well. Temperature control wells contained only culture media and pre-wetted screens. Islets were left to equilibrate after the seeding procedure by incubating for 1 h at 37 ^{o}C under air. Next, the microplate was transferred to a Seahorse XF24 extracellular flux analyser (maintained at 37 ^{o}C) and calibrated for 10-minutes. Post calibration, islet basal oxygen uptake rates were measured by a 4 loop cycle

consisting of a 1-min mix, 2-min wait and 3-min measure (Figure 2.3B). After measuring basal respiration, glucose was added by pneumatic injection and glucose-stimulated oxygen uptake rates were monitored for 8 further loops consisting of a 1-min mix, 2-min wait and 3-min measure (Figure 2.3B). After this point, oligomycin and a mixture of rotenone and antimycin A were added sequentially to, respectively, inhibit the mitochondrial ATP synthase or complex I and III of the electron transport chain to determine non-mitochondrial respiration (Figure 2.3B).

2.4.3 Glucose-stimulated respiration

Glucose-stimulated respiration was measured to determine the impact of exogenous NEFA exposure on the glucose-sensitivity of INS-1E cells or pancreatic islets. Specifically, glucose-stimulated respiration was calculated as a factor of the basal respiration by dividing total oxygen uptake activity in the presence of glucose by the basal respiratory rate (Figure 2.4). Rotenone and antimycin A-resistant respiratory activity was subtracted from all other activities to correct for non-mitochondrial oxygen consumption.

2.4.4 Coupling efficiency

The coupling efficiency of oxidative phosphorylation is defined as the proportion of respiration used to make ATP. The coupling efficiency was calculated by the amount of respiration that was inhibited by the ATP synthase inhibitor, oligomycin (Figure 2.4). Therefore the proportion of oxygen

consumption that was inhibited after the addition of oligomycin was used as an approximation of the amount of respiration coupled to ADP phosphorylation. The coupling efficiency of oxidative phosphorylation was approximated by expressing oligomycin-sensitive respiration as a fraction of total respiration. Rotenone and antimycin A-resistant respiratory activity was subtracted from all other activities to correct for non-mitochondrial oxygen consumption.

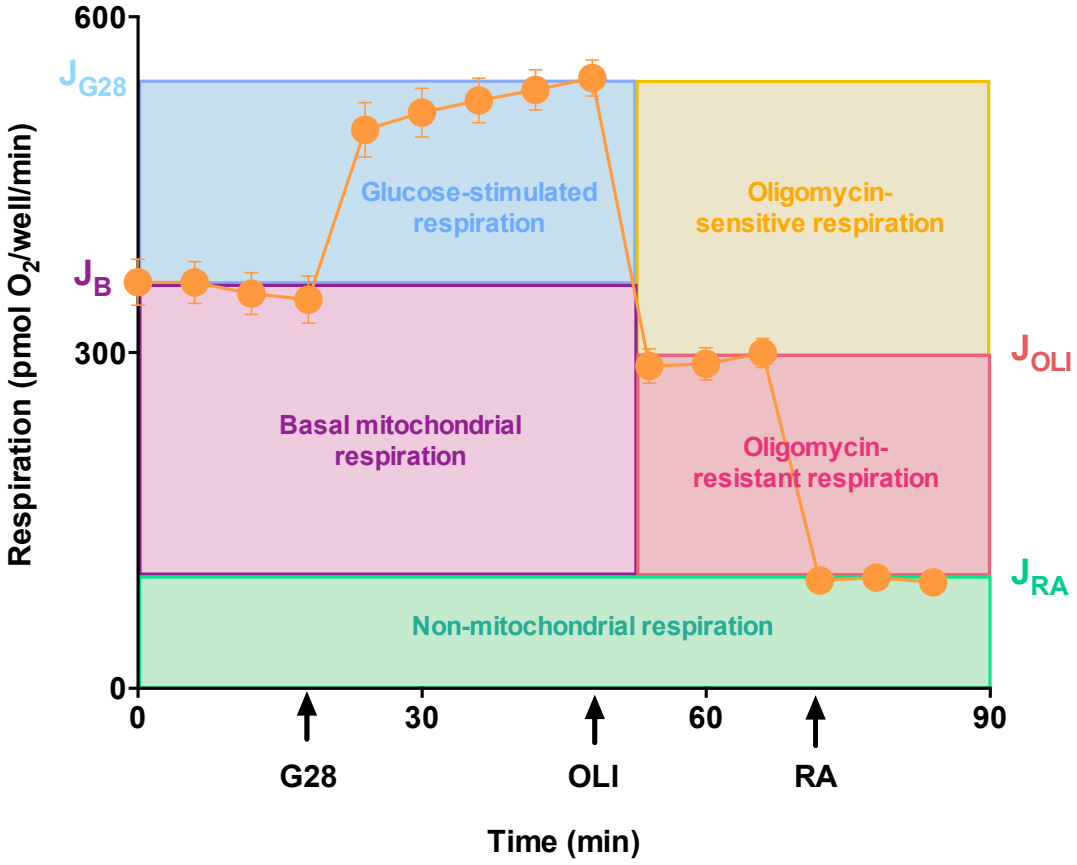

Figure 2.4 – Glucose-stimulated respiration and coupling efficiency of oxidative phosphorylation

INS-1E cells were washed into a glucose-free Krebs-Ringer buffer and then incubated in a Seahorse XF24 extracellular flux analyser. The basal oxygen consumption rate (J_B) was measured 4x after which the glucose concentration was raised to 28 mM (G28). After 5 further measurements, 1 µg/ml oligomycin (OLI) and a mix of 1 µM rotenone and 2 µM antimycin A (RA) were added sequentially to inhibit the mitochondrial ATP synthase and to determine the non-mitochondrial respiratory rate (J_{RA}), respectively. Coupling efficiency of oxidative phosphorylation is approximated by expressing the oligomycin-sensitive respiration (J_{OLI}) as a fraction of the total respiration (J_{G28}). JRA is subtracted from all rates to correct for the non-mitochondrial respiration. In equation: coupling efficiency = 1 – ((J_{OLI} – J_{RA})/(J_{G28} – J_{RA})). Data represent the averaged oxygen uptake rates ± SEM from 5 wells of a single XF24 microplate.

2.4.5 Absolute respiratory activity

Unlike the coupling efficiency of oxidative phosphorylation and glucose-stimulated respiration, absolute oxygen uptake rates are non-normalised bioenergetic parameters and may thus only be compared between experimental systems if normalised, for example, to cell number [157] or to islet DNA content [13]. To establish specific oxygen consumption rates, INS-1E cell density or islet DNA content was used to normalise oxygen uptake rates. For a detailed overview of these methods refer to sections 2.5 and 2.6 for INS-1E cell densities or section 2.8 for islet DNA content.

Briefly, cell densities of attached INS-1E cells seeded in XF24 microplates were probed for either their metabolic activity in each well using C_{12}- resazurin, a cell vitality probe that is reduced in metabolically active cells to the fluorescent product, C_{12}-resorufin [157] or for their nuclear content with 4',6-diamidino-2-phenylindole (DAPI), a fluorescent stain that binds to adenine or thymine regions in DNA by penetrating through cell membranes [158]. Total C_{12}-resorufin produced in metabolically active cells or DAPI stained nuclei was measured by detecting the total fluorescence in each well using a PHERAstar FS microplate reader (BMG LABTECH). Figure 2.5 highlights the dependence of total well C_{12}-resorufin and DAPI fluorescence on seeding density. Both C_{12}-resorufin and DAPI fluorescence are linear for cell seeding densities between 1

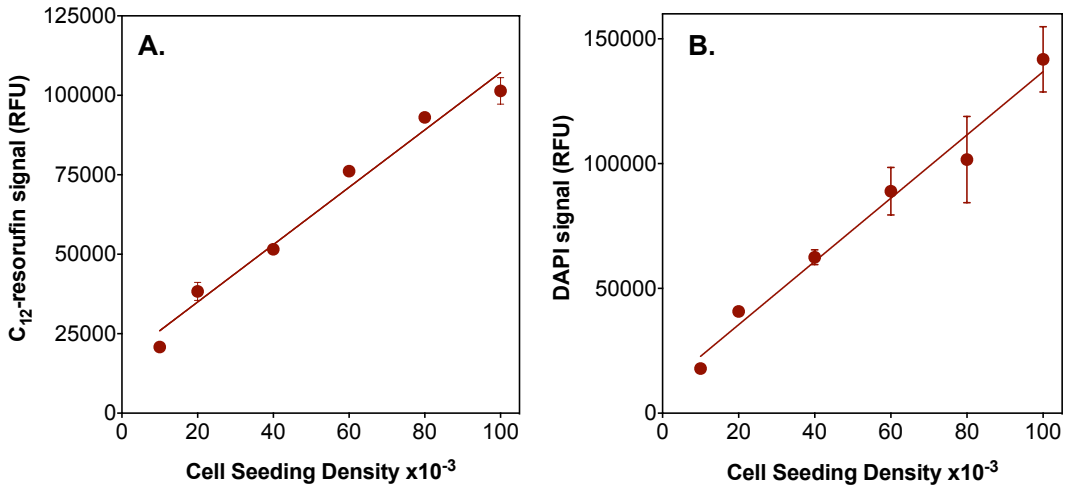

Figure 2.5 – The linearity of C_{12}-resorufin or DAPI fluorescence dependance on INS-1E cell seeding density

INS-1E cells were seeded on either XF24 (**A**) or 96-well (**B**) microplates at densities ranging from 1 x 10^4 to 1 x 10^5 cells in 200 ml RPMI medium per well and grown for 24 h. (**A**) Total C_{12}-resorufin formed during a 50-min incubation with 50 nM C_{12}-resazurin as described in section 2.5 (**B**) Total DAPI fluorescence measured after 20-min incubation as described in section 2.6. Data represent fluorescence means ± SEM expressed in relative fluorescence units (RFU) corrected for cell-free background fluorescence. Data were fitted to linear expressions.

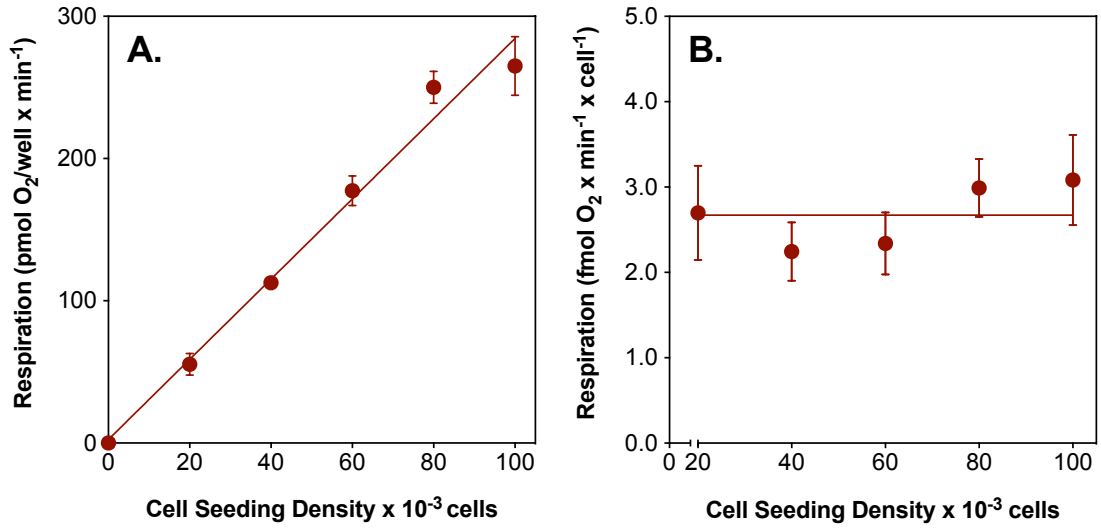

Figure 2.6 – Normalisation of basal respiration to INS-1E cell number

INS-1E cells were seeded on XF24 microplates and grown for 48 h. Basal respiration was measured 4x after which the cells were incubated for 50-min with 50 nM C_{12}-resazurin. Respiratory rates are plotted against applied seeding density and expressed as time resolved oxygen uptake per well (**A**) or per cell (**B**). Cell densities to which basal respiration was normalised were derived from the measured total C_{12}-resorufin fluorescence using data shown in Figure 2.3A. The plate reader's focal height was set at 2 mm, and its gain was fixed between different experiments. Data represent fluorescent means corrected for background fluorescence ± SEM calculated from 6 to 12 individual wells sampled from 2 to 3 separate plates. Data were fitted to linear expressions with slope kept variable (**A**) or set to zero (**B**).

x 10^4 and 1 x 10^5 cells per well. Typical seeding densities of INS-1E cells fall within this range, and therefore these assays are well suited to quantitatively detect the number of INS-1E cells in culture and therefore provided a suitable functional cell-normalising parameter [50,157]. Figure 2.6 demonstrates that normalisation of basal INS-1E cell respiration to C_{12}-resorufin fluorescence yields specific oxygen uptake rates that are consistent within a wide range of cell densities. Therefore, by quantifying INS-1E cell vitalities, absolute cellular respiration was determined from mitochondrial bioenergetic experiments [157].

It is of-course possible, however, that parameters normalised to cell vitality using the resazurin assay are confounded by effects of a particular treatment on the specific metabolic activity of cells, for these reasons to prove the lack of such effects, when C_{12}-resorufin fluorescence was used as a normalising tool it was also confirmed with DAPI staining (Figure 2.7). If the metabolic activity of cells was likely altered by specific treatments, for example after RNA interference (section 2.10.2) or when treated with mitochondrial pharmacological inhibitors, cell densities were obtained using the DAPI cell viability assay (section 2.6). To establish absolute respiration rates in pancreatic islets, respiratory data were normalised to DNA content using Quant-iT DNA assay kit (life technologies #Q33120), which is described in detail in section 2.8.

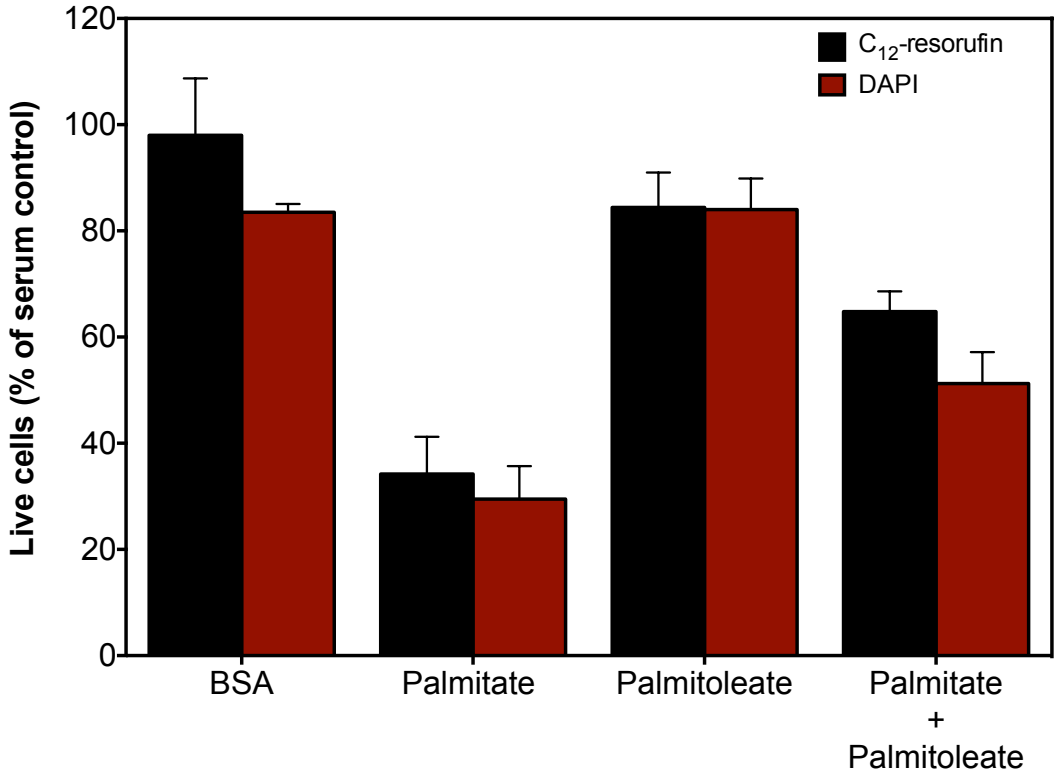

Figure 2.7 – The effect of NEFA exposure on INS-1E cell density measured by using two independent fluorescent probes

The vitality or viability of NEFA exposed INS-1E cells seeded on 96-well microplates was determined by C_{12}-resorufin fluorescence (black bars) or DAPI fluorescence (red bars), respectively. Cell vitality and viability was measured as described in sections 2.5.1 and 2.5.2 for C_{12}-resazurin and DAPI respectively. Cell densities were derived from the measured total fluorescence using data shown in Figure 2.3 and normalised to the serum control. Data represent fluorescent means corrected for background fluorescence ± SEM calculated from 16 to 20 individual wells sampled from 4 to 5 separate plates. There are no significant differences between the two data sets.

2.5 Cell Vitality

The density of INS-1E cells was not only determined to normalise data as described in section 2.4, but also to establish the effects of different treatments on INS-1E cell vitality. INS-1E cells were seeded at 6 x 10^4 cells/well into either XF24 microplates or 96-well Corning (Costar® 3595) culture plates, and at 70-80% confluence, exposed to different nutrient conditions and/or analysed for mitochondrial respiration. After specific treatments, for example to NEFAs or immediately after Seahorse measurements of basal oxygen uptake, the densities

of attached INS-1E cells were determined using the metabolic probe C_{12}-resazurin, a cell vitality probe that is reduced in metabolically active cells to fluorescent C_{12}-resorufin [157]. Lyophilized C_{12}-resazurin powder was bought as part of a commercial kit (Invitrogen #V-23110), dissolved to 10 mM in dimethylsulfoxide (Fisher #BPE231-100), and stored at -20 °C in 500 µl aliquots. On the day of use, C_{12}-resazurin was diluted in phosphate buffered saline (PBS, Sigma P4417) to 200 nM and protected from light. INS-1E cell cultures were washed into 100 µl/well supplemented RPMI to which 30 µl diluted C_{12}-resazurin was added, achieving a working concentration of 50 nM. After a 50 minute incubation period at 37 °C under carbogen total C_{12}-resorufin was measured by detecting the total fluorescence in each well using a PHERAstar FS microplate reader (BMG Labtech) in fluorescence intensity, bottom-reading and well-scanning mode. C_{12}-resorufin was excited at 540 nm and emitted light was detected at 590 nm. Cell densities were calculated from the total emitted C_{12}-resorufin fluorescence in relative fluorescent units (RFU) using the standard curve shown in Figure 2.5A.

2.6 Cell Viability

The cell viability of attached INS-1E cells was determined in 96-well culture plates by staining cell nuclei with DAPI, a fluorescent stain that binds strongly to adenine or thymine regions in DNA [158]. For the estimation of cell densities, treated cells were washed into 200 µl/well phosphate buffered saline (PBS), and

then fixed with 4% (w/v) paraformaldehyde (PFA) for 20 min at ambient temperature. After fixation, 0.5 μg/ml DAPI (Molecular Probes® #D1306) diluted in PBS was added to each well and left at room temperature for 15 min. To reduce background fluorescence, any unbound DAPI was removed by washing each well four times with 200 μl PBS. The fluorescence intensity of DAPI was measured by exciting at 358 nm and detecting emitted light at 461 nm using a multimode plate reader (PHERAstar FS, BMG Labtech) in bottom-reading and well-scanning mode. Cell densities were calculated from the total DAPI fluorescence using data from the standard curve shown in Figure 2.5B.

2.7 Insulin samples

2.7.1 Glucose-stimulated insulin secretion of INS-1E cells

INS-1E cells were seeded at 6 x 10^4 cells/well into 96-well Corning (Costar® 3595) culture plates, and at 80-90% confluence, starved for 2 h in glucose-free RPMI (Sigma #R8755) lacking sodium pyruvate, and containing only 1% (v/v) FBS. Cells were then washed into 100 μl/well glucose-free Krebs-Ringer buffer (KRH) comprising 135 mM NaCl, 3.6 mM KCl, 10 mM Hepes (pH 7.4), 0.5 mM $MgCl_2$, 1.5 mM $CaCl_2$, 0.5 mM NaH_2PO_4, 2 mM glutamine, and 0.1% (w/v) BSA and incubated in this medium for 30 min at 37 °C on a shaking plate incubator (Labnet International, Oakham, UK) set at 100 rpm. Next, glucose-free KRH was replaced with KRH containing 0 or 28 mM glucose or 4 mM glucose plus 50

mM KCl. After another 30 min incubation, supernatants were collected and centrifuged at 4 °C at 12,000 rpm (Heraeus™ Fresco™ 17 Microfuge, ThermoScientific) for 5 minutes to pellet any cells or cell debris. Aliquots of the supernatants were taken and stored at -20 °C until assayed for insulin by enzyme linked immunosorbent assay (ELISA).

2.7.2 Glucose-stimulated insulin secretion of pancreatic islets

Pancreatic islets were isolated as described in section 2.2, and maintained in culture at 37 °C with carbogen in CMRL culture medium. On the day of the assay, islet viability was inspected by eye using a stereomicroscope (Nikon, SMZ1000). In 10 µl of culture medium, islets were 'hand-picked' at random and transferred into a single well of a 'v' bottom 96 well culture microplate (Greiner bio-one #651101) containing 90 µl pre-warmed (37 °C) low-glucose KRH comprising 119 mM NaCl, 4.7 mM KCl, 2.5 mM CaCl, 1.2 mM KH_2PO_4 1.2 mM MgCl, 30.7 mM $NaHCO_3$, 10 mM Hepes (pH 7.4), 0.2 % BSA and 5.5 mM glucose. Once the islets had settled in the plate they were carefully washed by removing and adding 80 µl/well of KRH assay buffer. Following a second wash, the islet plate was incubated at 37 °C under carbogen for 2 hs. Half way through this incubation period the islets were washed once more by removing and adding 80 µl/well of KRH assay buffer. After the 2 h incubation period, supernatants were collected by removing 80 µl/well of the assay buffer. This was replaced with 80 µl/well KRH supplemented with 28 mM glucose. The

microplate was then placed back into the incubator for 1 h before collecting 80 µl/well of the supernatant following stimulation with high glucose. The supernatants were immediately centrifuged after collection at 12,000 rpm (MIKRO 220R, Hettich) for 5 minutes at 4 °C to pellet any cells or debris. Aliquots of the supernatant were taken and frozen at -80 °C until assayed for insulin by ELISA.

2.7.3 Islet insulin content

Immediately after the GSIS assay, islets were aspirated and homogenised in 100 µl RIPA buffer comprised of 0.1 % sodium dodecyl sulfate (SDS), 150 mM NaCl, 1 % octylphenyl-polyethylene glycol, 0.5 % sodium deoxycholate and 50 mM Tris-HCl (pH 8.0). Islet homogenates were prepared by shaking vigorously at 4 °C for 5 minutes using a mechanical tissue lyser set at 30 revolutions per second (TissueLyser II, Qiagen, Limburg, Netherlands). Islet homogenates were stored overnight at -80 °C and then centrifuged at 12,000 rpm (MIKRO 220R, Hettich) at 4 °C. Aliquots of the supernatant were taken and assayed immediately for insulin or stored at -80 °C.

2.7.4 Insulin quantification

Samples were assayed for insulin using ELISA using mouse insulin as standard. The principal of the ELISA used was based on a direct sandwich technique in which two monoclonal antibodies are directed against separate antigenic determinants on insulin molecules. The determination of insulin is finally

achieved by the addition of 3,3',5,5'-tetramethylbenzidine (TMB), a chromogenic substrate, that when oxidised by horseradish peroxidase which is linked to antibodies, yields a characteristic change that is detectable spectrophotometrically [159]. The enzymatic reaction between TMB and horseradish peroxidase is stopped by the addition of H_2SO_4, turning the TMB yellow, which absorbs light at a wavelength of 450 nm. The absorbance measured at 450 nm is proportional to insulin in the sample (Figure 2.8).

Specifically, on the day of the assay, insulin samples were thawed on ice and diluted appropriately in glucose-free KRH comprising 135 mM NaCl, 3.6 mM KCl, 10 mM Hepes (pH 7.4), 0.5 mM $MgCl_2$ and 1.5 mM $CaCl_2$. Dilution of the insulin sample was critical to ensure the insulin concentration remains within the sensitivity of the standard curve (Figure 2.8) and to avoid complex crowding which can limit the detection of insulin in the sample. Following dilution, insulin standards and samples were added to appropriate wells in the microplate, after which, peroxidase-conjugated anti-insulin antibodies were added to each well. The microplate was incubated for 2 hs at room temperature on a plate shaker set at 700 rpm. During this incubation, insulin bound to the anti-insulin antibodies bound to the microplate forming insulin bound anti-insulin complexes with the peroxidase-conjugated anti-insulin antibodies. After incubation, any unbound enzyme labeled antibody was removed by a series of 6 washes using 300 µl/well wash buffer. After the final wash, any residual wash

buffer was discarded from each well by inverting the microplate and tapping firmly onto absorbent tissue paper before adding TMB solution to each well for 15 minutes. The reaction was terminated by adding 0.5 M H_2SO_4 to each well and absorbance was measured spectrophotometrically at 450 nm using a PHERAstar FS microplate reader (BMG LABTECH). Insulin in the sample was proportional to the absorbance at 450 nm as shown in Figure 2.8. Insulin concentrations in each sample was therefore interpolated by comparing the relative optical density after spectrophotometric analysis at 450 nm with the standard curve.

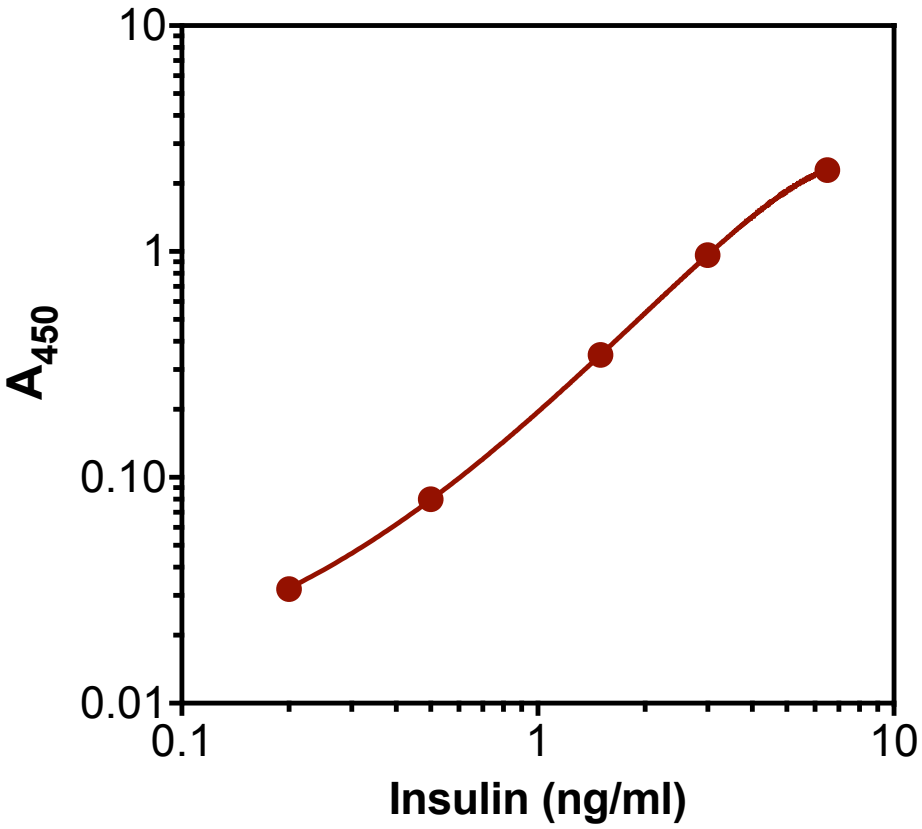

Figure 2.8 – Example standard curve using mouse insulin as standard

Mouse insulin standards of known concentrations (0.2, 0.5, 1.5, 3.0 and 6.5 ng/ml) were assayed for insulin using ELISA (Mercodia). Absorbance measured at 450 nm is plotted on a logarithmic scale against insulin concentration (ng/ml) and fitted to cubic spline regression.

2.8 DNA Content

The heterogeneity between pancreatic islet size, insulin content, cell composition and insulin secretory capabilities presents a situation that complicates the interpretation of islet data. This variation, which arises from well-to-well in the same experiments and from different experiments can be minimised by normalising islet data with known concentrations of double-stranded DNA (dsDNA) [13]. Measurements of dsDNA are indicative of cell number, providing a valuable tool for normalising islet bioenergetics (section 2.4) or insulin secretion (section 2.7). Specifically, normalising islet data to dsDNA corrects for the variation that arises between islet size and/or cell content. Indeed there are limitations to this assay, for example, dsDNA will be measured in all cells whether they are metabolically active or not. Furthermore, dsDNA will be quantified in islet cells which do not contribute to the secretion of insulin, which is an exclusive characteristic of pancreatic β-cells.

2.8.1 DNA samples

After measuring oxygen uptake or insulin secretion, pancreatic islets were aspirated and transferred to 100 µl RIPA buffer comprised of 0.1 % sodium dodecyl sulfate, 150 mM NaCl, 1 % octylphenyl-polyethylene glycol, 0.5 % sodium deoxycholate and 50 mM Tris-HCl (pH 8.0). Islets were homogenised as described in section 2.7.3. Islet homogenates were stored overnight at -80 ºC and centrifuged at 12,000 rpm (MIKRO 220R, Hettich) at 4 ºC. Aliquots of the

supernatant were taken and assayed immediately for dsDNA using Quant-iT™ PicoGreen® dsDNA assay kit (life technologies #P11496).

2.8.2 DNA quantification

Quant-iT™ PicoGreen® dsDNA reagent was used as a fluorescent nucleic acid stain for quantifying dsDNA in solution. On the day of the assay 1X Tris-EDTA (TE) buffer comprised of 10 mM Tris-HCl (pH 7.5) and 1 mM EDTA was prepared in DNase free H_2O and left to reach room temperature. Following this, a working concentration of Quant-iT™ PicoGreen® dsDNA reagent was prepared by making a 200-fold dilution of the concentrated stock solution using TE buffer. To avoid the reagent adsorbing to glass surfaces or being susceptible to photo-degradation it was prepared in a plastic container and stored away from direct light. To create a 5-point high-range standard curve a 100 µg/ml Lambda DNA stock solution was diluted in 1X TE buffer supplemented with 50 % RIPA buffer. 100 µl of each DNA standard (0, 2, 20, 200, 2000 ng/ml) was added to a single well of a 96-well microplate (Greiner-bio #). Next, 50 µl of each islet sample prepared as described in Section 2.8 was added to separate wells containing 50 µl 1X TE buffer. To each well, 100 µl working solution of Quant-iT™ PicoGreen® dsDNA reagent was added and the microplate was incubated for 5 minutes in a PheraStar fluorescence multiplate reader (BMG Labtech). Fluorescent products were excited at 480 nm and emission intensity was measured at 520 nm. The fluorometer gain and focal height were set

between each experiment and adjusted to accommodate the lower fluorescence signals. DNA in each sample was quantified by interpolating unknown X values from comparing RFU values with those on a standard curve of known dsDNA concentrations (Figure 2.9).

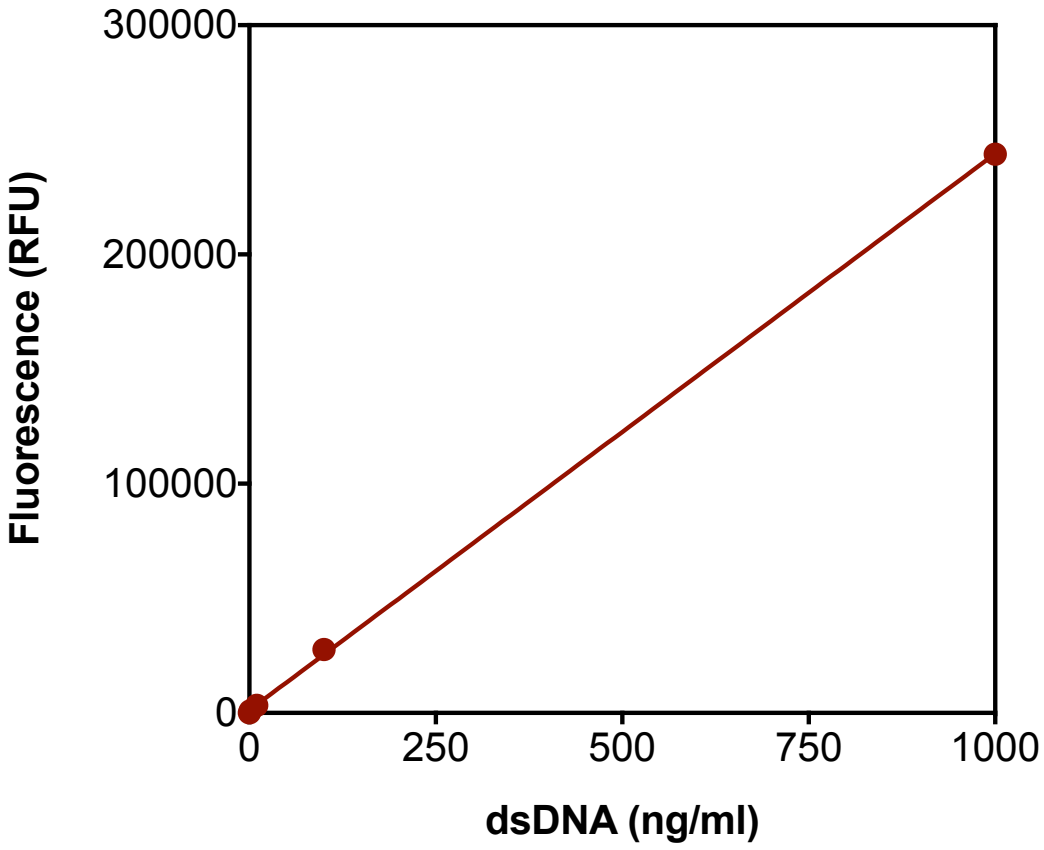

Figure 2.9 – Standard curve of Lambda dsDNA detected with Quant-iT™ PicoGreen® dsDNA reagent

Lambda DNA was diluted to create standards of known concentrations (0, 1, 10, 100 and 1000 ng/ml) and were quantified using Quant-iT™ PicoGreen® dsDNA reagent. The samples were excited at 480 nm and fluorescence emission intensity measured at 520 nm. Relative fluorescent units were plotted as a function of dsDNA and fitted with linear regression.

2.9 Reactive Oxygen Species

2.9.1 Mitochondrial reactive oxygen species

Mitochondria derived superoxide was detected in intact INS-1E cells using MitoSOX, a hydroethidene probe which is targeted to the mitochondria by a conjugated triphenylphosphonium moiety. In the presence of mitochondrial superoxide and to some extent hydrogen peroxide [160] MitoSOX is oxidised to fluorescent products, which are readily detected fluorometrically. INS-1E cells were seeded at 6 x 10^4 cells/well into 96-well Corning (Costar® 3595) microplates, and at 80-90% confluence washed into glucose-free Krebs-Ringer medium (KRH) comprising 135 mM NaCl, 3.6 mM KCl, 10 mM Hepes (pH 7.4), 0.5 mM $MgCl_2$, 1.5 mM $CaCl_2$, 0.5 mM NaH_2PO_4 and 2 mM glutamine and incubated in air at 37 ^oC for 30 minutes. Next, plates were transferred to a multimode plate reader (PHERAstar FS, BMG Labtech) and following injection of 5 μM MitoSOX fluorescence was monitored at 28-sec intervals for 30 min. Fluorescent MitoSOX oxidation products were excited at 510 nm and light emission was detected at 580 nm. The plate reader's focal height was set at 3.4 mm and its gain was fixed between different experiments. Since MitoSOX is primarily oxidised by mitochondrial superoxide, the rate at which mitochondrial superoxide was produced could be determined from the slope of the resultant progress curve over the 30 minute period post MitoSOX injection.

2.9.2 Cytoplasmic reactive oxygen species

Intracellular cytoplasmic superoxide was detected in intact INS-1E cells using hydroethidene (DHE). In the presence of superoxide and to some extent hydrogen peroxide [160] DHE is oxidised to fluorescent products, which are readily detected fluorometrically. Specifically, INS-1E cells were seeded at 6 x 10^4 cells/well into 96-well Corning (Costar® 3595) microplates, and at 80-90% confluence washed into glucose-free Krebs-Ringer medium (KRH) comprising 135 mM NaCl, 3.6 mM KCl, 10 mM Hepes (pH 7.4), 0.5 mM $MgCl_2$, 1.5 mM $CaCl_2$, 0.5 mM NaH_2PO_4 and 2 mM glutamine and incubated in air at 37 °C for 30 minutes. Next, plates were transferred to a multimode plate reader (PHERAstar FS, BMG Labtech) and following injection of 5 μM DHE fluorescence was monitored at 28-sec intervals for 30 min. Fluorescent DHE oxidation products were excited at 510 nm and light emission was detected at 580 nm. The plate reader's focal height was set at 3.4 mm and its gain was fixed between different experiments. Since DHE is primarily oxidised by cytoplasmic superoxide, the rate at which cytoplasmic superoxide was produced could be determined from the slope of the resultant progress curve over the 30 minute period post DHE injection.

2.10 Uncoupling protein-2

2.10.1 Uncoupling protein-2 protein detection

2.10.1.1 Sample preparation

INS-1E cells were seeded into 25 cm^2 tissue culture flasks (BD Bioscience) at a density of 1 x 10^6 cells/flask. At 80-90 % confluency, cells were washed twice with 5 ml ice-cold Dulbecco's modified phosphate buffered saline (DPBS) and removed from tissue culture flasks using a cell scraper. Cell suspensions in DPBS were centrifuged at 900 rpm (5810R, Eppendorf) for 5 minutes, supernatant was aspirated and the pelleted cells were lysed in ice-cold RIPA buffer containing 50 mM Tris-HCl (pH 8.0), 1 % (v/v) Nonidet P40, 0.25 % (w/v) sodium-desoxycholate, 0.1 % (v/v) SDS, 150 mM NaCl, 1 mM EDTA and 500x diluted protease inhibitor (Sigma-Aldrich #P8340). To aid cell lysis, samples in RIPA were agitated vigorously for 20 minutes at 4 °C. Following centrifugation of the cell lysates at 12,000 rpm (Heraeus™ Fresco™ 17 Microfuge, ThermoScientific) for 20 min at 4 °C , protein content of the supernatants were estimated with a bicinchonic acid assay (BCA) (ThermoScientific, #23227).

The BCA protein assay is based on a colorimetric detection that exhibits strong absorbance at 562 nm which is linear with increasing protein concentrations over a working range of 20-1500 μg/ml protein (Figure 2.10). Thus, quantification of total protein in unknown samples can be interpolated from a standard curve of known protein concentrations. To create the standard curve,

BSA standards were prepared at concentrations between 0 - 1500 μg/ml by diluting in RIPA buffer supplemented with 1:500 protease inhibitor. In non-tissue culture treated 96-well microplates (Sterilin #3875-096) 10 μl protein sample or standard was pipetted into allocated wells. Next, 200 μl BCA protein assay reagent (ThermoScientific #23228) was added to each well and incubated under air at 37 ºC for 30 minutes. After incubation, the absorbance of each well was read spectrophotometrically at 562 nm using a PheraStar multi-plate reader (BMG Labtech). The optical density at 562 nm was proportional to protein concentration and thus, unknown protein concentrations were determined from a standard curve using BSA as standard (Figure 2.10).

After protein quantification, sample volumes of protein extracts containing 50 μg protein were calculated and diluted 1:5 in ice-cold acetone to precipitate protein in the sample. Each sample was vortexed for approximately 10 seconds and left overnight at -20 ºC. The following day, each sample was centrifuged at 12,000 rpm (Heraeus™ Fresco™ 17 Microfuge, ThermoScientific) for 15 min at 4 ºC. The supernatant was aspirated and the precipitated protein was re-suspended in 20 μl loading buffer containing 10% (v/v) glycerol, 50 mM Tris-HCl (pH 6.8), 2% (v/v) SDS, 2% (v/v) mercaptoethanol, 0.1 mM EDTA and 0.01% (w/v) bromophenol blue. Complete solubilisation was ensured by, 3x 30-second vortexes during a 5-min incubation at 100 ºC. After a brief 2 min cool down period, samples were analysed immediately.

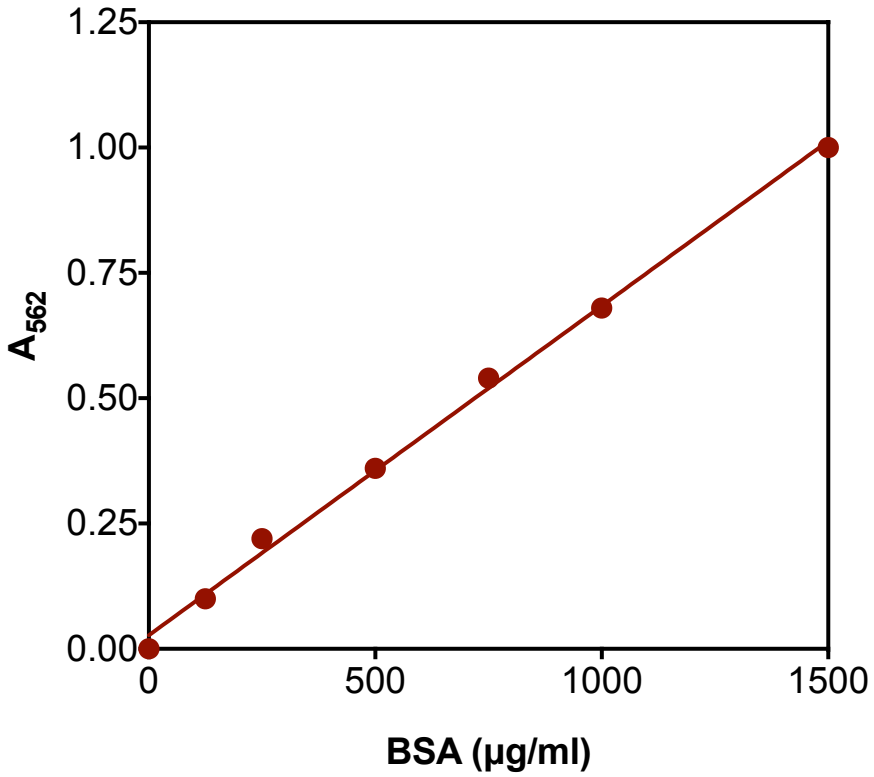

Figure 2.10 – The linearity of BSA standards probed with Pierce™ BCA reagents

BSA diluted in RIPA buffer to create standards of known concentrations (0, 125, 250, 500, 750, 1000, 1500 and 2000 µg/ml) was assayed for protein using BCA assay reagents. Absorbance was measured spectrophotometrically at 562 nm and plotted as a function of BSA concentration. Data were fitted to linear regression.

2.10.1.2 Western analysis

Proteins from cell lysates were separated on a 12 % SDS polyacrylamide gel by running it at 150 V for 1 h 45 min. Proteins were transferred onto nitrocellulose membrane (Whatman Protan, BA85) at ambient temperature using a semi-dry Trans-Blot SD (BIO-RAD) transfer cell set at 20 V for 30 min. After being washed with Tris-buffered saline (TBS) comprising of 20 mM Tris HCl (pH 7.5) and 50 mM NaCl, the membrane was blocked by continuous shaking at 65 rpm for 2 h in blocking buffer containing 3% (w/v) dried skimmed milk powder (MARVEL), 20 mM Tris-HCl (pH 7.5), 50 mM NaCl and 0.1% (v/v) Tween 20.

Primary UCP2 antibodies (sc-6525, Santa Cruz) were then added to the blocking buffer at 0.4 μg/ml [156]. Following overnight incubation at 4 ºC (rocked at 100 rpm), membranes were washed 4x over a period of 30 min with TBST, and then incubated for 2 h at room temperature with 0.2 μg/ml peroxidase-conjugated secondary antibodies. Following 4 TBST washes over a period of 30 min, antibody cross-reactivity was detected by chemiluminescence (ECL Prime, Amersham) using a LAS 4000 camera (GE Healthcare) collecting images at 30-sec intervals for 5 min. Membrane images were analysed with ImageQuant TL version 7.0 (GE Healthcare) (Figure 2.11A and 2.11B). As described fully in Figure 2.11, UCP2 protein levels were compared between samples by normalising to partially purified recombinant human UCP2 standards donated by Dr Paul Crichton (MRC Mitochondrial Biology Unit, Cambridge, UK). After UCP2 detection (Figure 2.11A) band intensities were normalised to total protein per lane by routinely staining membranes with Pierce™ GelCode Blue reagent (Catalogue #24590, ThermoScientific). This was achieved by rehydrating membranes in distilled water for 5 minutes and then staining for 5 min with GelCode® Blue reagent diluted 2x in distilled water. Following staining, the membranes were de-stained by washing in a mix of 50% (v/v) methanol and 1% (v/v) acetic acid for 45 min (Figure 2.11C).

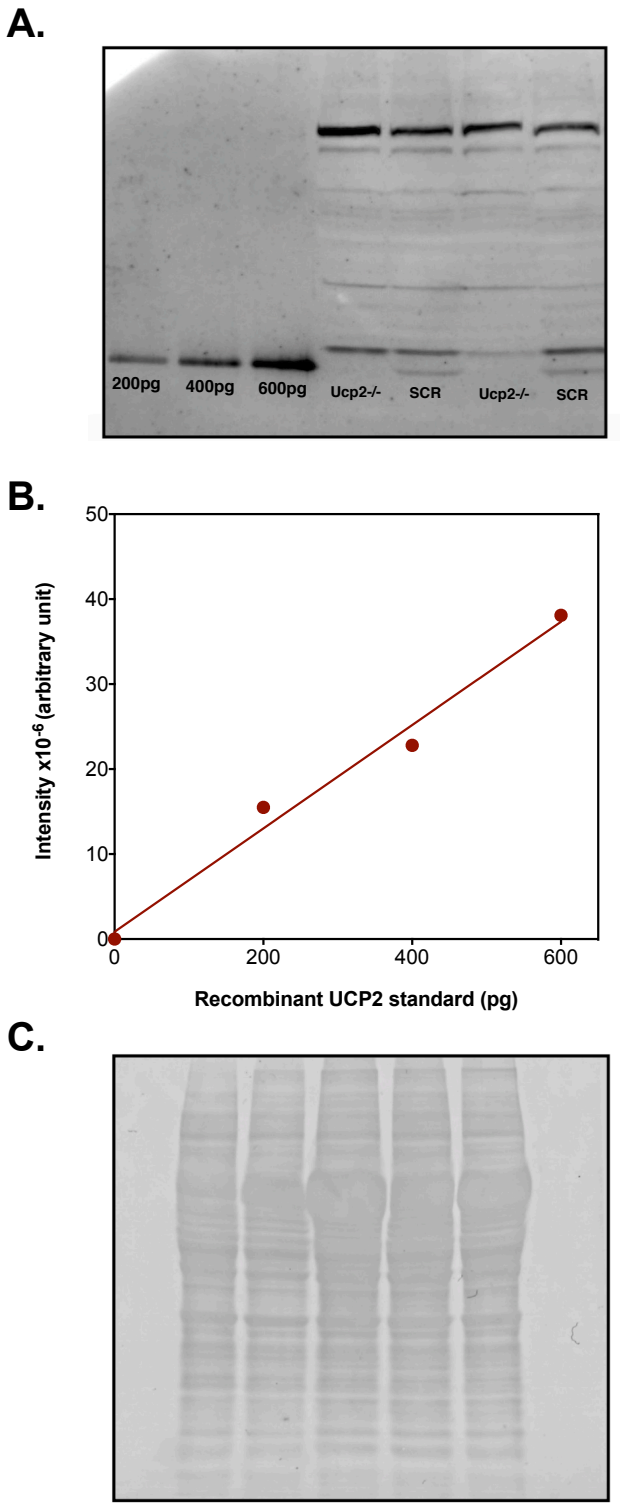

Figure 2.11 – Measuring UCP2 protein levels in INS-1E cells

(**A**)Typical Western blot showing cross-reactivity of UCP2 antibodies with partially purified recombinant hUCP2 (200pg, 400pg and 600pg) and INS-1E cell proteins separated by SDS-PAGE. Proteins were isolated from cells transfected with Ucp2-targeted or scrambled siRNA oligonucleotides (Ucp2-/- and Scr, respectively). (**B**) Typical relation between signal intensity and amount of hUCP2 as determined for each individual experiment (cf. panel **A**) to allow comparison of UCP2 levels between different samples. (**C**) Typical membrane stained for total protein with GelCode Blue reagent to allow for normalisation of protein loading between different lanes (cf. panel **A**). Membrane images were analysed with ImageQuant software using its 1D gel analysis feature. Panel B: background in defined lanes was subtracted by the rolling ball function, bands reflecting known hUCP2 amounts were boxed, and by applying the quantity calibration function the presented relation was generated.

2.10.2 Knockdown of uncoupling protein-2

UCP2 protein was knocked down in INS-1E cells by RNA interference using siRNA oligonucleotides targeted at exon 8 of the rat UCP2 (5'-3' sense sequence: CGUAGUAAUGUUUGUCACCtt) (Ambion #199050, AM16706) [156]. INS-1E cells were seeded at 6 x 10^4 cells/well in 96-well Corning (Costar®, 3595) microplates and incubated at 37 ºC with carbogen. Post 24 h seeding, cells were transfected with 200 nM UCP2 siRNA complexed with 1.7 μg/ml Lipofectamine™ 2000 (Invitrogen, UK) in RPMI lacking fetal bovine serum and antibiotics [157]. In parallel wells, cells were transfected with scrambled siRNA (Ambion, Silencer® Negative Control 1 #AM4635) to control for possible non-specific transfection events. Following a 24 h period of transfection, cell medium was exchanged for normal RPMI and after 24 h further growth, cell lysates were collected as described in section 2.10.1.1 and analysed for UCP2 protein by Western analysis (section 2.10.1.2). As shown in Figure 2.11A the expression of UCP2 protein disappeared after RNA interference with *Ucp2*-targeted oligonucleotides.

Chapter 3

NOVEL INSIGHTS IN PANCREATIC BETA CELL GLUCOLIPOTOXICITY FROM REAL-TIME FUNCTIONAL ANALYSIS OF MITOCHONDRIAL ENERGY METABOLISM IN INS-1E INSULINOMA CELLS

Permission to include the work from the following publication: Barlow, J. and Affourtit, C. (2013) Novel insights in pancreatic beta cell glucolipotoxicity from real-time functional analysis of mitochondrial energy metabolism in INS-1E insulinoma cells. Biochemical Journal. 456, 417-426 was granted by Portland Press Ltd.

3.0 Abstract

High circulating glucose and free fatty acid levels can cause pancreatic β-cell failure. The molecular mechanisms of this β-cell glucolipotoxicity are yet to be established conclusively. In this chapter the involvement of mitochondrial dysfunction in fatty acid-induced β-cell failure is examined by using extracellular flux technology to functionally probe mitochondrial energy metabolism in intact INS-1E insulinoma cells in real-time. It is reported that 24 h palmitate exposure at high glucose attenuates the glucose-sensitivity of mitochondrial respiration and lowers coupling efficiency of glucose-stimulated oxidative phosphorylation. These mitochondrial defects coincide with an increased level of ROS, impaired GSIS and decreased cell viability. Palmitate lowers absolute glucose-stimulated respiration coupled to ATP synthesis, but does not affect mitochondrial proton leak. Palmitate is not toxic when administered at low glucose unless fatty acid beta oxidation is inhibited. Palmitoleate, on the other hand, does not affect mitochondrial respiration, ROS levels, GSIS or cell viability. Whilst palmitoleate protects against the palmitate-induced ROS increase and cell viability loss, it does not protect against respiratory and insulin secretory defects. It is concluded that mitochondrial dysfunction contributes to fatty acid-induced GSIS impairment, and that glucolipotoxic cell viability and GSIS phenotypes are mechanistically distinct.

3.1. Introduction

The risk of developing Type 2 diabetes is greatly increased in obese individuals [22] and a major mediator of this risk is a chronic elevation of circulating NEFAs [161]. It is generally accepted that there is a causal relationship between chronically high NEFA levels and pancreatic β cell failure [9]. This pathological link, which is often referred to as 'β-cell lipotoxicity' [162], is responsible for the impaired insulin secretion that contributes to the development of obesity-related hyperglycaemia [163].

The precise mechanisms by which NEFAs lead to β-cell failure are subject of ongoing debate, which is partly due to the relatively complicated nature of lipotoxicity [18,59]. Exposure time, for example, is a critical factor that determines whether or not a particular fatty acid will be detrimental (long exposure) for β-cell performance or in fact beneficial (short exposure). It is worth stressing in this respect that the exposure necessary for toxic effects is poorly defined and varies dramatically between experimental systems ranging from a few hours in cultured cell models to many years in human subjects [18]. Moreover, not all fatty acids are equal as it has been reported that the toxic effect of NEFAs on β-cells depends on carbon chain length and double bond configuration [100]. Long-chain saturated NEFAs such as palmitate are generally harmful to β-cells, whereas mono-unsaturated molecules such as palmitoleate are relatively well tolerated and may even protect against the

adverse effects of their saturated equivalents [100]. Importantly, even chronic exposure to high levels of saturated NEFAs is not necessarily harmful to β-cells, as toxicity often depends on a high glucose level – given this glucose permissibility, lipotoxicity is more correctly referred to as 'glucolipotoxicity' [16].

Glucolipotoxicity is an umbrella term that covers the combined deleterious effects of supraphysiological glucose and NEFA levels on both the viability and function of pancreatic β-cells [18]. Cellular defects that may be responsible for NEFA-induced β-cell death [164] or loss of insulin secretory function [165], are in abundance: glucolipotoxicity has for example been associated with regulatory gene transcription changes [166], epigenetic alterations [64], inflammation [167], defected cell signaling [154], oxidative stress [73], endoplasmic reticulum stress [168], and with mitochondrial dysfunction [29]. However, the relative importance of these multifarious NEFA effects and, indeed, their causal relations are unclear at present. Some important mechanistic questions are yet to be answered too. For example, anabolic derivatives, which likely emerge from the glycerolipid/free fatty acid cycle [28], are widely held responsible for the detrimental effects of fatty acids, but the nature of such derivatives remains elusive [18]. The mechanism by which mono-unsaturated NEFAs offer cytoprotection against the harmful effects of their saturated equivalents remains equally obscure [169] and, although such

protection prevents cellular death [100], it is unclear if it equally applies to the many other glucolipotoxic effects.

Following the observation that mitochondrial UCP2 dampens GSIS in mouse islets [81], mitochondrial dysfunction has been linked causally to β-cell glucolipotoxicity and to the development of Type 2 diabetes [29]. However, the GSIS improvement observed in mice after global UCP2 knockout on a mixed genetic background [81] is fully lost when the protein is knocked out on congenic backgrounds [82]. Instead, genetically pure mice exhibit impaired GSIS, which has been attributed to the persistent oxidative stress such animals face [82]. Given these results, the UCP2 up-regulation observed under glucolipotoxic conditions was interpreted as a stress response preventing fuel-induced oxidative damage [73], probably by allowing proton leak across the mitochondrial inner membrane [50,91]. Recent studies with pancreatic islets isolated from β-cell-specific UCP2 knockout mice [84] and INS-1E insulinoma cells [50] show that UCP2 attenuates GSIS and lowers reactive oxygen species (ROS) levels. These findings are consistent with a dual role for UCP2 in GSIS regulation and oxidative stress protection. Whilst the UCP2 role in glucolipotoxicity is yet to be established firmly [18], it is likely that other defects in mitochondrial function contribute to the harmful NEFA effects on β-cell function and viability [170]. When mitochondrial dysfunction is explored in cells [141], it is important to define explicitly which aspects of mitochondrial

physiology are important for the specific function of a given cell. In pancreatic β-cells, glucose-sensitivity of respiration and the coupling between respiration and ATP synthesis are two features of mitochondrial function that are essential for triggering GSIS (Figure 3.1A, [171]). Furthermore, ROS that are involved in non-canonical GSIS [47] are at least partly mitochondria-derived [50].

In this chapter, extracellular flux technology was exploited to probe mitochondrial function in INS-1E insulinoma cells [156] that were exposed to glucolipotoxic conditions that cause loss of cell viability and GSIS impairment. By comparing the effects of palmitate and its mono-unsaturated counterpart palmitoleate on basal mitochondrial respiration and both glucose-sensitivity and coupling efficiency of oxidative phosphorylation, it is revealed that (i) mitochondrial dysfunction contributes significantly to palmitate-induced GSIS defects, (ii) palmitate-provoked loss of cell vitality and GSIS phenotypes are mechanistically distinct, (iii) proton leak does not contribute to palmitate-induced mitochondrial dysfunction, and (iv) fatty acid beta oxidation restricts palmitate-induced mitochondrial dysfunction.

3.2. Experimental

3.2.1 Cell Culture

INS-1E insulinoma cells were maintained as described in section 2.1 and seeded at 6 x 10^4 cells/well into XF24 (Seahorse bioscience) or 96-well (Costar, Corning) microplates. At 70-80% confluence, cells were exposed to NEFAs for 24 h in

serum-free RPMI containing 4 or 11 mM glucose. NEFA exposure at low glucose was executed ± 50 μM etomoxir. NEFAs were conjugated to bovine serum albumin (BSA), so control cells were exposed to BSA alone.

3.2.2 Preparation of fatty acid conjugations with bovine serum albumin

Essentially fatty acid-free BSA (Sigma A7030) dissolved at 1.6 mM in medium containing 135 mM NaCl, 3.6 mM KCl, 10 mM Hepes (pH 7.4), and 0.5 mM $MgCl_2$ was conjugated to different fatty acids (palmitate, palmitoleate or palmitate and palmitoleate) as described in section 2.3. When added to cultures, BSA:NEFA mixtures were diluted 40x. The applied BSA and NEFA concentrations were chosen because of published binding parameters [151] that predict the respective molar ratios should result in similar total unbound NEFA levels.

3.2.3 Insulin secretion

Cells were seeded and exposed to NEFAs for 24 h in serum-free RPMI-1640 containing 4 or 11 mM glucose on 96-well culture plates. After NEFA exposure, cells were tested for GSIS as described in section 2.7. Insulin samples were assayed for insulin by ELISA (Mercodia, Uppsala, Sweden) using mouse insulin as standard.

3.2.4 Mitochondrial bioenergetics

Mitochondrial function was probed in intact attached INS-1E cells as described in section 2.4.1. Briefly, cells seeded and NEFA-exposed on XF24 culture plates (Seahorse Bioscience) were washed into glucose-free KRH lacking BSA and incubated in this medium for 30 min at 37 ºC under air. XF24 microplates were transferred to a Seahorse XF24 extracellular flux analyser (controlled at 37 ºC) for a 10-min calibration and 4 measurement cycles to record basal cellular respiration (Figs 3.1B and 3.1C). Glucose (4, 11 or 28 mM) was then added to stimulate respiration and, subsequently, 5 μg/mL oligomycin and a mixture of 1 μM rotenone plus 2 μM antimycin A were added to, respectively, inhibit the ATP synthase and to determine non-mitochondrial respiration.

3.2.5 Mitochondrial reactive oxygen species

ROS levels were estimated from MitoSOX oxidation rates as described in section 2.9. Cells seeded and NEFA-exposed on 96-well plates were washed into glucose-free KRH lacking BSA, incubated in this medium for 30 min at 37 ºC under air, and then transferred to a multimode plate reader (PHERAstar FS BMG LABTECH). Following injection of 5 μM MitoSOX (Invitrogen M36008), fluorescence was monitored at 28-sec intervals for 30 min. The fluorescent MitoSOX oxidation products were excited at 510 nm and light emission was detected at 580 nm. The plate reader's focal height was set at 3.5 mm and its gain was fixed between different experiments.

3.2.6 Cell vitality

Cell densities were determined to quantify NEFA effects on cell vitality and to normalise absolute respiratory and MitoSOX oxidation data. For both purposes, the metabolic activity of INS-1E cells was probed on Seahorse XF24 plates by adding 50 nM C_{12}-resazurin in 100 µL RPMI to each well as described in section 2.5. Metabolically active cells reduce C_{12}-resazurin to the fluorescent C_{12}-resorufin ($\lambda_{ex/em}$ = 540/590 nm), which was detected using a PHERAstar FS plate reader (BMG LABTECH) in fluorescence intensity, bottom- reading and well-scanning mode. For the normalisation of respiratory data (Figures 3.2A and 3.4), KRH was replaced with RPMI containing C_{12}-resazurin immediately after measuring basal oxygen uptake, i.e., in the absence of any respiratory effectors. The respiratory activity in a particular well was normalised using the cell density measured in that same well [157]. MitoSOX oxidation data (Figure 3.5) were normalised using averaged cell vitalities (Figure 3.8).

3.2.7 Statistical analysis

Significance of mean differences was tested by ANOVA – applying Tukey's multiple comparison post-hoc analysis – using GraphPad Prism Version 6.0 for Mac OS X (GraphPad software, San Diego, CA, USA).

3.3 Results

3.3.1 Mitochondrial respiration

When blood glucose rises, β-cells increase their oxidative catabolism of glucose, which leads to increased mitochondrial respiratory activity that is coupled to ATP synthesis (Figure 3.1A). As discussed in section 1.2.2, in canonical GSIS, the glucose-induced increase in the ATP/ADP ratio is the key signal that triggers insulin release [2]. The typical respiratory trace shown in Figure 3.1B illustrates that INS-1E cells indeed increase their oxygen uptake rate when subjected to 28 mM glucose. This cellular respiratory response to glucose tends to be dampened in cells that were exposed for 24 h to palmitate in the presence of 11 mM glucose (Figure 3.1C). As expected, the oxygen consumption rate of control and palmitate-exposed cells is inhibited by both oligomycin and a mixture of rotenone and antimycin A (Figures 3.1B and 3.1C). The data shown in Figures 3.1B and 3.1C are normalised to basal respiration measured in the absence of glucose. When corrected for non-mitochondrial oxygen uptake, which ranges from 0.5 to 0.6 fmol O_2/min/cell (Figure 3.2A), the magnitude of this basal respiration is 2 fmol O_2/min/cell (Figure 3.2A). Exposure to palmitate or palmitoleate, alone or combined, does not significantly affect either the basal mitochondrial or non-mitochondrial respiratory rates (Figure 3.2A). However, when cells were cultured with 11 mM glucose, palmitate exposure lowers the glucose sensitivity of mitochondrial respiration (Figure 3.2B). Basal

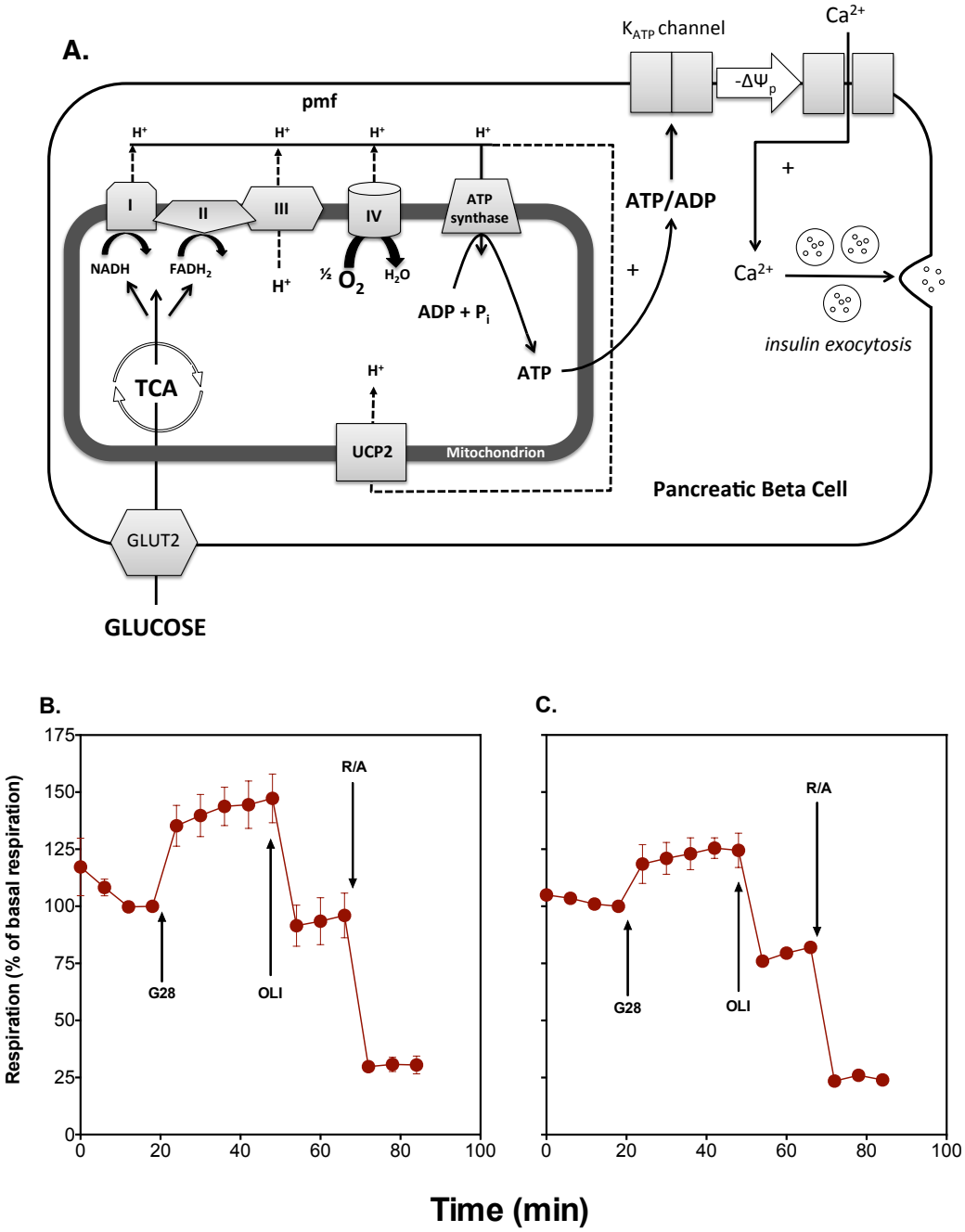

Figure 3.1 – Real-time detection of palmitate-induced mitochondrial dysfunction in intact INS-1E cells

(**A**) Mitochondrial function is essential for canonical GSIS: glucose is taken up by pancreatic beta cells via an insulin-insensitive transporter (GLUT2) and broken down oxidatively, which leads to increased activity of the mitochondrial tricarboxylic acid (TCA) cycle and the mitochondrial respiratory chain (complexes I-IV), and an increased mitochondrial protonmotive force (pmf). The pmf drives ATP synthesis but may also be dissipated by mitochondrial uncoupling protein-2 (UCP2) activity. The glucose-induced rise in ATP/ADP triggers closure of ATP-sensitive potassium (K^{ATP}) channels, depolarization of the plasma membrane (Δψp), Ca^{2+} influx and exocytosis of insulin-containing granules. (**B** and **C**) – Typical traces (normalised as % of basal respiration) reflecting respiration of cells exposed for 24 hr at 11 mM glucose to BSA (**B**) or BSA-conjugated to palmitate (**C**). Cellular oxygen uptake was measured as described in section 2.4 – 28 mM glucose (G28), 5 µg/mL oligomycin (OLI), and a mixture of 1 µM rotenone and 2 µM antimycin A (RA) were added as indicated. Data are means ± SEM of 5 separate wells from a single XF24 plate and are expressed as a percentage of basal respiration.

mitochondrial oxygen consumption of control cells increases up to 2-fold when 4, 11 or 28 mM glucose is administered, whereas oxygen consumption of palmitate-exposed cells increases maximally 1.4-fold (Figure 3.2B). Similar exposure to palmitoleate does not affect glucose-sensitivity of INS-1E mitochondrial respiration, and palmitoleate does not provide significant prevention against the desensitising effect of palmitate (Figure 3.2B). When cells were cultured with 4 mM glucose, palmitate and palmitoleate, alone or combined, do not significantly affect the mitochondrial respiratory response to glucose (Figure 3.2C). Probably due to differential glucose limitation, BSA control cells cultured with 4 mM glucose (Figure 3.2C) tend to increase their oxygen consumption rate to a greater extent when stimulated with increasing glucose concentrations compared with cells cultured in 11 mM glucose (Figure 3.2B).

3.3.2 Coupling efficiency

Coupling efficiency of oxidative phosphorylation is defined as the proportion of mitochondrial respiration linked to ATP synthesis [141]. Coupling efficiency can be approximated from the oligomycin-sensitivity of mitochondrial oxygen consumption (Figure 2.4) and may thus be derived from data as shown in Figure 3.1. Because the inner membranes of INS-1E mitochondria allow an unusually high proton leak [172], INS-1E cells exhibit exceptionally low coupling efficiency [50,91] as is reflected by Figure 3.3A, which shows that

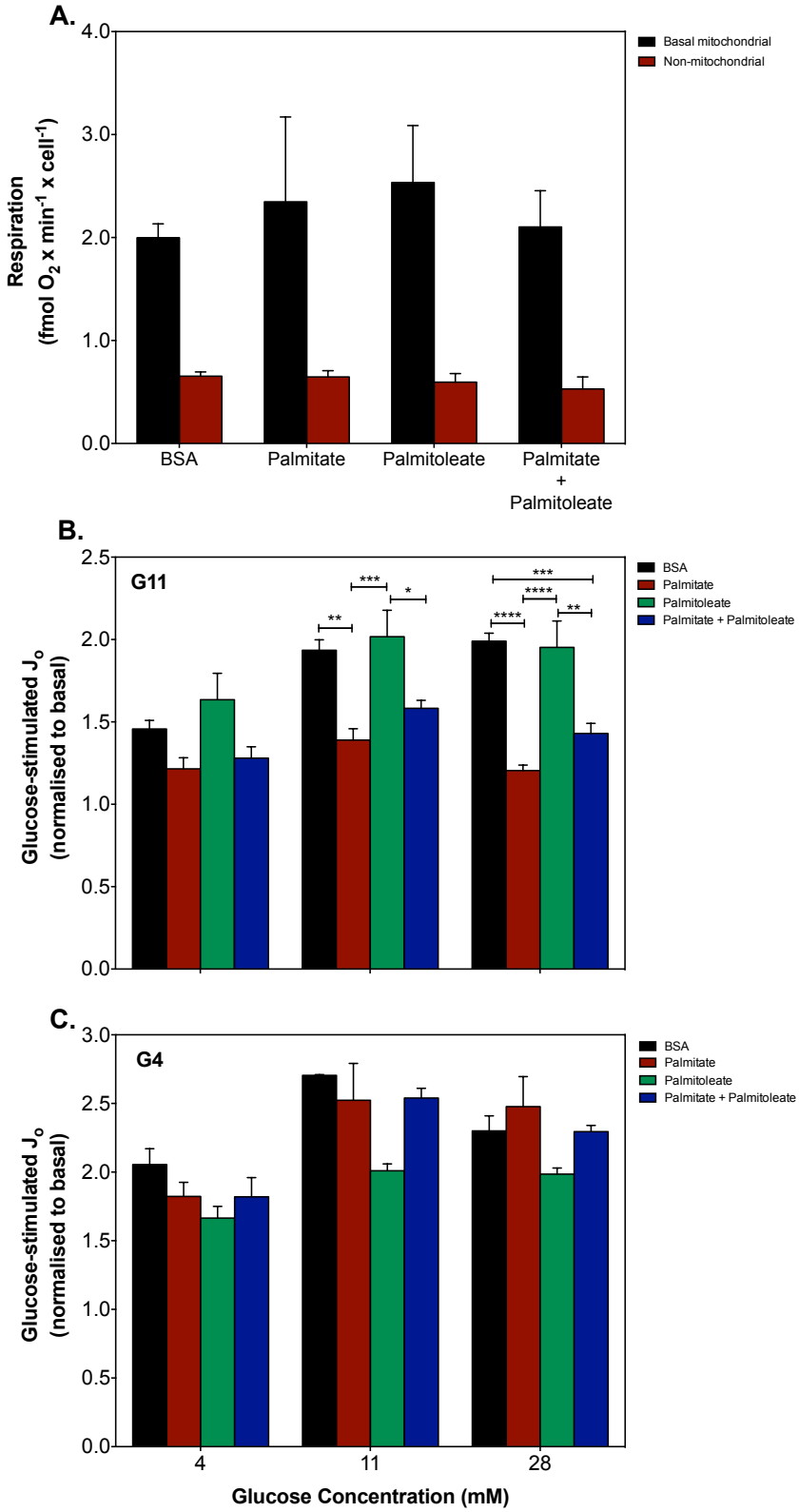

Figure 3.2 – Palmitate exposure at high glucose dampens the glucose-sensitivity of mitochondrial respiration

(**A**) Absolute basal mitochondrial (black bars) and non-mitochondrial (red bars) oxygen uptake in cells exposed to BSA-conjugated NEFAs or BSA alone at 11 mM glucose. (**B** and **C**) Glucose-sensitivity of mitochondrial respiration in cells exposed for 24 h to BSA- conjugated NEFAs or BSA alone at 11 mM glucose (**G11**) or 4 mM glucose (**G4**). Data are means ± SEM for three to five independent experiments that each involved three or four replicates per treatment. Statistical significance of mean differences was tested for by two-way ANOVA. (**A**) Not significant. (**B**) **P* < 0.05, ***P* < 0.01, ****P* < 0.001 and *****P* < 0.0001. (**C**) Not significant.

control cells use just 50-55% of their glucose-stimulated mitochondrial respiratory activity to make ATP. Interestingly, palmitate exposure at high glucose lowers the coupling efficiency further, such that only 40% of the respiratory activity drives ATP synthesis at any applied glucose level (Figure 3.3A). Palmitoleate exposure causes a small, statistically insignificant, rise in coupling efficiency (Figure 3.3A). Mirroring the NEFA effects on the glucose-sensitivity of mitochondrial respiration (Figure 3.2), palmitoleate does not prevent the negative effect of palmitate on coupling efficiency (Figure 3.3A), and palmitate nor palmitoleate lower coupling efficiency when incubated at low glucose (Figure 3.3B).

Coupling efficiency reflects all major processes underlying oxidative phosphorylation including substrate oxidation, ADP phosphorylation and proton leak across the mitochondrial inner membrane [156]. The detrimental palmitate effect in cells stimulated with either 11 or 28 mM glucose on coupling efficiency (Figure 3.3A) could, therefore, in principle be due to inhibitory effects on substrate oxidation and/or ADP phosphorylation, and/or to a stimulatory effect on proton leak. To distinguish between these possibilities, we calculated the absolute total glucose-stimulated respiratory activity (substrate oxidation) as well as absolute oligomycin-sensitive (ADP phosphorylation) and oligomycin-resistant (proton leak) activities. Figure 3.4 shows that palmitate exposure causes statistically significant drops in both the total and the

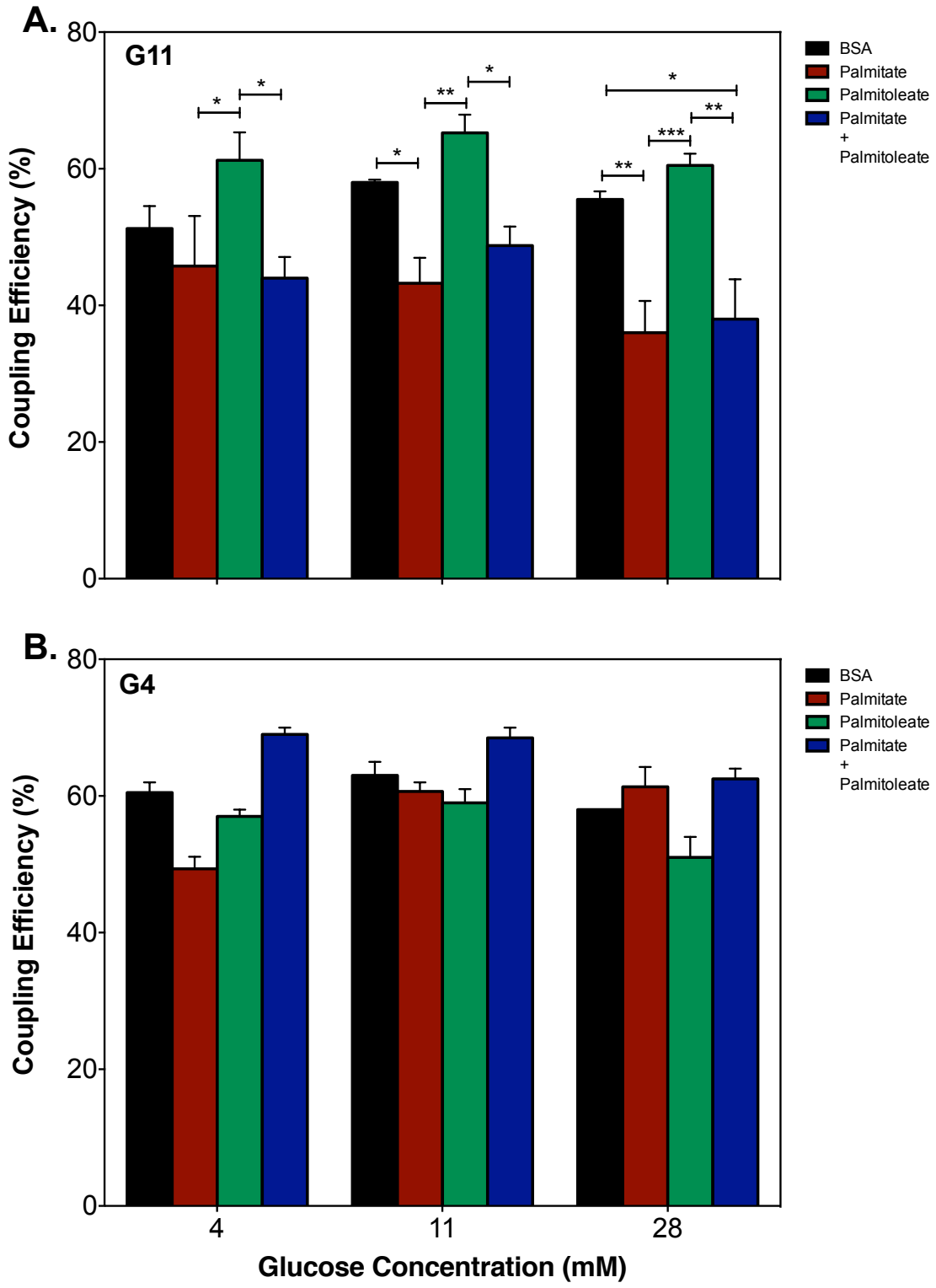

Figure 3.3 – Palmitate exposure at high glucose attenuates mitochondrial coupling efficiency

Coupling efficiency of oxidative phosphorylation – assayed at 4, 11 and 28 mM glucose, was calculated as the percentage of glucose-stimulated mitochondrial respiration that is sensitive to oligomycin in cells that had been exposed for 24 h to BSA-conjugated NEFAs or BSA alone at 11 mM glucose (**A - G11**) or 4 mM glucose (**B - G4**). Values are means ± SEM from three to five independent experiments that each involved three to four replicates per treatment. Statistical significance of mean differences was tested for by two-way ANOVA. (**A**) **P* < 0.05, ***P* < 0.01 and ****P* < 0.001. (**C**) Not significant.

oligomycin-sensitive glucose-stimulated mitochondrial respiratory activities, indicating that ADP phosphorylation-coupled substrate oxidation has been compromised. Palmitoleate exposure on the other hand lowers neither substrate oxidation nor ADP phosphorylation, but instead causes a small, statistically insignificant, stimulation of these processes compared with BSA control cells (Figure 3.4). Importantly, proton leak is not affected by exposure to palmitate and/or palmitoleate (Figure 3.4).

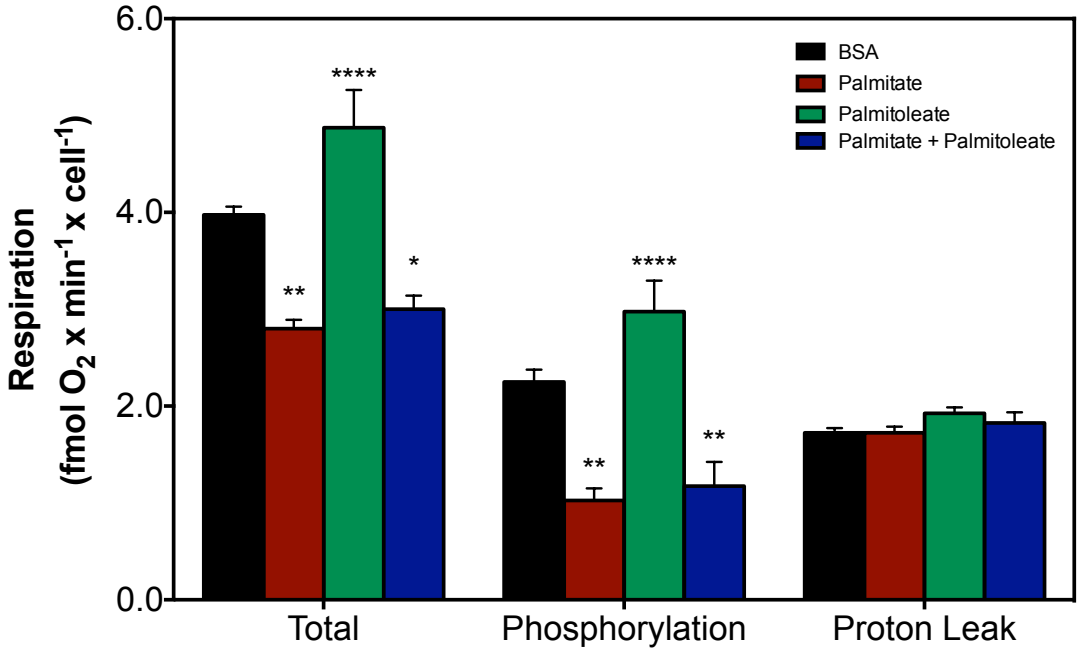

Figure 3.4 – Palmitate exposure at high glucose decreases ADP phosphorylation-coupled glucose-stimulated mitochondrial respiration, but does not affect proton leak

Absolute mitochondrial respiratory activity of INS-1E cells stimulated with 28 mM glucose (**Total**), absolute oligomycin-sensitive (**Phosphorylation**) and oligomycin-resistant (**Proton Leak**) activities were calculated from cell number-normalised basal mitochondrial respiration (Figure 3.2A), the sensitivity of basal mitochondrial respiration to 28 mM glucose (Figure 3.2B), and the coupling efficiency of oxidative phosphorylation at 28 mM glucose (Figure 3.3A). Values are means ± SEM from four separate experiments that each involved three to four replicates per treatment. Statistical significance of differences between groups was tested for by two-way ANOVA. * $P < 0.05$, differs from BSA conditions; ** $P < 0.01$, differs from BSA conditions; **** $P < 0.0001$, differs from 'palmitate' and 'palmitate + palmitoleate' conditions.

3.3.3 Mitochondrial reactive oxygen species

In addition to their textbook role in GSIS (Figure 3.1A), mitochondria play an important part in less well understood, non-canonical GSIS mechanisms (see section, 1.2.2.2). For example, ROS have been implicated as insulin secretion signals [47], and at least some of these ROS are mitochondria-derived [50]. To assess the effect of NEFAs on mitochondrial ROS, MitoSOX oxidation was probed in cells exposed to palmitate and palmitoleate, alone or in combination, at 11 or 4 mM glucose (Figure 3.5). MitoSOX is a mitochondria-targeted hydroethidine analogue that is oxidised mainly by superoxide, and to a lesser extent by hydrogen peroxide [160]. The MitoSOX oxidation rate, calculated from fluorescence progress curves (Figures 3.5A and 3.5B), is thus proportional to mitochondrial ROS levels. The data shown in Figure 3.5C reveal that palmitate exposure at 11 mM glucose causes a significant rise in ROS, whereas the equivalent palmitoleate exposure is without effect. Interestingly, palmitoleate dampens the palmitate-induced ROS increase (Figure 3.5C). Palmitate nor palmitoleate stimulate ROS when cells are exposed at 4 instead of 11 mM glucose. The mechanism by which palmitate increases mitochondrial ROS at high glucose is unclear at present (see Chapter 4). Therefore it is possible that the palmitate-induced ROS measured here arise due to the activation of pancreatic β-cell NADPH oxidase, as suggested previously [49]. Irrespective of their origin, palmitoleate lowers palmitate-induced ROS

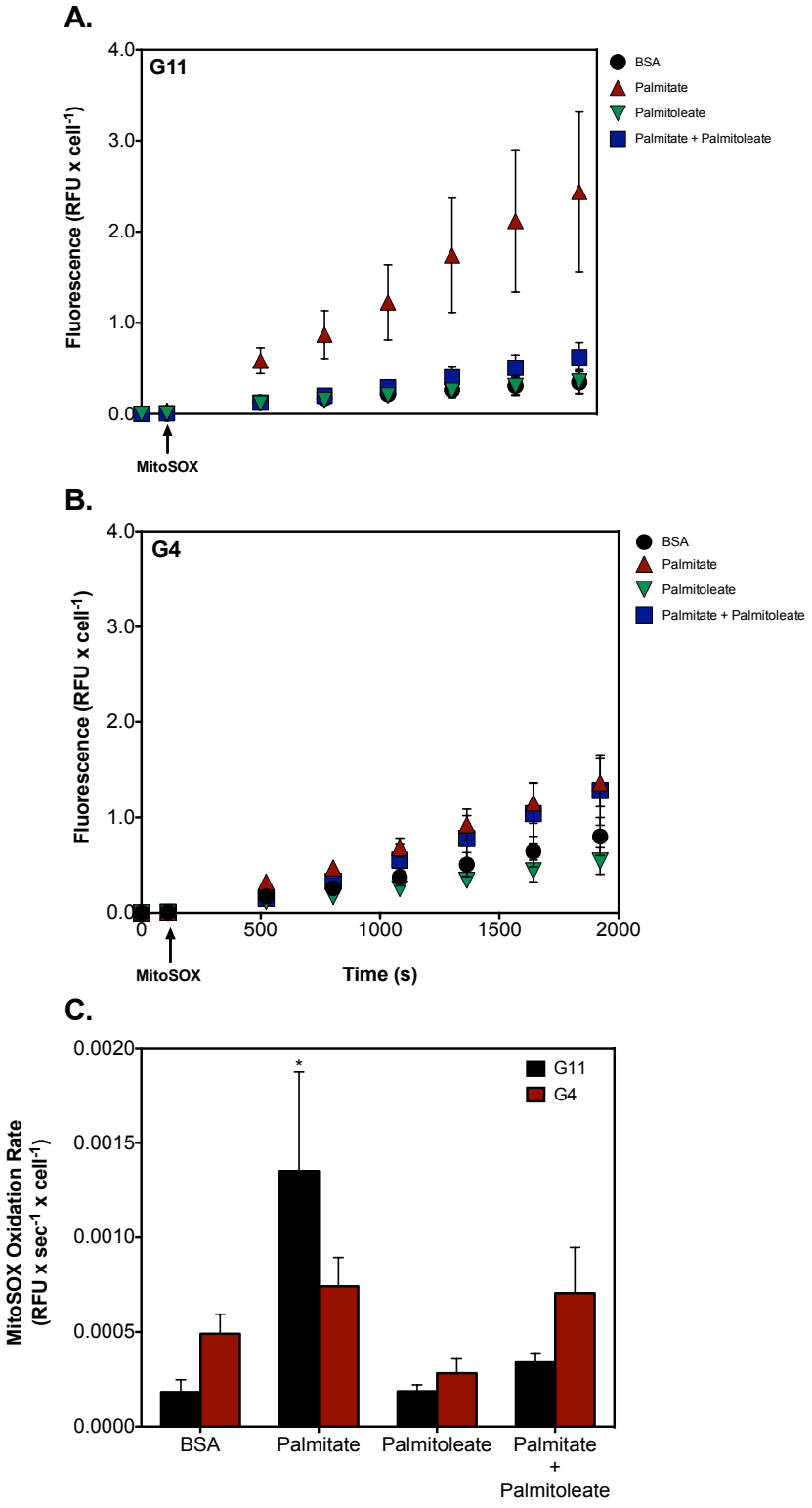

Figure 3.5 – Palmitate exposure at high glucose increases ROS

Mitochondrial superoxide was estimated from MitoSOX oxidation in INS-1E cells exposed for 24 hr to BSA-conjugated NEFAs or BSA alone at 11 mM (**A - G11**) or 4 mM (**B - G4**) glucose. (**A** and **B**) MitoSOX (5 *μM*) was injected during the assay as indicated by the arrow and fluorescence was recorded at 28-sec intervals; for clarity, only a selection of measurements is shown. Relative fluorescence units (RFU) were corrected for low background fluorescence observed in cell-free controls and were normalised to cell number using averaged cell vitality data shown in Figure 3.6. (**C**) MitoSOX oxidation rates were calculated from the slopes of the progress curves shown in (**A** and **B**). Except for the first 4 measurements, all data recorded following MitoSOX addition were included in these calculations. Data are means ± SEM of 3-6 independent experiments that involved 7-8 replicates per treatment. Statistical significance of differences between groups was tested for by two-way ANOVA: * $P < 0.05$, differs from the equivalent G11 conditions..

significantly (Figure 3.5C). This apparent palmitoleate prevention against oxidative stress disconnects the effect of palmitate on ROS (Figure 3.5) from its effects on oxidative phosphorylation (Figures 3.2-3.4).

3.3.4 Glucose-stimulated insulin secretion and cell viability

To assess if the palmitate-induced defects in oxidative phosphorylation (Figures 3.2-3.4) and rise in ROS (Figure 3.5) relate to any other lipotoxic effects, insulin secretion (Figure 3.6) and cell vitality (Figure 3.8) were measured. INS-1E insulin secretion is stimulated considerably by glucose, which is why this insulinoma cell line is widely used as a β-cell model [147]. In these experiments, basal INS-1E insulin secretion is more than doubled by high glucose and increased 1.6-fold by KCl (Figure 3.6A). Although these responses are somewhat lower than those reported elsewhere [147], they nonetheless allow NEFA effects to be assessed. Palmitate exposure at 11 mM glucose blunts both glucose-stimulated (Figure 3.6B) and KCl-stimulated (Figure 3.6C) insulin secretion completely, although the effect on KSIS appears not statistically significant. Palmitoleate exposure at high glucose, on the other hand, has no significant effect on GSIS (Figure 3.6B) or KSIS (Figure 3.6C). Importantly, the deleterious effects of palmitate on GSIS (Figure 3.6B) and KSIS (Figure 3.6C) are not prevented significantly by palmitoleate. This lack of protection mirrors the relative inconsequentiality of palmitoleate with respect to palmitate-induced defects in oxidative phosphorylation (Figures 3.3-3.4). Similar to the

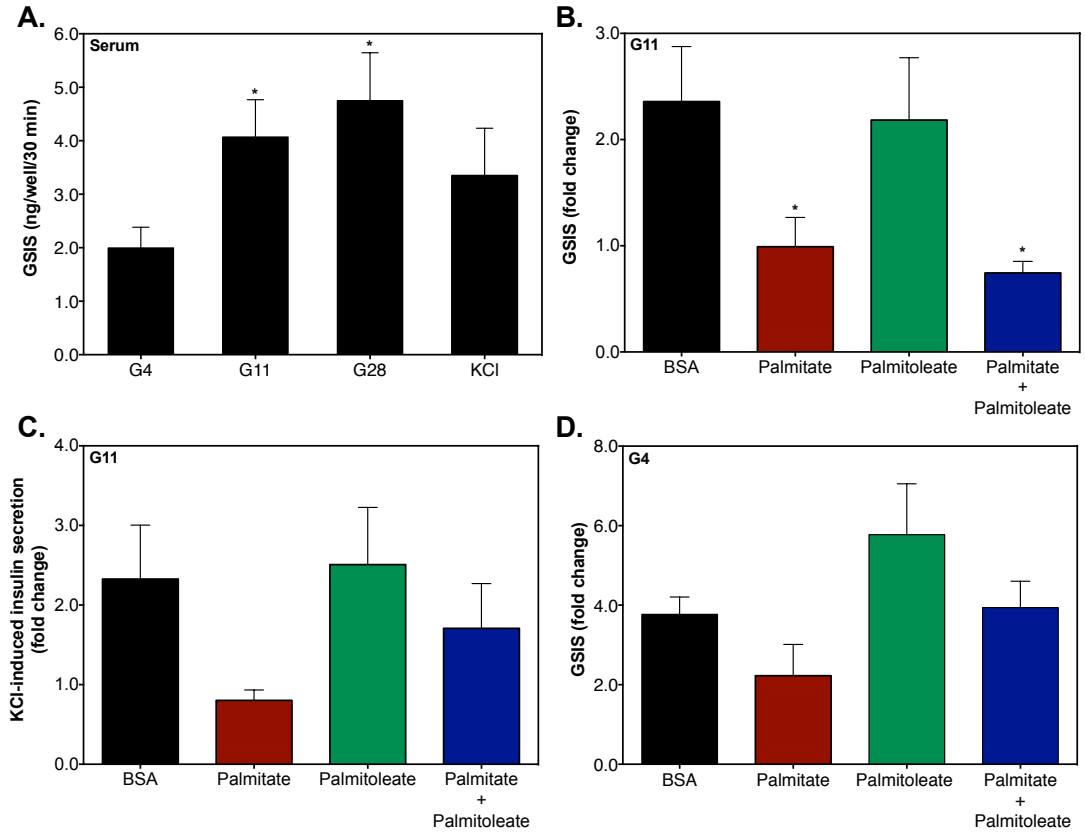

Figure 3.6 – Palmitate exposure at high glucose impairs glucose-stimulated and KCl- induced insulin secretion

Insulin secretion (ng/well/30 min) was measured in INS-1E cells grown in RPMI growth medium containing serum (**A - Serum**) and in cells exposed for 24 hr to BSA-conjugated NEFAs or BSA alone at 11 mM glucose (**B** and **C - G11**) or 4 mM glucose (**D - G4**). Following glucose starvation, cells were subjected to 4-28 mM glucose (**A**, G4, G11, G28) or to 4 mM glucose plus 50 mM KCl (**A**, KCl). GSIS was expressed as the G28/G0 insulin secretion ratio (**B** and **D**) and KCl-induced insulin secretion was normalised to insulin secretion at 4 mM glucose (**C**). Data are means ± SEM of four to six independent experiments that involved three to five replicates per treatment. Statistical significance of mean differences was tested for by one-way ANOVA: * $P < 0.05$ differs from G4 condition (**A**) or BSA condition (**B**).

bioenergetic phenotypes, the lipotoxic GSIS effects also depend on the presence of a relatively high glucose level, since palmitate exposure at low glucose does not significantly impair GSIS (Figure 3.6D). Reminiscent of the mitochondrial respiratory response to glucose (Figures 3.1B and 3.1C), GSIS in BSA control cells is a little, but not significantly, higher at 4 mM than at 11 mM glucose (Figures 3.6D and 3.6B). Furthermore, the NEFA defects on mitochondrial respiration (Figure 3.2 and 3.3) connect positively with the GSIS defects (Figure 3.7).

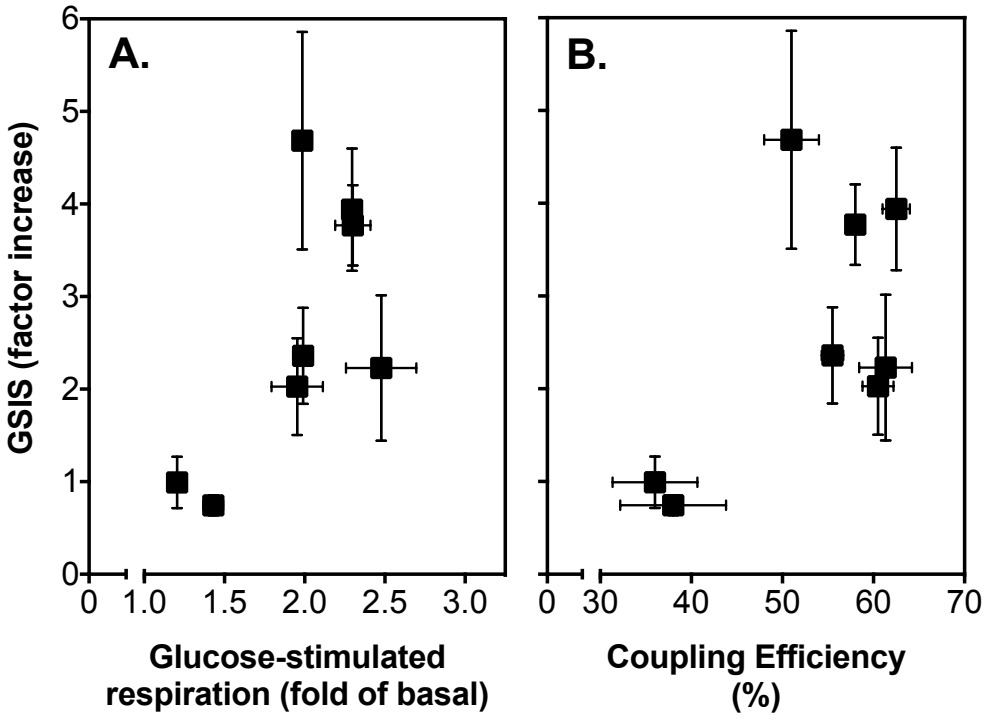

Figure 3.7 – Relationship between mitochondrial bioenergetics and GSIS

G28/G0 GSIS ratio plotted correlatively with glucose-stimulated mitochondrial respiration at 28 mM glucose (**A**) or coupling efficiency in the presence of 28 mM glucose (**B**) in cells exposed to BSA-conjugated NEFAs or BSA alone at 4 and 11 mM glucose. Data shown are replotted from figures 3.2B and 3.2C and figures 3.3A and 3.3B for glucose-stimulated mitochondrial respiration and coupling efficiency, respectively. Data are means ± S.E.M for three to six independent experiments that involved three to five replicates per treatment.

In line with the ROS, GSIS and mitochondrial respiratory effects, palmitate exposure at high glucose lowers cell vitality (cell survival < 40%), whereas palmitoleate is relatively harmless (Figure 3.8). Palmitate and/or palmitoleate do not cause statistically significant changes in cell vitality when administered at low glucose (Figure 3.8), which mirrors the glucose dependence of the ROS, GSIS and bioenergetic effects. Unlike the GSIS and bioenergetic phenotypes, palmitoleate prevents some of the palmitate-induced loss in cell vitality at high glucose exposure (Figure 3.8). Such protection is indeed consistent with the prevention of palmitate-induced ROS by palmitoleate (Figure 3.5C).

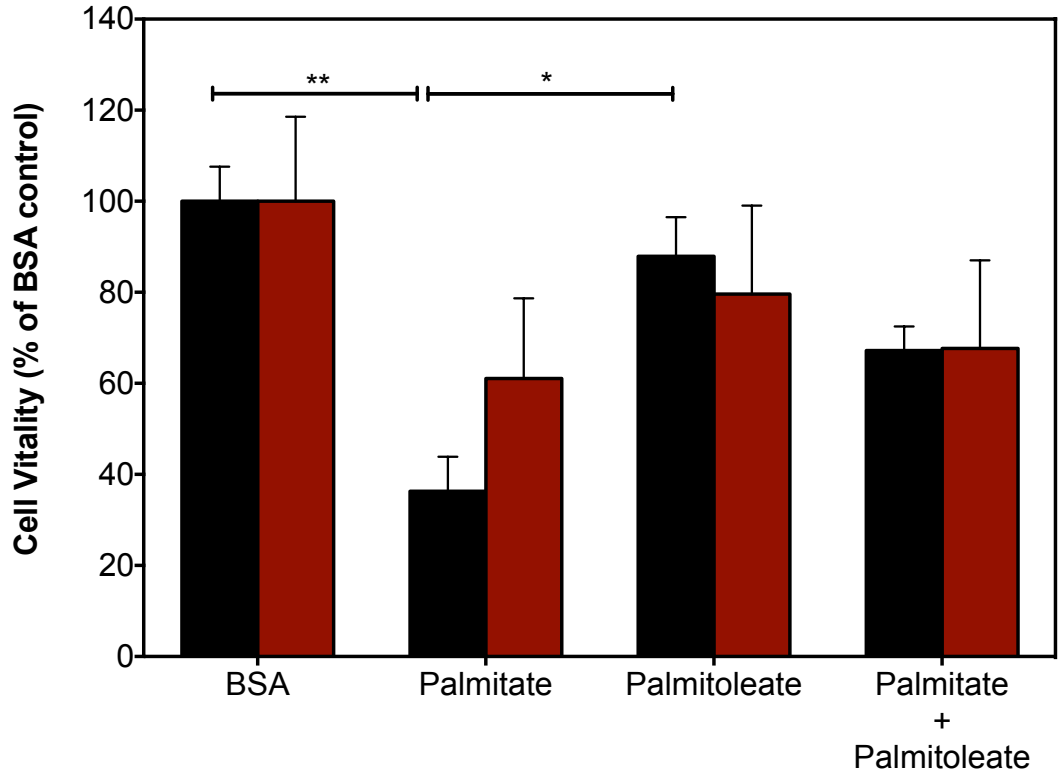

Figure 3.8 – Palmitate exposure causes loss of cell vitality at high glucose

Cell vitality was determined by measuring the total metabolic activity within individual microplate wells that contained cells exposed for 24 hr to BSA-conjugated NEFAs or BSA alone at 11 mM glucose (**black bars**) or 4 mM glucose (**red bars**). To quantify cell vitality, total metabolic activity in each well was expressed as a percentage of the activity exhibited by wells that contained cells grown in fully supplemented RPMI – it was confirmed by light microscopy that these RPMI wells showed no visible signs of cell dysfunction. Cell vitality percentages were then normalised to the BSA controls. BSA alone causes about 5% and 20% loss in cell vitality when administered in serum-free RPMI at 11 and 4 mM glucose, respectively. Data are means ± SEM of four to five independent experiments that each involved three to four replicates per treatment. Statistical significance of mean differences was tested by two-way ANOVA: $*P < 0.05$ and $**P < 0.01$.

3.3.5 Mitochondrial palmitate toxicity at low glucose

Palmitate only causes harm to INS-1E cells when administered at 11 mM glucose (Figures 3.2-3.3, 3.5-3.6 and 3.8). This exclusivity is likely explained by the Randle 'cycle' [68]: high glucose oxidation leads to accumulation of cytoplasmic malonyl-CoA, which inhibits CPT-1 thus preventing mitochondrial β oxidation of fatty acids and promoting NEFA engagement in esterification-hydrolysis cycles [28] – this order of events is generally held responsible for the glucose permissibility of lipotoxicity [16]. To test if palmitate-induced effects on

mitochondrial respiration would be enhanced when its breakdown were prevented, INS-1E cells were exposed to palmitate at 4 mM glucose in the presence of etomoxir, a specific CPT1 inhibitor [173] that inhibits acute palmitate oxidation by INS-1E cells [1]. Figure 3.9A shows that 'BSA-etomoxir' control cells increase mitochondrial respiration about 2.2-fold in response to 28 mM glucose. The equivalent response by 'palmitate-etomoxir' cells is just a 1.7-fold rise (Figure 3.9A). Cells exposed to BSA at low glucose in the absence of etomoxir respond to 28 mM glucose by increasing mitochondrial oxygen uptake roughly 2.5-fold – this response is not affected by palmitate (Figures 3.9A and 3.2C). The respiratory response to 28 mM glucose by cells exposed to BSA at 11 mM glucose, is lowered significantly by palmitate from a 2-fold to a 1.2-fold stimulation (Figures 3.9A and 3.2B). Figure 3.9A thus demonstrates that statistically significant palmitate toxicity arises at 4 mM glucose when NEFA catabolism is impeded. The emerging palmitate lipotoxicity on glucose-sensitivity of mitochondrial respiration becomes even more apparent when glucose responses are normalised to the respective BSA control responses (Figure 3.9B). Interestingly, etomoxir's presence at 4 mM glucose exposure does not lead to the palmitate-induced drop in coupling efficiency – assayed at 28 mM glucose – that is seen at 11 mM glucose exposure (Figure 3.9C, *cf*. Figure 3.3). The limited mitochondrial dysfunction caused by palmitate at lower glucose concentrations in the presence of etomoxir suggests that palmitate

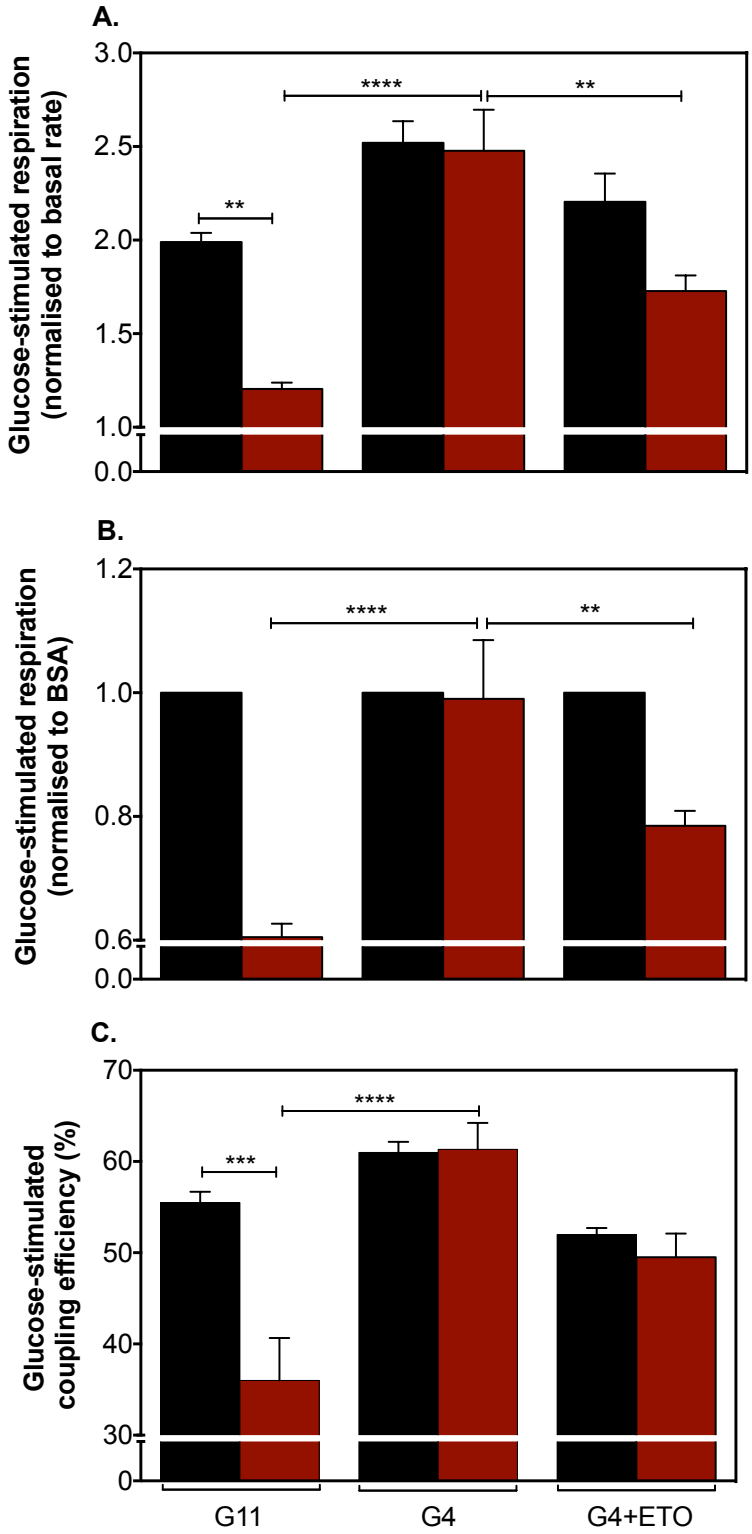

Figure 3.9 – Mitochondrial toxicity of palmitate exposure emerges at low glucose when NEFA oxidation is inhibited

The glucose-sensitivity of mitochondrial respiration (**A** and **B**) and coupling efficiency of oxidative phosphorylation (**C**) were measured in cells exposed for 24 hr to BSA-conjugated palmitate (red bars) or BSA alone (black bars) at 11 mM glucose (G11), at 4 mM glucose (G4), or at 4 mM glucose with 50 µM etomoxir (G4+ETO). Mitochondrial respiration stimulated by 28 mM glucose was either normalised to basal respiration (**A**) or to the respective glucose-stimulated BSA conditions (**B**). Data are means ± SEM of three to five independent experiments that each involved three to four replicates per treatment. Statistical significance of mean differences was tested for by two-way ANOVA: ** $P < 0.01$, ***$P < 0.001$ and ****$P < 0.0001$.

inhibits glucose oxidation at multiple targets that have different affinities for palmitate or its toxic derivative(s).

3.4 Discussion

3.4.1 Mitochondrial dysfunction contributes to palmitate-induced glucose-stimulated insulin secretion defects

The functional bioenergetic analysis shown in this chapter reveals that palmitate impairs aspects of mitochondrial function that underpin the insulin secretion ability of INS-1E cells: both glucose-sensitivity of mitochondrial respiration and coupling efficiency of oxidative phosphorylation are lowered (Figures 3.2B and 3.3A). These results thus demonstrate that mitochondrial dysfunction contributes to the NEFA-induced GSIS defects reported here (Figures 3.6B and 3.7) and by others [165]. Agreeing with current concensus [18], the deleterious palmitate effects on mitochondrial function and GSIS depend on glucose (Figures 3.2C, 3.3B, 3.6D) and, therefore, appear glucolipotoxic effects [16]. Functional insight in mitochondrial NEFA effects is scarce, but a recent study [64] associates palmitate-induced GSIS defects in INS-1 cells with (epi)genetic and metabolic changes, including diminished mitochondrial respiration. Consistent with the findings in Figure 3.4, palmitate lowers glucose-stimulated oxygen uptake coupled to phosphorylation, but does not affect proton leak [64]. Discrepant with the findings in Figures 3.2B and 3.3A, most likely because of experimental differences, palmitate does not seem

to affect normalised glucose-sensitivity of mitochondrial respiration or coupling efficiency [64]. Palmitate exposure leads to a significantly increased ROS level (Figure 3.5). Palmitate-induced ROS possibly arise from cytoplasmic NADPH oxidase activity [146], although a mitochondrial origin for some or all of the ROS measured in this study cannot be excluded (see Chapter 4). Irrespective of where they arise, however, palmitate-induced ROS do almost certainly not contribute to impaired GSIS, because palmitoleate prevents the emergence of ROS (Figure 3.5C), whereas this unsaturated NEFA does not protect against palmitate-induced GSIS defects (Figure 3.6B). Although these data demonstrate involvement of mitochondrial dysfunction in palmitate-induced GSIS impairment, palmitate also likely acts on non-mitochondrial processes relevant to GSIS, e.g. K_{ATP} channel closure [174], Ca^{2+} channel opening [175] and exocytosis [95]. Attenuation of KSIS by palmitate (Figure 3.6C) agrees with such non-mitochondrial action.

This chapter highlights the power of measuring β-cell oxidative phosphorylation in real-time, revealing that mitochondrial function correlates with GSIS (Figure 3.7). This approach is somewhat limited to cells, which is unfortunate, as pancreatic islets arguably yield more insight in glucolipotoxic pathophysiology than insulinoma cells. Respirometry has been applied to islets (see Chapter 5), but it is hard to causally link islet bioenergetics, which are accounted for by many cell types, to insulin secretion, which is mediated by β-

cells alone [1]. Reassuringly, previous INS-1E predictions – high proton leak [91] and a dual UCP2 role in GSIS regulation and oxidative stress protection [50] – have come true in islets [73,84,176].

3.4.2 Glucolipotoxic vitality and glucose-stimulated insulin secretion phenotypes are mechanistically distinct

Unlike palmitate, palmitoleate does not increase ROS (Figure 3.5) and does not compromise oxidative phosphorylation, insulin secretion or cell vitality (Figures 3.2B, 3.3A, 3.6B, 3.8A). Instead, palmitoleate protects against palmitate-induced loss of cell vitality (Figure 3.8A), which mirrors published data [96,100], and prevents a palmitate-induced rise in ROS (Figure 3.5). Importantly, palmitoleate does not ameliorate palmitate-induced defects in oxidative phosphorylation (Figures 3.2B, 3.3A) and GSIS (Figure 3.6B). Such differential palmitoleate protection suggests that glucolipotoxic effects on cell vitality and GSIS phenotypes are mechanistically distinct: whereas blunted mitochondrial glucose-sensitivity and coupling efficiency at least partly account for GSIS impairment (Figure 3.7), these defects unlikely cause cell vitality impairment. NEFA-induced cell vitality damage might result from other mitochondrial dysfunction [115], likely involving ROS (Figures 3.5 and 4.6). These results thus support the idea that the many and varied glucolipotoxic manifestations are not explained by one unifying mechanism [18] – the data also shed light on causal interrelations between the multifarious palmitate effects.

Some structural aspects critical to the cytoprotective properties of mono-unsaturated NEFAs are known, and protection may involve activation of G-protein-coupled receptors, inhibition of caspases and NEFA esterification. Despite this knowledge, the mechanism of cytoprotection remains elusive. Importantly these data exclude mitochondrial oxidative phosphorylation from any mechanistic model, and thus weaken the reported idea [169] that unsaturated NEFAs enhance the clearance of saturated species by increasing fatty acid beta oxidation. Moreover, mono-unsaturated NEFAs may indeed save β-cells from glucolipotoxic-induced cell death, but it is unlikely that they prevent functional deterioration of the surviving cells.

3.4.3 Mechanism of palmitate-induced mitochondrial dysfunction

UCP2 has been implicated in β-cell failure and development of Type 2 diabetes [29], but its glucolipotoxic role is contentious (see Chapter 4). Palmitate effects on glucose-sensitivity of respiration, coupling efficiency, and GSIS (Figures 3.2B, 3.3A, 3.6B) closely mirror UCP2 effects on INS-1E cells reported before [50]. However, these results demonstrate that palmitate exposure does not affect mitochondrial proton leak (Figure 3.4). This important observation most likely rules out UCP2 involvement in the mitochondrial dysfunction reported here, since UCP2 contributes considerably to proton leak of INS-1E cells [50,91]. Related, possible palmitate stimulation of UCP2 expression and/or activity is expected to increase overall mitochondrial respiration [50,91,177], which

appears not the case (Figures 3.2A and 4.2). It remains unclear how palmitate exposure impedes glucose-fuelled oxidative phosphorylation, but multiple targets are likely [178].

3.4.4 Fatty acid beta oxidation restricts palmitate-induced mitochondrial dysfunction

Palmitate blunts the mitochondrial respiratory response to glucose when administered at low glucose in the presence of etomoxir (Figure 3.9A and 3.9B). Such etomoxir-induced palmitate toxicity agrees with the widely accepted notion that malonyl CoA accumulation accounts for glucose permissibility of lipotoxicity [16]. The observation shown here predicts that NEFA toxicity at high glucose may be ameliorated by stimulating fatty acid β oxidation (Figure 3.10), which would lower the chance that toxic NEFA derivatives emerge from esterification-hydrolysis cycles [28]. The stimulatory effect of palmitoleate – a relatively harmless NEFA – on absolute mitochondrial respiration (Figure 3.4) supports this prediction, although the effect is statistically not significant. The relative ease, compared to their saturated counterparts, by which mono-unsaturated NEFAs are converted to stable triglyceride [60] and thus removed from esterification-hydrolysis cycles, further explains the harmless nature of palmitoleate. Promotion of palmitate oxidation [169] and triglyceride formation [60] have both been suggested to explain the protective effect of mono-unsaturated NEFAs against palmitate toxicity, but lack of palmitoleate

protection against mitochondrial respiratory defects (Figures 3.2B, 3.3A, 3.6) weakens the 'protection through oxidation' model.

It is hypothesised that harmful NEFA effects could be outweighed by beneficial effects that are triggered by NEFAs per se or by their catabolites (Figure 3.10), and that the experimental phenotype of any NEFA exposure reflects the balance of these harmful and beneficial effects. Palmitate for example, acutely benefits β-cell function by potentiating GSIS [101], however such potentiation is not seen after sustained exposure because palmitate toxicity dominates the phenotype time-dependently. This metabolic balance model explains why 24 h palmitate exposure impairs GSIS at high glucose and is inconsequential at low glucose and, at the same time, why palmitoleate is inconsequential at high glucose and in fact potentiates GSIS at low glucose even after 24 h exposure (Figure 3.6B and

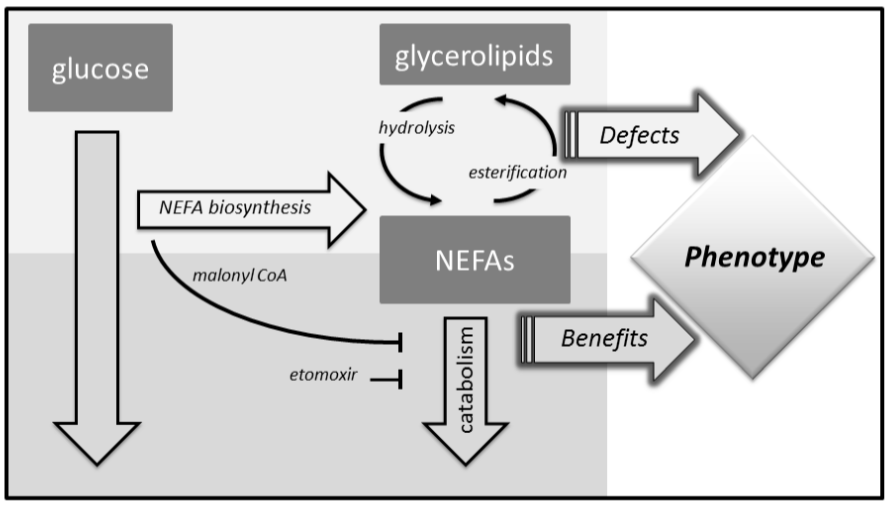

Figure 3.10 – A metabolic balance model of glucolipotoxicity

NEFA and glucose exposure phenotypes are the net result of deleterious and beneficial NEFA-induced processes. See text for further details.

3.6D). It is therefore suggested that beneficial and deleterious NEFA processes are not necessarily separated in time, but may coincide.

3.5 Conclusion

Cellular bioenergetics yield powerful insight in pancreatic β-cell function as mitochondrial activity appears to positively correlate with GSIS. Data in this chapter provide new information on some of the causal interrelations between the multifarious glucolipotoxicity phenotypes. However, the data also underscore the complicated nature of NEFA toxicity, suggesting many targets for even the damaging effect of palmitate on glucose oxidation alone. The occurrence of multiple targets hampers the development of drugs to manage NEFA-induced β-cell failure, but these findings suggest an alternative: as glucolipotoxicity may be ameliorated by promoting mitochondrial fatty acid β oxidation, thereby stimulating such oxidation, may prove an attractive therapeutic possibility. Notably these data were obtained using a pancreatic β-cell model and it is likely that glucolipotoxic effects differ between model cell lines and primary pancreatic β-cells (Chapter 5). It is also important to note that INS-1E insulinoma cells are derived from rats and since a human pancreatic β-cell line is not readily available, consideration should be taken into account when comparing these data with that from human islet studies.

Chapter 4

UNCOUPLING PROTEIN-2 ATTENUATES PALMITOLEATE PROTECTION AGAINST THE CYTOTOXIC PRODUCTION OF MITOCHONDRIAL REACTIVE OXYGEN SPECIES IN INS-1E INSULINOMA CELLS

4.0 Abstract

High glucose and fatty acid levels impair pancreatic β-cell function. In chapter 3 it was shown that palmitate-induced loss of INS-1E insulinoma cells is related to increased ROS production, as both toxic effects are ameliorated by palmitoleate (see Chapter 3, Figure 3.5A). In this chapter it is revealed that palmitate-induced ROS are mostly mitochondrial: oxidation of MitoSOX, a mitochondria-targeted superoxide probe, is increased by palmitate, whilst oxidation of the equivalent non-targeted probe hydroethidine (DHE) is unaffected. Moreover, mitochondrial respiratory inhibition with antimycin A stimulates palmitate-induced MitoSOX oxidation. Furthermore, palmitate does not change the level of mitochondrial UCP2 and UCP2 knockdown does not affect palmitate-induced MitoSOX oxidation. Palmitoleate does not influence MitoSOX oxidation in INS-1E cells ± UCP2 and largely prevents the palmitate-induced effects. Importantly, UCP2 knockdown amplifies the preventive effect of palmitoleate on palmitate-induced ROS. Consistently, viability effects of palmitate and palmitoleate are similar between cells ± UCP2, but UCP2 knockdown significantly augments the palmitoleate protection against palmitate-induced cell loss at high glucose. It is concluded that UCP2 neither mediates palmitate-induced mitochondrial ROS generation and the associated cell loss, nor protects against these deleterious effects. Instead, UCP2 dampens palmitoleate protection against palmitate toxicity.

4.1 Introduction

High levels of circulating glucose and NEFAs impair pancreatic β-cell function and thus contribute to the pathogenesis of Type 2 diabetes [18]. Chapter 3 provides evidence in INS-1E insulinoma cells that mitochondrial dysfunction is involved in this β-cell glucolipotoxicity. Specifically, overnight palmitate exposure at high glucose causes oxidative phosphorylation defects (Figures 3.2, 3.3 and 3.4) that are related to impaired glucose-stimulated insulin secretion (Figure 3.6 and 3.7). Concomitantly, palmitate exposure leads to increased ROS (Figure 3.5) that are associated with cell loss (Figure 3.8). In agreement with the notion that unsaturated NEFAs provide protection against the harmful effects of saturated NEFAs [100] the deleterious effects of palmitate on ROS and INS-1E viability are largely prevented by its mono-unsaturated counterpart palmitoleate (Figures 3.5 and 3.8). Oxidative stress has been linked extensively to β-cell dysfunction and death that give rise to Type 2 diabetes [128,179-181]. Indeed, ROS scavenging has been reported to improve β-cell health under glucolipotoxic conditions [182,183]. β-cells generate ROS in the cytoplasm through activity of a plasma-membrane-bound NADPH oxidase and in mitochondria as a consequence of nutrient catabolism [128]. The origin of the palmitate-induced ROS in INS-1E cells (Figure 3.5A) is unclear at present as is the mechanism underlying the protective effect of palmitoleate.

ROS are non-canonical signals in GSIS [47,48] and studies with isolated islets [84] and INS-1E cells [50] have revealed that UCP2 attenuates GSIS by dampening ROS production. This acute regulatory effect of UCP2 on β-cell function is consistent with the relatively strong GSIS exhibited by the first-established *Ucp2*-ablated mouse strain [81], which suggested a pathological role for UCP2 in the development of β-cell dysfunction and Type 2 diabetes [29]. Indeed, studies involving this original genetic knockout strain demonstrated that UCP2 restricts the insulin secretory capacity of mice fed a high fat diet [85] and that UCP2 mediates β-cell defects caused by free fatty acids [86]. However, work on more recently established *Ucp2*-deficient mouse strains [82] has suggested a physiological instead of a pathological role for UCP2 as the protein has been attributed a protective function in assisting β-cells to deal with sustained oxidative stress [181]. Such stress is for example encountered after chronic fatty acid exposure [184,185]. A protective physiological role for UCP2 is consistent with its reported ROS-dampening effect at high glucose [50], but predicts that UCP2 activity would ameliorate harmful effects of free fatty acids and high fat diet rather than mediate them. Evidently, UCP2 involvement in β-cell glucolipotoxicity remains unclear [18].

The aims of the current chapter were (i) to establish in which cellular compartment ROS arise in INS-1E cells incubated under glucolipotoxic conditions and (ii) to clarify if and how UCP2 regulates ROS production in

NEFA-exposed cells. The work in this chapter reveals that palmitate-induced ROS predominantly emerge from mitochondria and that these ROS correlate strongly with loss of cell viability. Surprisingly, neither palmitate nor palmitoleate significantly affect UCP2 protein level and knockdown of UCP2 by RNA interference does not alter palmitate-induced mitochondrial ROS or associated cell loss. Interestingly, UCP2 knockdown amplifies the dampening effect of palmitoleate on palmitate-induced ROS and augments palmitoleate protection against palmitate-provoked cell loss at high glucose.

4.2 Experimental

4.2.1 Cell culture

INS-1E insulinoma cells were maintained in RPMI-1640 medium containing 11 mM glucose as described in section 2.1.1. INS- 1E cells were seeded at 6 x 10^4 cells/well and, at 70-80% confluence, exposed to NEFAs for 24 h in serum-free RPMI containing 11 mM or 4 mM glucose. NEFAs were administered in conjugation to BSA as described in section 2.3 and control cells were exposed to BSA alone. For RNAi experiments, INS-1E cells were seeded at 60,000 cells/well, grown overnight to 50-60% confluence and then transfected with 200 nM *Ucp2*-targeted or scrambled siRNA oligonucleotides that were complexed with 1.67 μg/mL Lipofectamine 2000 in serum-free RPMI. After 24 h incubation with siRNA-lipofectamine complexes, growth medium was replaced with serum-free

RPMI supplemented with either 11 mM or 4 mM glucose and with appropriate NEFA:BSA conjugations. Transfected cells were exposed to NEFAs for 24 h.

4.2.2 Measurements of reactive oxygen species

Mitochondrial and cytoplasmic ROS levels were estimated from MitoSOX and DHE oxidation rates respectively as described in section 2.9. Cells seeded, transfected and NEFA-exposed on 96-well plates were washed into glucose-free KRH medium comprising 135 mM NaCl, 3.6 mM KCl, 10 mM Hepes (pH 7.4), 0.5 mM $MgCl_2$, 1.5 mM $CaCl_2$, 0.5 mM NaH_2PO_4 and 2 mM L-glutamine, and incubated in this medium (± 15 μM antimycin A) for 30 min in a 37 ^oC air incubator. Next, plates were transferred to a multimode plate reader (PHERAstar FS, BMG Labtech) and following injection of either 5 μM MitoSOX or 100 μM DHE, fluorescence was monitored at 28-sec intervals for 30 min. Fluorescent MitoSOX and DHE oxidation products were excited at 510 nm and light emission was detected at 580 nm. The plate reader's focal height was set at 3.4 mm and its gain was fixed between different experiments.

4.2.3 Cell viability

Densities of attached INS-1E cells were determined by fluorescent DAPI-staining as described in section 2.6. Briefly, cells seeded, transfected and NEFA-exposed on 96-well plates were washed into 200 μL/well PBS, fixed with 4% (w/v) PFA for 20 min at room temperature, and then incubated with DAPI (0.5 μg/mL in PBS) for another 15 min at room temperature. To minimise background

fluorescence, excess DAPI was removed by washing 4x with PBS before measuring total-well fluorescence ($\lambda^{ex/em}$ = 358/461 nm) using a multimode plate reader (PHERAstar FS, BMG Labtech) in bottom-reading and well-scanning mode. Standard curve-derived cell numbers (Figure 2.5B) were used to quantify NEFA effects on cell viability (Figures 4.5 and 4.6) and to normalise ROS probe oxidation rates (Figures 4.1, 4.3 and 4.4).

4.2.4 Uncoupling protein-2

UCP2 was determined in INS-1E cells as described in section 2.10. In summary, INS-1E cells were seeded in 25 cm^2 tissue culture flasks at 1 x 10^6 cells/flask and transfected with scrambled or *Ucp2*-targeted siRNA. After 24 h incubation, cells were washed into serum-free RPMI and exposed to NEFA:BSA conjugations for 24 h. Samples of 50 μg protein were estimated from cell lysates and precipitated overnight. Precipitated protein was pelleted by centrifugation and solubilised in 20 μL loading buffer. Proteins were separated by SDS-PAGE and transferred to nitrocellulose membrane at room temperature using a semi-dry transfer cell. Blocked membranes incubated with primary and secondary antibodies were anlaysed for cross-reactivity by chemiluminescence using a LAS 4000 camera collecting images at 30-sec intervals for 5 min. Membrane images were analysed with ImageQuant TL version 7.0. As described in Figure 4.2, UCP2 protein

levels were compared between samples by normalising to partially purified recombinant human UCP2 standards.

4.2.5 Statistical analysis

Statistical significance of mean differences was tested by Student's t-test or ANOVA as specified in the figure legends using GraphPad Prism Version 6.0 for Mac OS X (GraphPad software, San Diego, CA, USA).

4.3 Results

4.3.1 Palmitate-induced reactive oxygen species emerge from mitochondria

INS-1E cells exposed for 24 h to palmitate in the presence of high glucose exhibit a MitoSOX oxidation rate that is significantly higher than the rate observed in BSA-exposed control cells (Figure 4.1A). This observation agrees with previous results (Figure 3.5A) and strongly suggests that palmitate provokes an increase in mitochondrial ROS, as MitoSOX is a widely used mitochondria-targeted superoxide probe [160]. Not all MitoSOX will accumulate in the mitochondrial matrix, however, and it is thus formally possible that the data in Figure 4.1A reflect a palmitate-induced rise in cytoplasmic superoxide that is secondary to stimulated NADPH oxidase activity [146]. Importantly, DHE is oxidised at the same rate by palmitate-exposed and BSA control INS-1E cells (Figure 4.1B). DHE is the non-targeted equivalent of MitoSOX and its oxidation is therefore dominated by cytoplasmic

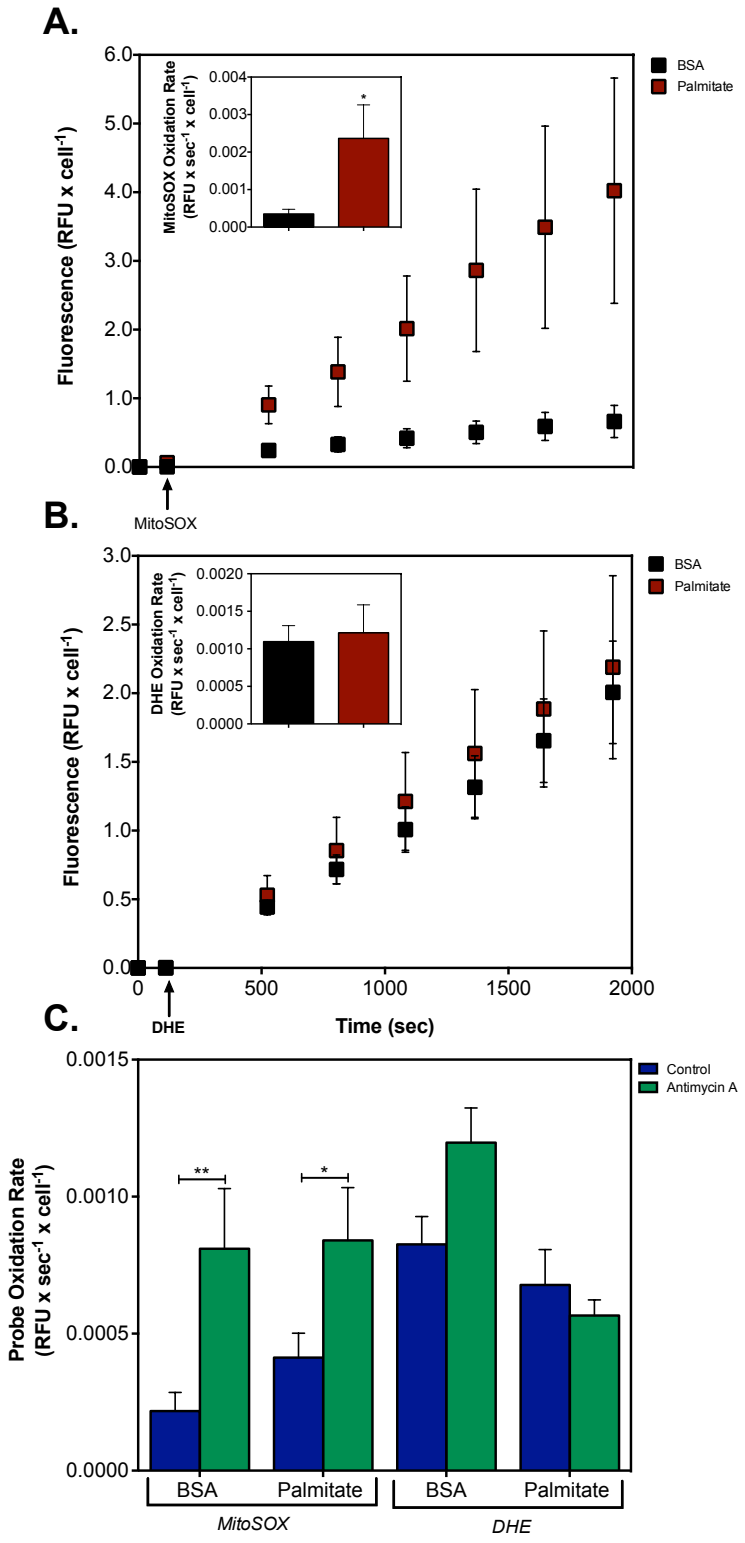

Figure 4.1 – Palmitate-induced ROS are mitochondrial

Mitochondrial and cytoplasmic superoxide levels were estimated from MitoSOX (5 µM, **A** and **C**) and DHE (100 µM, **B** and **C**) oxidation rates, respectively, in INS-1E cells exposed for 24 hr to BSA-conjugated palmitate or BSA alone at 11 mM glucose. Probes were injected at times indicated by the arrows and background-corrected fluorescence was recorded at 28-second intervals; for clarity, only a selection of measurements is shown (**A** and **B**). Probe oxidation rates (insets) were calculated from the slopes of the progress curves; except for the first 4 measurements after probe addition, all data were included in these calculations (**A** and **B**). Probe oxidation rates were also determined ± 15 µM antimycin A (**C**). Relative fluorescence units (RFU) were normalized to cell number using mean INS-1E viability data (Figure 4.5). Data are means ± SEM from three to eleven independent experiments that each involved 7-8 replicates per treatment. Statistical significance of mean differences was tested for by Student's t-test (**A** and **B**) and two-way ANOVA (**C**): **P* < 0.05 and ***P* < 0.01.

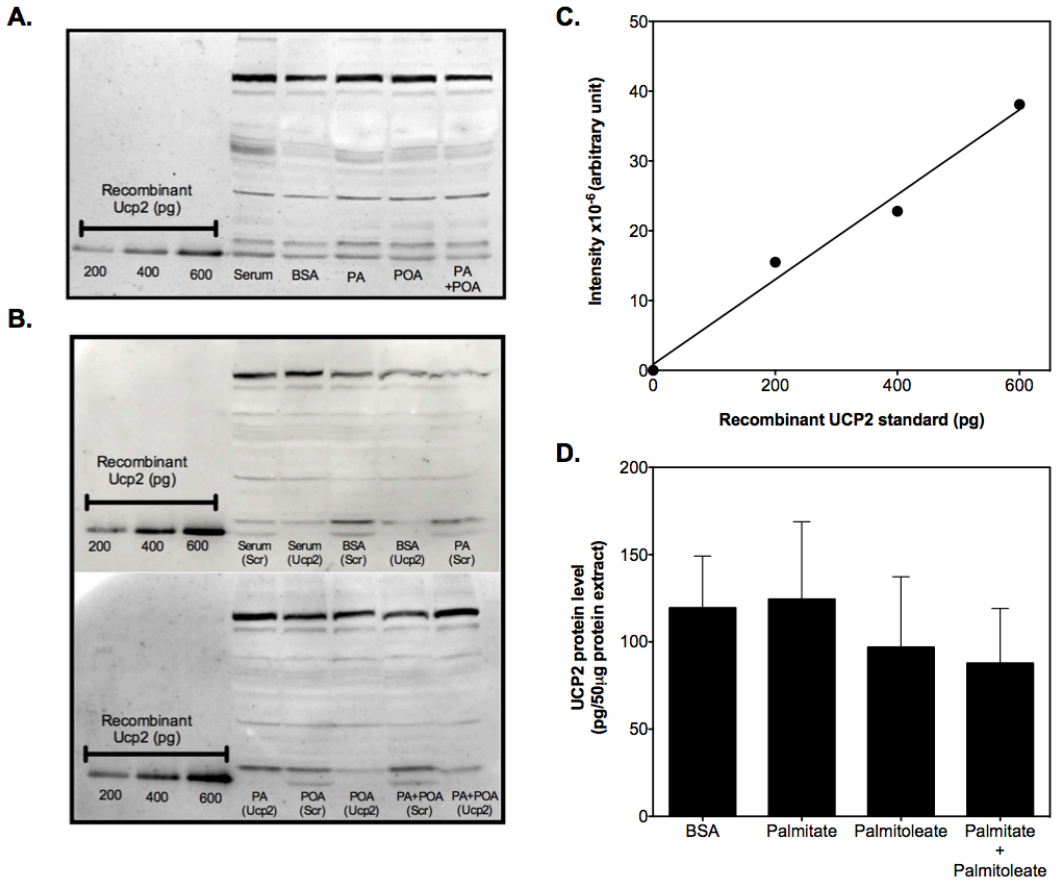

Figure 4.2 – UCP2 protein in INS-1E cells is not affected by palmitate and/or palmitoleate

Typical Western blot showing cross-reactivity of UCP2 antibodies with partially purified recombinant human UCP2 (hUCP2) and INS-1E proteins separated by SDS-PAGE (see Experimental) (**A**). Proteins were isolated from cells exposed for 24 hr to BSA-conjugated to NEFAs or BSA alone at 11 mM glucose. Typical blots showing data from cells transfected with *Ucp2*-targeted or scrambled siRNA oligonucleotides (Ucp2 and Scr, respectively) before fatty acid exposure (**B**). Palmitate (PA), palmitoleate (POA), palmitate plus palmitoleate (PA+POA), BSA alone (BSA) or serum-supplemented growth medium (Serum) (**A** and **B**). Typical relation between signal intensity and amount of hUCP2 as determined for each individual experiment (*cf.* **A** and **B**) to allow comparison of UCP2 levels between different samples (**C**). Membrane images were analysed with ImageQuant software using its *1D gel analysis* feature: background in defined lanes was subtracted by the *rolling ball* function, bands reflecting known hUCP2 amounts were boxed, and by applying the *quality calibration* function the presented relation was generated. UCP2 content approximated as picograms per 50 µg total extracted protein (**D**). Data are means ± SEM from three independent fatty acid exposures. Statistical significance of mean differences was tested for by one- way ANOVA revealing no significant differences between conditions.

ROS suggesting that, in our experiments, palmitate has not affected superoxide generation by NADPH oxidase. In a separate set of experiments, we tested the effect of mitochondrial respiratory inhibition with antimycin A on ROS production in INS-1E cells (Figure 4.1C). Although the palmitate effect on the MitoSOX oxidation rate was relatively modest in these particular experiments (Figures 4.1C, 4.1A and 4.3A), it is clear that antimycin A significantly

stimulates MitoSOX oxidation in both palmitate-exposed and BSA control cells (Figure 4.1C). Antimycin A also increases DHE oxidation a little in BSA control cells, but not to a statistically significant extent. Importantly, antimycin A has no effect on DHE oxidation in palmitate-treated cells (Figure 4.1C). Together, the effects of antimycin A support our assertion that glucolipotoxic ROS emerge from the mitochondria.

4.3.2 Palmitate does not affect uncoupling protein-2 protein levels

Next, we explored possible UCP2 involvement in the palmitate-induced rise in mitochondrial ROS, in the first instance by probing the effect of palmitate and palmitoleate on UCP2 protein level. Detection and relative quantification of UCP2 protein by Western analysis is complicated by the notorious non-specificity of commercially available UCP2 antibodies. To conclusively identify bands that represent UCP2 in INS-1E samples, these set of experiments included partially purified recombinant hUCP2 protein and UCP2-depleted cells as positive and negative controls, respectively. Figure 4.2A shows a typical Western blot that stresses the necessity of these controls: many bands cross-react with UCP2 antibodies across the entire molecular weight range including a protein doublet at the position to which hUCP2 migrates – only the lower band of this doublet is absent in INS-1E cells transfected with *Ucp2*-targeted siRNA (Figure 4.2B). As the intensity of this band consistently falls within the linear range of hUCP2 intensities (Figure 4.2C), normalisation to hUCP2 allows

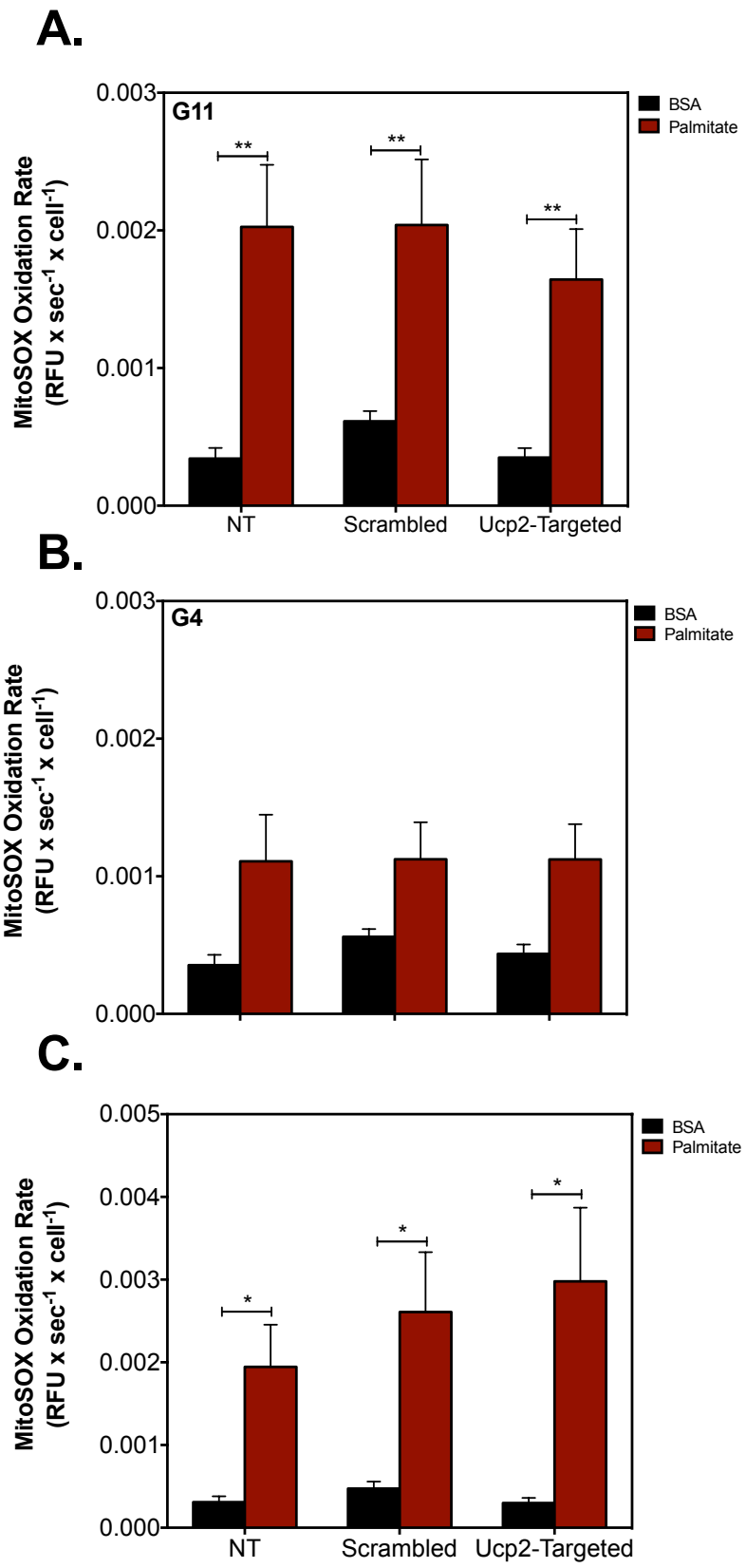

Figure 4.3 – UCP2 knockdown does not change the effect of palmitate on mitochondrial ROS

MitoSOX oxidation rates were determined in non-transfected INS-1E cells (NT) or cells transfected with scrambled or *Ucp2*-targeted siRNA oligonucleotides. Cells were exposed for 24 hr to BSA-conjugated to palmitate or BSA alone at 11 mM (**A -G11**) or 4 mM (**B - G4**) glucose. Cells exposed for 24 hr to BSA-conjugated to palmitate or BSA alone in the presence of 10 μM verapamil (**C**). Data are means ± SEM of four to eleven separate exposures with 3-8 replicates per treatment. Statistical significance of mean differences was tested for by two-way ANOVA: **P* < 0.05 and ***P* < 0.01.

relative quantification of UCP2 protein in NEFA-exposed INS-1E cells. Although the absolute values in Figure 4.2D bare little relevance given the impurity of hUCP2 and the possible differential antibody reactivity with human and rat proteins, it is clear that the level of UCP2 protein is unchanged in INS-1E cells exposed to palmitate for 24 h at high glucose. Similar exposure to palmitoleate, alone or in combination with palmitate, tends to lower UCP2 protein moderately, but not to a statistically significant extent (Figure 4.2D). Equally, palmitate and/or palmitoleate have no obvious effect on UCP2 levels in INS-1E cells transfected with scrambled siRNA (Figure 4.2B). The relatively stable UCP2 protein level is consistent with the observation that mitochondrial proton leak in INS-1E cells is unaffected by NEFA exposure (Figure 3.4).

4.3.3 Knockdown of uncoupling protein-2 amplifies palmitoleate protection against palmitate-induced reactive oxygen species

Figure 4.2B confirms that the NEFA-sensitivity of UCP2 protein is similar in non-transfected cells and cells transfected with scrambled siRNA, and that transfection with *Ucp2*-targeted siRNA leads to UCP2 depletion in both untreated cells and in cells exposed to BSA-conjugated NEFAs or to BSA alone. Therefore, RNAi was used to directly assess UCP2 involvement in NEFA-induced ROS formation. MitoSOX oxidation was measured in non-transfected and transfected INS-1E cells exposed to palmitate for 24 h at 4 and 11 mM glucose (Figure 4.3). In line with data shown in Figures 4.1A and 4.1C, palmitate

exposure causes a significant increase in MitoSOX oxidation in non-transfected cells incubated at high glucose – importantly, the effect of palmitate is near-identical in cells transfected with scrambled siRNA (Figure 4.3A). MitoSOX

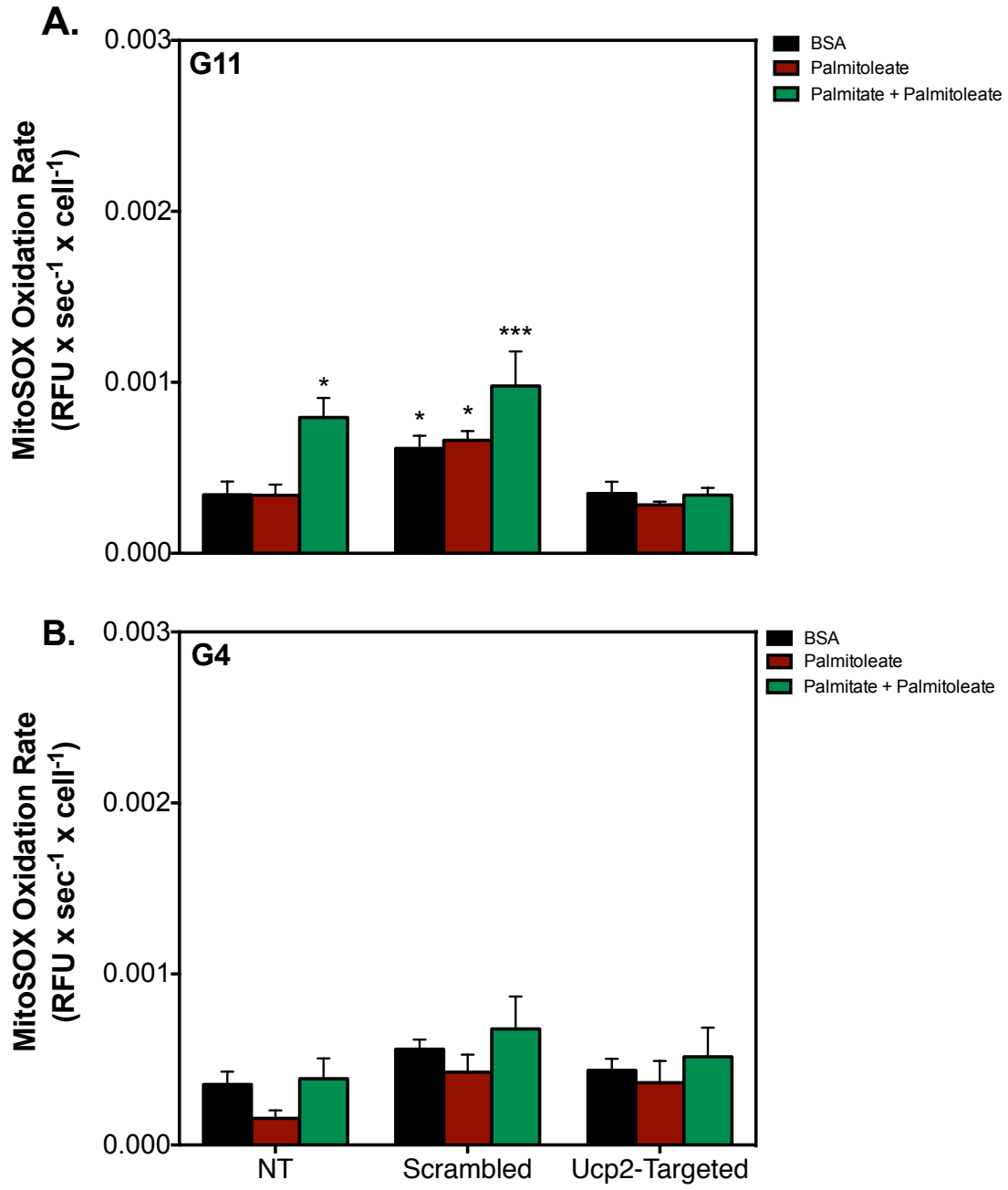

Figure 4.4 – UCP2 knockdown amplifies attenuation by palmitoleate of palmitate-induced mitochondrial ROS

MitoSOX oxidation rates were determined (see Figure 4.1) in non-transfected INS-1E cells (NT) or cells transfected with scrambled or *Ucp2*-targeted siRNA oligonucleotides. Cells were exposed for 24 hr to BSA-conjugated NEFA or BSA alone at 11 mM (**A - G11**) or 4 mM (**B - G4**) glucose. Data are means ± SEM of three to five separate experiments with 3-8 replicates per treatment. Statistical significance of mean differences was tested for by two-way ANOVA: **P* < 0.05, ****P* < 0.001 differs from the equivalent *Ucp2*-targeted condition.

oxidation in UCP2-depleted cells exposed to palmitate tends to be somewhat decreased, but the drop is not statistically significant (Figure 4.3A). Palmitate-induced MitoSOX oxidation is relatively modest when cells are exposed at low glucose (Figure 4.3B), but again, palmitate-sensitivity does not depend on the presence of UCP2 (Figure 4.3B). These data indicate that UCP2 does not mediate palmitate-induced mitochondrial ROS, and does not protect against their formation either. To control for multiple drug resistance (MDR) that could lower net uptake of fluorescent dyes, MitoSOX oxidation was measured in transfected and non-transfected INS-1E cells exposed to palmitate in the presence of verapamil – an MDR inhibitor [186] (Figure 4.3C). Under all conditions, verapamil stimulated MitoSOX oxidation modestly, but not to a statistically significant extent (Figure 4.3C) and importantly, did not influence NEFA or UCP2 phenotypes (Figure 4.3).

Irrespective of glucose exposure or the presence of UCP2, MitoSOX oxidation is not affected by palmitoleate (Figure 4.4). When administered in combination with palmitate, palmitoleate dampens the rate of palmitate-induced MitoSOX oxidation at high glucose in non-transfected INS-1E cells from 0.002 to 0.0008 RFU x sec^{-1} x $cell^{-1}$ (Figures 4.3A and 4.4A, respectively), which is consistent with data shown in Figure 3.5A. The preventive effect of palmitoleate is similar in cells transfected with scrambled siRNA (Figures 4.3A and 4.4A). Interestingly, palmitoleate lowers palmitate-induced MitoSOX even further, to

about 0.0003 RFU x sec^{-1} x $cell^{-1}$, in UCP2-depleted cells (Figure 4.4A). Generally, MitoSOX oxidation in BSA-exposed control cells tends to be marginally higher in cells transfected with scrambled siRNA than in non-transfected or *Ucp2*-transfected cells (Figures 4.3 and 4.4).

4.3.4 Knockdown of uncoupling protein-2 amplifies palmitoleate protection against palmitate-induced cell loss

Next, the viability of non-transfected and transfected INS-1E cells was measured to probe the effect of UCP2 knockdown on palmitate-provoked cell loss (Figure 3.8). Reflecting the effect of transfection on MitoSOX oxidation, absolute numbers of scrambled-transfected BSA control cells are lower than their non-transfected and *Ucp2*-transfected counterparts (Figure 4.6D), but the relative effects of NEFAs on cell viability are comparable between scrambled-transfected and non-transfected cells (Figure 4.5). Serum withdrawal tends to have a modest negative effect on the viability of both cell types, particularly at high glucose (Figure 4.5A), as reflected by relatively small drops in the number of BSA-exposed control cells. Interestingly, UCP2 knockdown appears to improve cell resistance against the lack of serum, although the viability difference between BSA-exposed cells transfected with scrambled and *Ucp2*-transfected siRNA is not statistically significant (Figure 4.5A). At high and low glucose (Figures 4.5A and 4.5B, respectively), palmitate decreases cell number considerably further, whereas palmitoleate does not exert any effect in addition

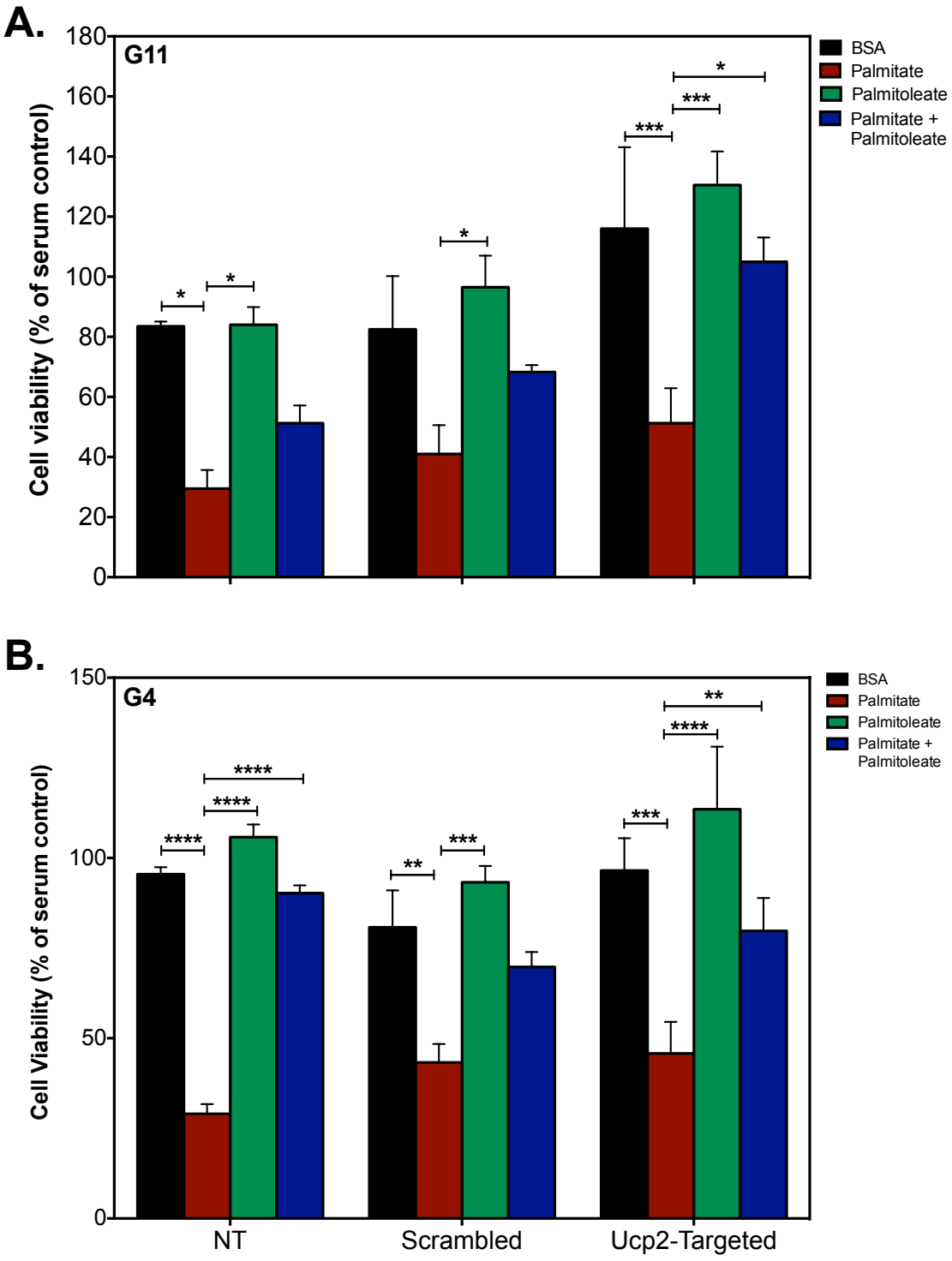

Figure 4.5 – Effect of UCP2 knockdown on the viability of NEFA-exposed INS-1E cells

Cell viability was determined as described in 'Experimental' using non-transfected cells and cells transfected with scrambled or *Ucp2*-targeted siRNA oligonucleotides. Cells were exposed for 24 hr to BSA-conjugated to NEFAs or to BSA alone at 11 mM (**A - G11**) or 4 mM (**B - G4**) glucose. Absolute cell numbers (*cf.* Figure 4.6) were expressed as a percentage of control values obtained with cells grown in standard serum-supplemented growth medium. Data are means ± SEM of four independent experiments with 3-5 replicates per treatment. Statistical significance of mean differences was tested for by two-way ANOVA: **P* < 0.05, ***P* < 0.01, ****P* < 0.001 and *****P* < 0.0001.

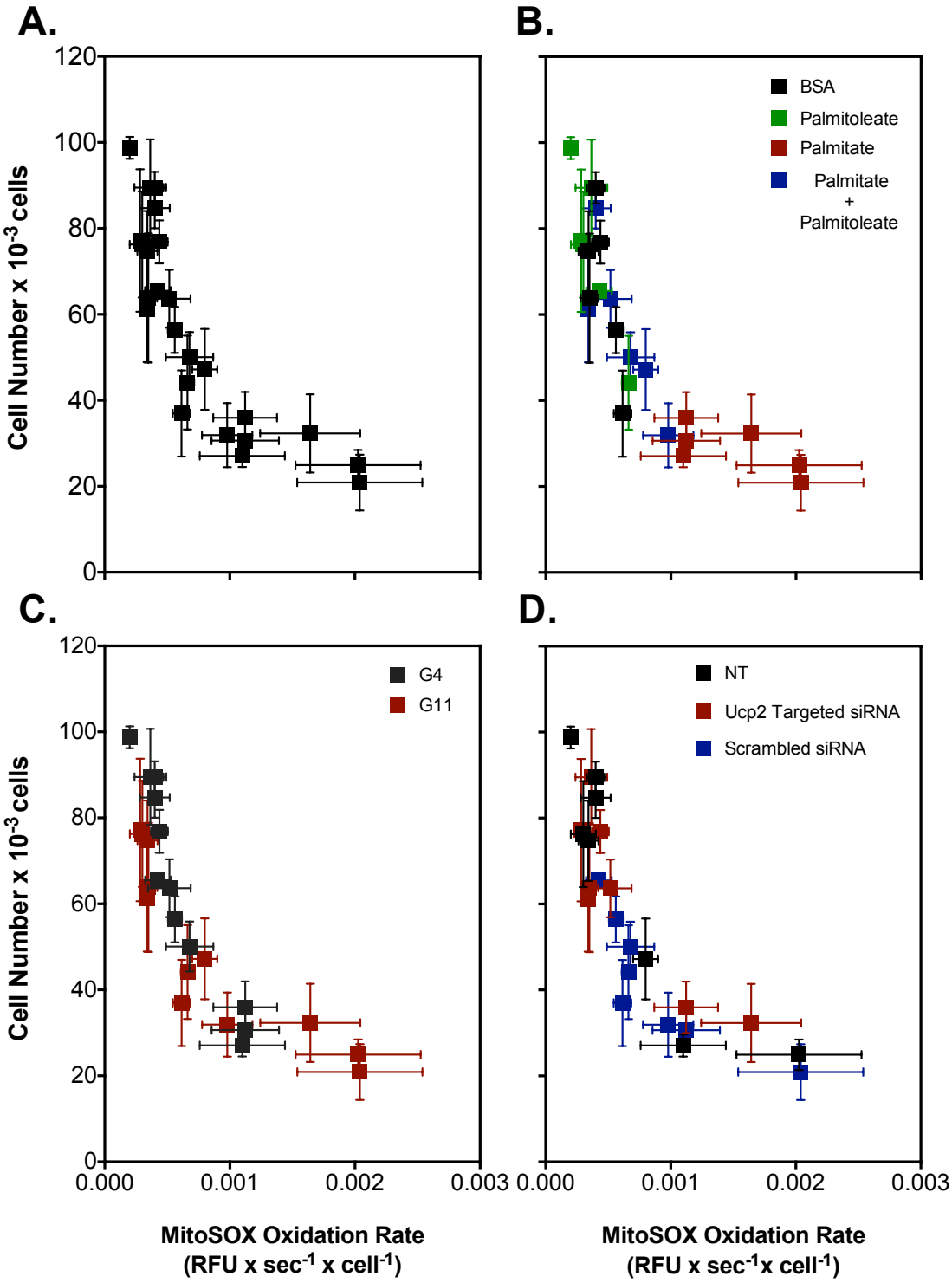

Figure 4.6 – INS-1E cell viability correlates inversely with mitochondrial ROS.

Absolute cell number (*cf.* Figure 4.5) was plotted as a function of the MitoSOX oxidation rate (*cf.* Figures 4.3 and 4.4). Data reflect the behavior of non-transfected (NT) cells and that of cells transfected with scrambled or *Ucp2*-targeted siRNA oligonucleotides after 24 hr exposure to BSA-conjugated NEFAs or to BSA alone at 11 mM (G11) and 4 mM (G4) glucose.

to serum withdrawal – UCP2 knockdown does not change these NEFA responses. Palmitoleate ameliorates palmitate-induced cell loss, but more strongly at low than high glucose (Figure 4.5). Strikingly, the relatively modest protective effect of palmitoleate at high glucose is amplified significantly after UCP2 knockdown (Figure 4.5A).

4.3.5 Inverse correlation between mitochondrial reactive oxygen species and cell viability

In line with the suggested causative role of ROS in glucolipotoxic β-cell failure [182,183], palmitate affects MitoSOX oxidation and INS-1E cell number in opposite directions (Figures 4.3 and 4.5, respectively). These palmitate phenotypes are both attenuated by palmitoleate – a protection that is regulated by UCP2 (Figures 4.4 and 4.5) – suggesting a mechanistic relation between mitochondrial ROS and INS-1E cell viability. Indeed, combined analysis of the data demonstrates an unequivocal inverse correlation between absolute numbers and specific MitoSOX oxidation rates (Figure 4.6). The relation between cell number and mitochondrial ROS is not linear as cell loss starts to tail off from a MitoSOX oxidation rate just below 0.001 RFU x sec^{-1} x $cell^{-1}$ (Figure 4.6A). A correlative analysis of our data illustrates persuasively that palmitate is indeed toxic to INS-1E cells and that this toxicity is prevented by palmitoleate (Figure 4.6B). The inverse correlation between cell number and MitoSOX oxidation appears independent of the applied glucose level (Figure

4.6C), suggesting that the glucose permissibility on palmitate toxicity is rather weak (Figures 4.6B and 4.6C). The inverse correlation between cell number and MitoSOX oxidation is the same in non-transfected cells as in cells transfected with scrambled or *Ucp2*-targeted siRNA (Figure 4.6D), which suggests that the relatively low number of scrambled-transfected cells is owed to comparably high mitochondrial ROS.

4.4 Discussion

In this chapter it is shown that palmitate-induced ROS in INS-1E cells have a mitochondrial origin (Figure 4.1) and that cell viability exhibits a strong inverse correlation with these mitochondrial ROS (Figure 4.6). Moreover, it is demonstrated that UCP2 is not needed for the palmitate effects on mitochondrial ROS or INS-1E cell viability, and does not ameliorate such effects either (Figures 4.3 and 4.5, respectively). Importantly, a new and unexpected phenotype is revealed as UCP2 appears to attenuate palmitoleate protection against palmitate toxicity (Figures 4.4 and 4.5).

4.4.1 Palmitate induces mitochondrial reactive oxygen species

Palmitate increases the oxidation of hydroethidine by INS-1E cells, but only when this superoxide probe is targeted to mitochondria through conjugation to a triphenylphosphonium moiety (Figure 4.1). Palmitate-induced oxidation of the targeted hydroethidine (MitoSOX) is further increased following inhibition of mitochondrial respiration with antimycin A (Figure 4.1C). Together, these

data indicate that palmitate triggers formation of mitochondrial superoxide in INS-1E cells. A mitochondrial origin of palmitate-induced ROS seems at odds with glucolipotoxicity-provoked expression and activity of a cytoplasmic superoxide-generating NADPH oxidase [146]. Such activity, however, is expected to increase DHE oxidation, which in previous experiments appears unaffected by palmitate (Figure 4.1B). Superoxide formation by NADPH oxidase is also expected to increase cytoplasmic oxygen uptake, but palmitate does not change such non-mitochondrial respiration in INS-1E cells (Figure 3.2A). Although the likely nature of palmitate-induced ROS is superoxide, it should be kept in mind that hydroethidine probes are also oxidised, albeit to a lesser extent, by hydrogen peroxide (in the presence of peroxidases) and intracellular oxidoreductases [160]. Additionally, MitoSOX accumulation into the mitochondrial matrix is dependent on mitochondrial membrane potential so changes in MitoSOX oxidation may arise from differential probe availability. As discussed before [50], however, this eventuality is unlikely given the saturating MitoSOX concentration applied in the reported experiments. Related, it is conceivable that MitoSOX oxidation is limited by multiple drug resistance (MDR) that could lower net uptake of fluorescent dyes by INS-1E cells. However, by exposing transfected and non-transfected INS-1E cells to palmitate in the presence of verapamil – an MDR inhibitor [186] – any MDR-related limitations are excluded (Figure 4.3C). Under all conditions, verapamil

stimulated MitoSOX oxidation modestly, but not to a statistically significant extent (Figure 4.3C) – verapamil did not influence NEFA or UCP2 phenotypes.

4.4.2 Physiological role of uncoupling protein-2

The first evidence for β-cell UCP2 emerged some time ago [87] but the physiological role of UCP2 in pancreatic β-cells has still not been established unequivocally [140]. Indeed, the exact molecular role of UCP2 remains subject of debate as this carrier has recently been shown to export carbon compounds from the mitochondrial matrix [80]. Such a function clearly differs from the widely assumed uncoupling activity of UCP2 that would result in partial dissipation of the mitochondrial protonmotive force [187]. In light of the unclear molecular and physiological roles, it is perhaps not surprising that UCP2 involvement in glucolipotoxicity remains contentious [18]. Several functional UCP2 models have been proposed, which include roles in β-cell pathology and consequent development of Type 2 diabetes [29], and in protecting β-cells against oxidative stress [181]. These fundamentally different roles suggest opposite UCP2 involvement in glucolipotoxicity: the pathological model predicts UCP2 is required for palmitate-provoked ROS formation, whereas the protective model predicts UCP2 prevents such formation instead. Our findings do not provide support for either model as UCP2 knockdown does not decrease or increase palmitate-induced mitochondrial ROS production significantly (Figure 4.3). Although caution is due when inferring physiological meaning

from insulinoma cell data, our results would suggest UCP2 does not mediate harmful effects of palmitate in β-cells and does not protect against such effects either. Consistently, palmitate does not change the level of UCP2 protein (Figure 4.2). This lack of effect is discrepant with literature that suggests UCP2 expression is relatively high in palmitate-exposed insulinoma cells as well as in islets from mouse models of Type 2 diabetes and lipotoxicity (reviewed in [72]), and in islets of Type 2 diabetic patients [188]. The discrepancy likely arises from the relative difficulty of quantifying UCP2 protein: (i) measuring mRNA level is insufficient as UCP2 expression is strongly controlled by translation [149], (ii) detecting protein in pancreatic islets is confounded by the presence of UCP2 in both β-cells and other islet cell types [90], and (iii) Western analysis is complicated by the notorious non-specificity of commercial UCP2 antibodies (Figures 4.2A and 4.2B). In this study positive and negative protein controls were used to unequivocally identify UCP2 protein in homogenous INS-1E cell lysates, and relative protein amounts were quantified in NEFA-exposed cells by normalising antibody cross-reactivity to partially purified recombinant human UCP2 protein (Figure 4.2).

4.4.3 Uncoupling protein-2 regulates palmitoleate protection

Palmitoleate protects INS-1E cells against mitochondrial ROS formation and the associated loss of cells (Figure 4.6B). Interestingly, UCP2 knockdown amplifies the protective effect of palmitoleate against palmitate-induced ROS (Figure 4.4)

and cell loss (Figure 4.5). These observations suggest an unexpected role for UCP2 in the regulation of β-cell protection by unsaturated NEFAs against cytotoxicity. It has been well established that unsaturated fatty acids protect β-cells against the toxic effects of their saturated counterparts [100] but mechanistic understanding of this phenomenon is incomplete [169]. Interestingly, cytoprotection is not restricted to lipotoxic stress as unsaturated NEFAs also prevent cell loss after serum withdrawal or cytokine exposure [17]. In this respect, it is worth notice that UCP2 knockdown protects against the moderate viability loss of control INS-1E cells that were deprived from serum and exposed overnight to BSA alone at high glucose (Figure 4.5A). Although these data do not explain how UCP2 activity may dampen palmitoleate protection, they firmly implicate mitochondrial energy metabolism in this poorly understood process.

4.4.4 Glucose dependence of palmitate toxicity

NEFA-induced β-cell defects are often – but not always [17] observed at a high glucose level, which is why such defects are generally referred to as glucolipotoxicity [16]. Indeed, in previous experiments, there were statistically insignificant effects of palmitate on MitoSOX oxidation and INS-1E cell viability when administered overnight at low glucose (Figure 3.8). Although the effect on MitoSOX oxidation remains insignificant in the current experiments, palmitate consistently tends to increase mitochondrial ROS in non-transfected

and transfected cells following exposure at low glucose (Figure 4.3B), albeit it to a lesser extent than at high glucose (Figure 4.3A). Consistently, palmitate causes statistically significant cell loss at both high and low glucose, and in non-transfected as well as in transfected cells (Figure 4.5). Quantitative differences with the previously reported cell numbers (Figure 3.8) likely arise from application of different assays to determine cell number (viability/vitality), but the glucose dependence of the palmitate viability phenotype appears weak irrespective of such experimental differences. Indeed, the combined analysis of mitochondrial ROS and INS-1E viability data confirms that palmitate is most toxic at high glucose, but causes significant damage at low glucose too (Figures 4.6B and 4.6C).

4.5 Conclusion

In conclusion, these results support the notion that oxidative stress contributes to pancreatic β-cell glucolipotoxicity and shed important new light on the elusive mechanism by which unsaturated NEFAs protect against the harmful effects of their saturated counterparts. In addition, such findings inform the ongoing debate on the physiological role of pancreatic β-cell UCP2. Importantly, since INS-1E cells are a pancreatic β-cell line that show clear differences from primary β-cells (Chapter 5), to establish the physiological significance of these data, these experiments should be performed using primary islet cells. Importantly, previous observations from INS-1E cells have

come true in pancreatic islets and although primary β-cells may respond differently, we are confident that UCP2 protein in INS-1E cells is not affected by overnight palmitate exposure at high glucose. To firmly establish a role of UCP2 in the glucolipotoxicity of pancreatic β-cells, UCP2 needs to be probed and knocked out specifically in the β-cells of isolated islets. Previous studies are often confounded by the presence of UCP2 in other islet cells or knock out of the protein in other tissues.

Chapter 5

FATTY ACID-INDUCED DEFECTS IN GLUCOSE-STIMULATED INSULIN SECRETION ARE DISCONNECTED FROM IMPAIRMENT OF MITOCHONDRIAL OXIDATIVE PHOSPHORYLATION IN PANCREATIC MOUSE ISLETS

5.0 Abstract

Recent evidence in INS-1E insulinoma cells suggests that the molecular mechanisms of pancreatic β-cell glucolipotoxicity are related to mitochondrial dysfunction (Chapter 3). To investigate the physiological impact of these findings, in this chapter, mitochondrial energy metabolism is probed using Seahorse extracellular flux technology in NEFA exposed pancreatic islets. In line with INS-1E cells (Figures 3.2 and 3.6) prolonged exposure of palmitate at high glucose attenuates the glucose-sensitivity of mitochondrial respiration and insulin secretion in pancreatic islets. Palmitate exposure does not alter basal respiration. Surprisingly, however, palmitate stimulates basal insulin secretion which is stimulated further by high glucose. Consistent with INS-1E cells (Figures 3.2 and 3.6), palmitoleate does not ameliorate the palmitate-induced defects in GSIS. Unlike INS-1E cells (Figures 3.2 and 3.6), palmitoleate alone tends to dampen GSIS and in combination with palmitate, palmitoleate protects against the palmitate impairment of glucose-stimulated mitochondrial respiration. Moreover the exposure of islets to palmitate, palmitoleate or palmitate plus palmitoleate have no effects on the coupling efficiency of oxidative phosphorylation in islets. These data suggest that NEFA-induced impairment of mitochondrial respiration is disconnected from NEFA-induced GSIS defects.

5.1 Introduction

The rapidly increasing prevalence of Type 2 diabetes makes the study of pancreatic islets a fundamental area of research in the modern world. It is now well accepted that obesity is in part responsible for this rise and has been linked with the glucolipotoxic actions of supra-physiological NEFA and glucose levels that circulate in the obese state [16]. Many papers have been published on the topic of pancreatic β-cell glucolipotoxicity, which have emerged from studies in clonal β-cell lines [15,97,152,189] and pancreatic islets isolated from both rodents [14,85,118] and humans [62,66,190]. Despite this extensive list, the underlying mechanisms responsible for glucolipotoxic-induced defects in β-cells is still subject of ongoing debate. Recent findings in this thesis using INS-1E insulinoma cells have provided new insights into the involvement of mitochondrial energy metabolism in glucolipotoxicity, as well as confirming glucolipotoxic-induced defects in GSIS and cell viability (Chapters 3 and 4). It was reported in chapter 3 that palmitate exposure leads to a loss of glucose sensitivity and lowered coupling efficiency of oxidative phosphorylation in INS-1E cells which correlated with palmitate-induced defects in GSIS. Due to this relationship it was concluded that the mechanisms responsible for palmitate-induced impairment of mitochondrial function and GSIS are related. Studies of mitochondrial dysfunction in pancreatic islets using methods that measure rates of oxygen uptake are scarce [84,177,191]. The benefits of

measuring respirometry in whole islets is important to test the physiological impact of cell studies. Due to the recent development of a novel islet respirometry assay [176], probing mitochondrial bioenergetics in intact islets has become more readily available.

In the present chapter mitochondrial energy metabolism in intact isolated mouse islets exposed to glucolipotoxic conditions was probed using Seahorse extracellular flux technology. By exposing pancreatic islets to palmitate it is reported that (i) palmitate lowers glucose-stimulated mitochondrial respiration but does not affect basal activity, and (ii) palmitate impairment of GSIS is due to amplification of basal insulin secretion. These observations suggest that mitochondrial dysfunction is disconnected from NEFA-induced GSIS defects.

5.2 Experimental

The experimental work in this chapter was carried out in the division for mitochondrial biology directed by Dr Martin Jastroch in the institute of Diabetes and Obesity at the HMGU research center.

5.2.1 Ethics

The Institute for Diabetes and Obesity of the HMGU takes the issue of animal welfare very seriously. German animal welfare laws are strictly enforced at HMGU, and its animal facilities are clean, well-organized and properly maintained. All animal housing and handling were performed in accordance

with the directive 2010/63/EU of 22nd November 2010 of the European Council on the protection of animals used for scientific purposes and its revisions, and with the laws governing the use of animals for research in Germany and Upper Bavaria.

5.2.2 Animals

Pancreatic islets were isolated from 12-18 week old male and female C57BL/6 mice. All animals were housed in air conditioned rooms maintained at 26 °C ± 2 °C with a 12 h light and dark cycle.

5.2.3 Isolation of pancreatic islets

Pancreatic islets were isolated by direct injection of liberase into the common bile duct as described in section 2.2. Freshly isolated islets were left to recover for 24 h in CMRL growth medium (Gibco, #21530027) containing 5.5 mM glucose and supplemented with 15 % FBS, 50 U/ml penicillin, 50 µg/ml streptomycin, 50 µM β-mercaptoethanol, 17.8 mM $NaHCO_3$, and 2 mM L-glutamine under humidified carbogen conditions at 37 °C.

5.2.4 Treatment of pancreatic islets

For experimental investigation, isolated islets were pooled from the pancreata of 10-12 mice and 'hand picked' at random using a stereomicroscope into sterile petri-dishes containing 10-15 ml CMRL growth medium supplemented with 11 mM glucose in the presence or absence of BSA-conjugated NEFAs (palmitate,

palmitoleate and palmitate plus palmitoleate) or BSA alone. Islets were incubated in this medium under humidified carbogen conditions at 37 ºC for 24 h or 48 h and then placed into either 'v' bottom 96-well culture microplates or XF24 islet capture microplates for measurements of insulin secretion and mitochondrial oxygen uptake rates, respectively.

5.2.5 Preparation of fatty acid conjugations with bovine serum albumin

BSA:NEFA conjugations were adapted from section 2.3 so that the molar ratios of BSA:NEFA resulted in similar $NEFA_u$ levels of 40 nM. To achieve these ratios the following concentrations of NEFAs were used - palmitate (9.2 mM), palmitoleate (5.42 mM) or a combination of palmitate (7 mM) and palmitoleate (1.22 mM) and conjugated to 1.6 mM BSA [151].

5.2.6 Glucose-stimulated insulin secretion

NEFA-exposed pancreatic islets were 'hand-picked' using a stereomicroscope and transferred into 'v' bottom 96-well culture microplates containing pre-warmed (37 ºC) KRH (*cf.* section 2.7.2) supplemented with 5.5 mM glucose at a density of 7 islets/well. Islets were incubated in this medium at 37 ºC under carbogen conditions for 1 h, washed into fresh KRH and then incubated again for 1 h. Next, supernatant was collected and replaced with KRH supplemented with 28 mM glucose. After 1 h incubation at 28 mM glucose, supernatant was collected. Samples taken at 5.5 mM and 28 mM glucose were diluted 1:2 or 1:10 in KRH, respectively, and then assayed for insulin content by Mouse Insulin

ELISA (Mercodia, upssala, Sweden, *cf.* section 2.7.4). Secreted insulin values were normalised to islet DNA content as described in section 2.8.

5.2.7 Islet insulin content

Immediately after insulin secretion experiments, NEFA-exposed islets were homogenised as described in section 2.7.3 and assayed for insulin content using Mouse Insulin ELISA (Mercodia, upssala Sweden, *cf.* section 2.7.4).

5.2.8 Islet DNA content

After experiments of mitochondrial respiration and GSIS, NEFA exposed pancreatic islets were taken from microplate wells, homogenised in RIPA buffer and analysed for their DNA content using Quant-iT™ PicoGreen® dsDNA assay kit (life technologies) as described in section 2.8. DNA content was used to normalise data from oxygen uptake rates and insulin secretion assays.

5.2.9 Mitochondrial bioenergetics

Mitochondrial oxygen uptake rates, glucose sensitivity and coupling efficiency of oxidative phosphorylation were determined with an XF24 extracellular flux analyser as previously described in section 2.4. Briefly, NEFA-exposed islets were placed into an XF24 islet capture microplate at a density of 20-30 islets/ well in a total volume of 500 μL DMEM supplemented with 5.5 mM glucose. After 1 hr incubation in this medium at 37 °C under air, the microplate was transferred to a Seahorse XF24 extracellular flux analyser (maintained at 37 °C)

and after a 10-minute calibration, oxygen uptake rates were measured. Islet basal oxygen uptake rates were measured by a 4 loop cycle consisting of a 1-min mix, 2-min wait and 3-min prior to adding 28 mM glucose. Glucose-stimulated respiration was monitored for 8 further loop cycles, after which, 10 μg/ml oligomycin and a mixture of 2 μM rotenone and 2 μM antimycin A were added sequentially to, respectively, inhibit the mitochondrial ATP synthase or complex I and III of the electron transport chain.

5.2.10 Statistical analysis

Significance of mean differences was tested for by one-way ANOVA – applying Tukey's multiple comparison post-hoc analysis – using GraphPad Prism Version 6.0 for Mac OS X (GraphPad software, San Diego, CA, USA).

5.3 Results

5.3.1 Mitochondrial respiration of pancreatic islets

In canonical GSIS, the presence of high glucose stimulates an increase in mitochondrial respiration, leading to an elevation of the ATP/ADP ratio, providing a key signal for the triggering of insulin secretion [2] or suppression of glucagon secretion [192] from pancreatic β-cells and α-cells, respectively. Isolated pancreatic islets, indeed, increase their oxygen uptake rate 1.75-2.25 fold, when glucose is raised from 5.5 mM to 28 mM (Figure 5.1). This cellular respiratory response to glucose is unchanged in islets exposed to palmitate for

24 h (Figure 5.1A), but tends to be dampened to 1.5 fold after 48 h palmitate exposure (Figure 5.1B). As expected, the oxygen consumption rate of control and palmitate-exposed islets is inhibited by both oligomycin and a mixture of rotenone and antimycin A (Figure 5.1). Notably, this inhibition is slower in islets than in INS-1E cells (Figures 3A and 3B), which is likely due to the extended time it takes for these chemicals to successfully penetrate the islet cells [176]. The data shown in Figure 5.1 are normalised to the basal rate of respiration in the absence of glucose, an internally normalised function which cannot be used to confirm differences in basal or absolute mitochondrial respiratory activity. For these reasons, it is necessary to normalise oxygen uptake rates to a secondary parameter, for example, to islet DNA (Figure 5.2) [13]. Prior to normalisation it would be concluded that palmitate exposure has no effect on glucose sensitivity, since the rate of respiration after the glucose concentration is raised to 28 mM is similar between palmitate and BSA treated islets (Figure 5.2A). Once the data were normalised, however, it is revealed that palmitate lowers glucose-stimulated mitochondrial respiration from 65 pmol O_2/well/ min^{-1} x $ngDNA^{-1}$ to 35 pmol O_2/well/min^{-1} x $ngDNA^{-1}$ (Figure 5.2B). Normalising to DNA also makes it possible to make inferences about basal and non-mitochondrial respiratory oxygen uptake rates (Figure 5.3A). The absolute basal rate of islet mitochondrial respiration measured in the absence of glucose is about 15 pmol O_2 x min^{-1} x ng DNA^{-1} after subtracting non-mitochondrial

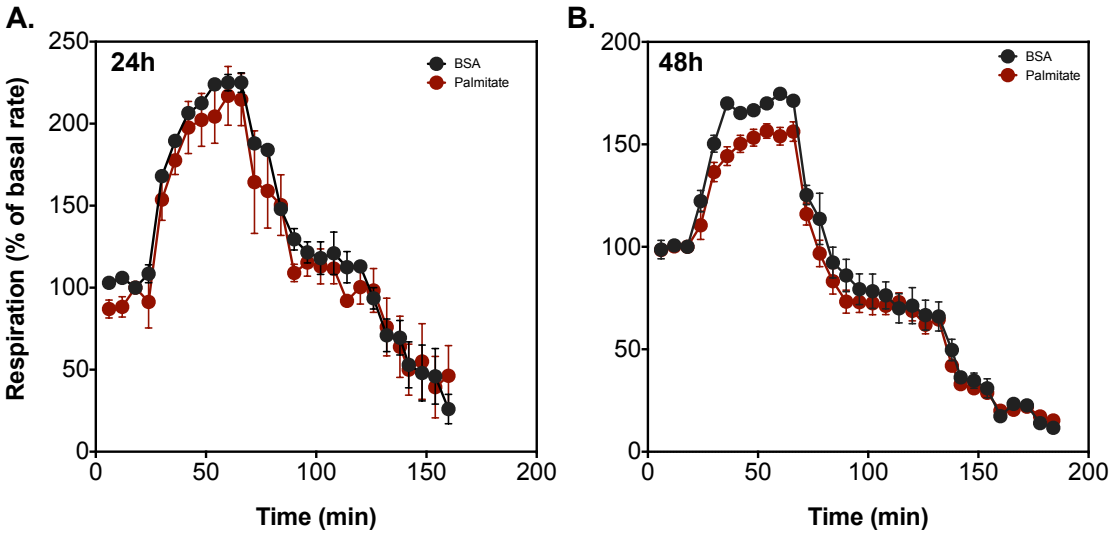

Figure 5.1 – Real-time detection of palmitate-induced mitochondrial dysfunction in isolated pancreatic islets

Typical oxygen uptake trace reflecting respiration of islets exposed for 24 hr (**A - 24h**) or 48 hr (**B - 48h**) to BSA-conjugated to palmitate or to BSA alone at 11 mM glucose. Islet oxygen uptake was measured as described in section 2.4 – 28 mM glucose (G28), 10 µg/mL oligomycin (OLI), and a mixture of 2 µM rotenone and 2 µM antimycin A (RA) were added as indicated. Data are means ± SEM of 3-4 separate wells from a single XF24 plate and are expressed as a percentage of basal respiration.

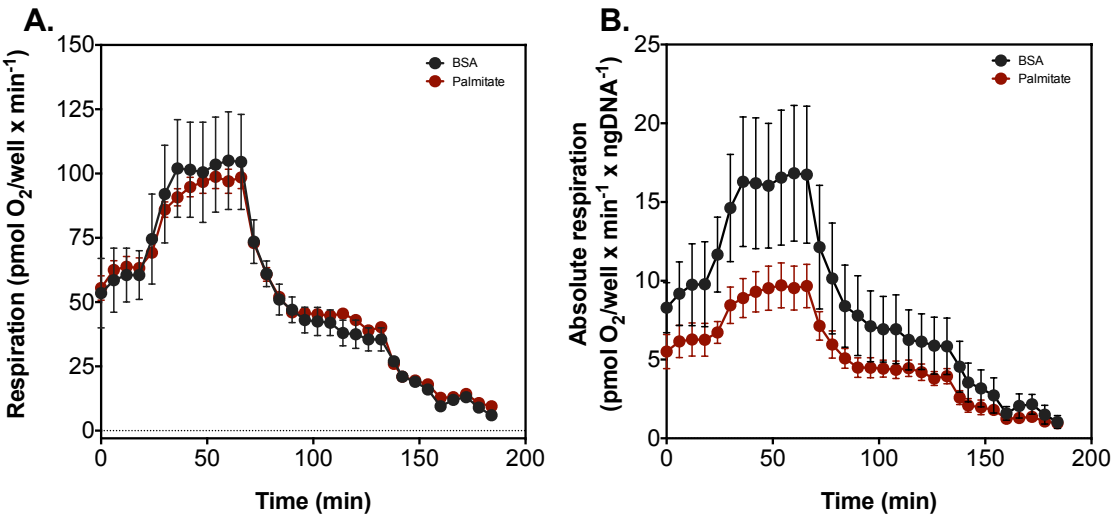

Figure 5.2 – Real-time detection of palmitate effects on mitochondrial respiration in isolated pancreatic islets

Typical oxygen uptake rates reflecting respiration of islets exposed for 48 hr to BSA-conjugated to palmitate or BSA alone at 11 mM glucose (**A**). Oxygen uptake rates normalised to DNA reflecting respiration of islets exposed for 48 hr to BSA-conjugated to palmitate or BSA alone at 11 mM glucose (**B**). Cellular oxygen uptake was measured as described in section 2.4. Data are means ± SEM of 2-4 separate wells from a single XF24 plate and are expressed as pmol O_2/well x min^{-1} or pmol O_2/well x min^{-1} x ng DNA^{-1} for (**A**) and (**B**) respectively.

respiration which is about 4 pmol O_2 x min^{-1} x ng DNA^{-1} (Figure 5.3A). Exposure to palmitate slightly decreases basal mitochondrial respiration to about 13 pmol O_2 x min^{-1} x ng DNA^{-1}, whilst palmitoleate plus or minus palmitate stimulates it a little, although none of these effects are statistically significant (Figure 5.3A). Furthermore, in agreement with observations in INS-1E cells (Figure 3.2A), non-mitochondrial respiration is unchanged in islets treated with NEFAs when exposed at high glucose (Figure 5.3A). In control islets, raising the glucose concentration from 5.5 mM to 28 mM glucose stimulates a 2.3-fold increase in mitochondrial respiration (Figure 5.3B). Palmitate exposure on the other hand lowers this stimulation to 1.7-fold (Figure 5.3B). Palmitoleate also lowers glucose-stimulated respiration in islets and in combination with palmitate does not influence the palmitate effect (Figure 5.3B). Notably the effects of palmitoleate plus or minus palmitate on glucose-sensitivity (Figure 5.3B) are not statistically significant from control islets and are most likely explained by the small increases in basal mitochondrial respiration (Figure 5.3A).

5.3.2 Coupling efficiency

Coupling efficiency of oxidative phosphorylation, which is defined as the proportion of respiration used to make ATP is an important mitochondrial bioenergetic parameter that can be estimated from the oligomycin-sensitive proportion of respiration (Figure 2.3). The coupling efficiency reported here is

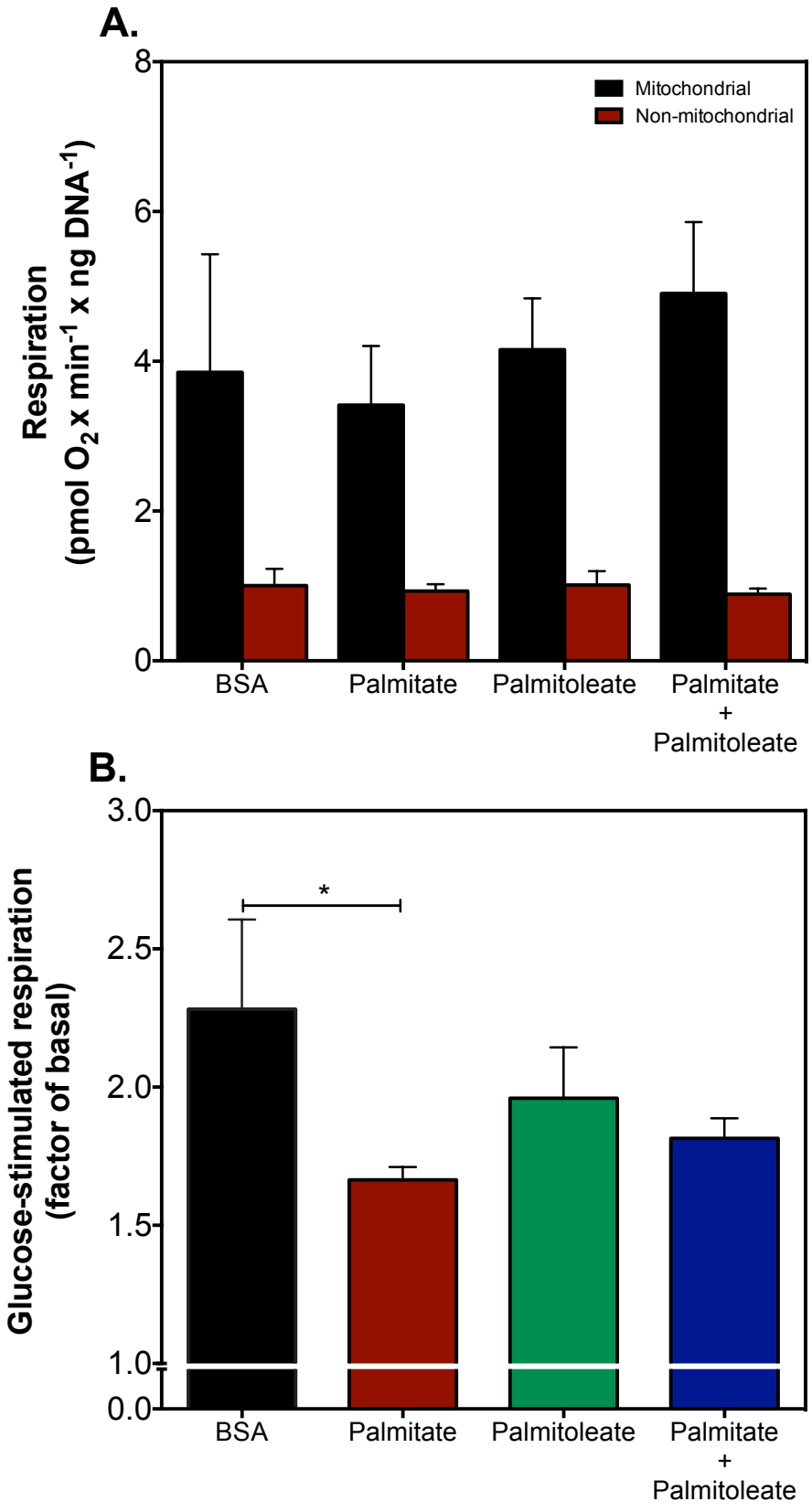

Figure 5.3 – Palmitate exposure at high glucose dampens the glucose-sensitivity of mitochondrial respiration in isolated pancreatic islets

Absolute basal mitochondrial and non-mitochondrial oxygen uptake rates (**A**) and glucose-sensitivity of mitochondrial respiration (**B**) were measured in pancreatic islets exposed for 48 hr to BSA-conjugated NEFAs or BSA alone at 11 mM glucose. Data are means ± SEM for two independent experiments that each involved three or four replicates per treatment. Statistical significance of mean differences was tested for by one-way ANOVA: $P < 0.05$.

estimated to be about 60% in control islets subjected to 28 mM glucose, suggesting that 40% of respiration is dissipated as heat via proton leak across the inner mitochondrial membrane (Figure 5.4). Importantly, this observation agrees with the coupling efficiency reported previously in INS-1E cells (Figure 3.3A) and in islets [176]. Interestingly, the coupling efficiency of islets subjected to 28 mM glucose is unaffected by NEFA exposure (Figure 5.4), which differs from INS-1E cells when 24 h exposure of palmitate and the combination of palmitate and palmitoleate lowers coupling efficiency (Figure 3.3A). To identify where these differences may arise, absolute respiration was determined from normalised oxygen uptake rates of NEFA exposed islets (Figure 5.5). Consistent with the effects of palmitate on the internally normalised respiratory response of islets to 28 mM glucose (Figure 5.3B), absolute mitochondrial respiration and respiration coupled to ADP phosphorylation tends to be lower in palmitate teated islets (Figure 5.5). Interestingly and different from INS-1E cells (Figure 3.4), respiration used to drive proton leak is also somewhat lower in palmitate treated pancreatic islets (Figure 5.5). Importantly, these small palmitate effects on absolute respiration rates in islets are not statistically significantly different from the BSA control or the other NEFA treatments. In contrast to palmitate, palmitoleate alone also has no effect on absolute mitochondrial respiration stimulated by 28 mM glucose (Figure 5.5). Importantly and unlike the situation in INS-1E cells (Figure 3.4), palmitoleate prevents the small defects of palmitate

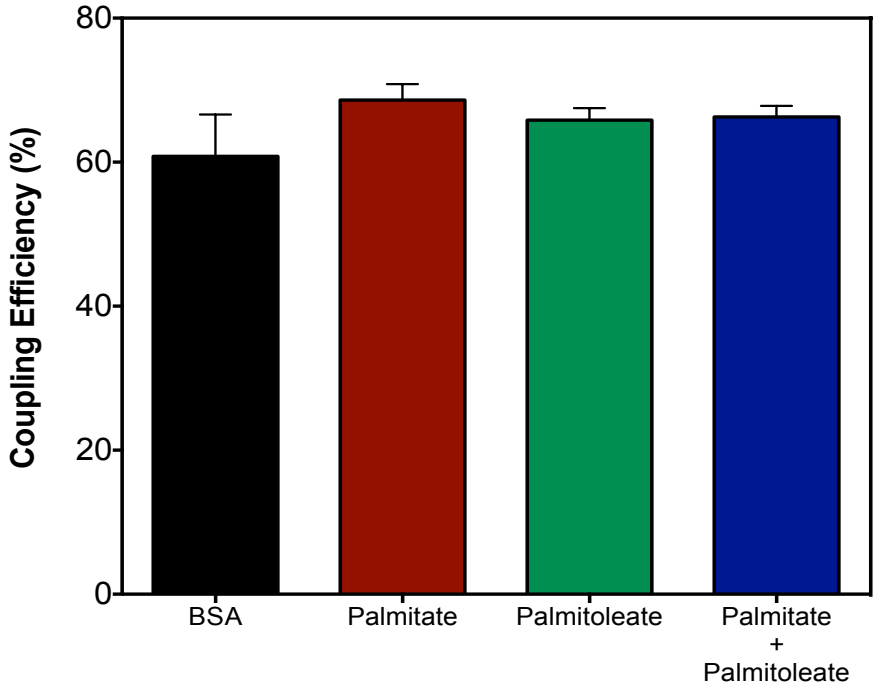

Figure 5.4 – Effect of NEFA exposure at high glucose on mitochondrial coupling efficiency in isolated pancreatic islets

Coupling efficiency of oxidative phosphorylation – assayed at 28 mM glucose, was calculated as the percentage of glucose-stimulated mitochondrial respiration that is sensitive to oligomycin in islets that had been exposed for 48 hr to BSA-conjugated NEFAs or BSA alone at 11 mM glucose. Data are means ± SEM from two independent experiments that each involved 3-4 replicates per treatment. Statistical significance of mean differences was tested for by one-way ANOVA - revealing no significant differences between conditions.

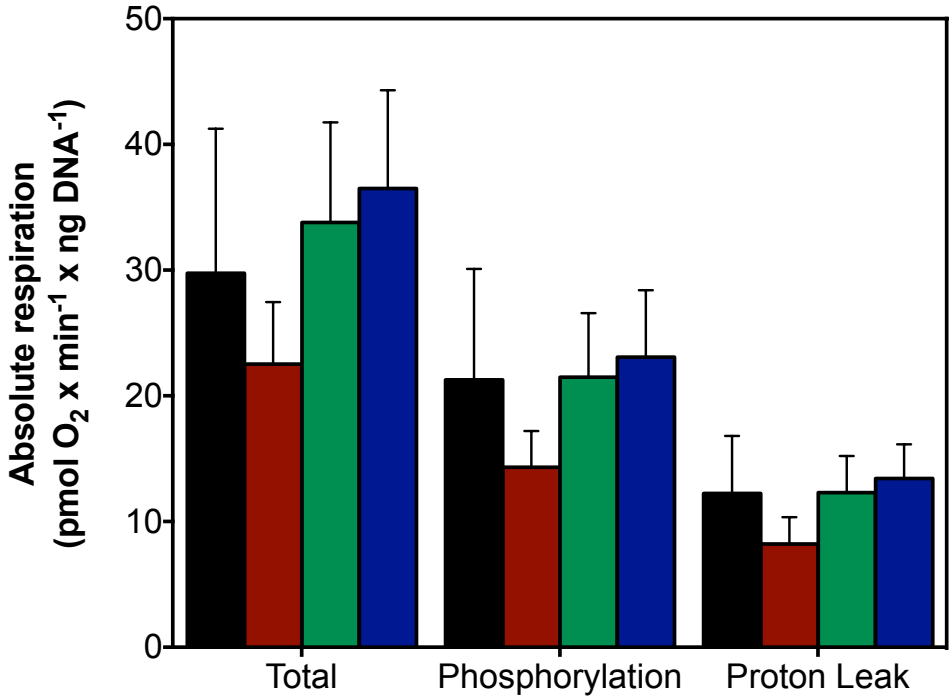

Figure 5.5 – Effects of NEFAs on absolute respiration

Absolute mitochondrial respiratory activity at 28 mM glucose (Total), absolute oligomycin-sensitive (Phosphorylation) and oligomycin-resistant (Proton Leak) activities were calculated from DNA content-normalised oxygen uptake rates (Figure 5.2B). Data are means ± S.E.M from two separate experiments that each involved 3-4 replicates per treatment. Statistical significance of differences between groups was tested for by two-way ANOVA - revealing no significant differences between conditions.

on glucose-stimulated mitochondrial oxidative phosphorylation (Figure 5.5).

5.3.3 Glucose-stimulated insulin secretion and insulin content

To asses if palmitate-induced defects in glucose-stimulated mitochondrial respiration relate to other lipotoxic effects, as is the case in INS-1E cells (Figure 3.7), the insulin secretory capacity of pancreatic islets exposed to NEFAs was measured (Figure 5.6). Basal insulin secretion in control islets is stimulated 10-fold from 0.25 ng insulin^{-1} x ng DNA^{-1} to 2.5 ng insulin^{-1} x ng DNA^{-1} by raising the glucose concentration from 5.5 mM to 28 mM (Figure 5.6), which is comparable with published data [13,14]. In islets exposed to palmitate basal insulin secretion is amplified to 0.6 ng insulin^{-1} x ng DNA^{-1} (Figure 5.6A). Interestingly, by increasing the glucose concentration to 28 mM in palmitate treated islets, insulin secretion is only stimulated 3-fold to 2.0 ng insulin^{-1} x ng DNA^{-1} (Figure 5.6B). In contrast, palmitoleate does not alter basal insulin secretion (Figure 5.6A). In combination with palmitate, palmitoleate prevents the palmitate-induced potentiation of basal insulin secretion (Figure 5.6A). When stimulated with high glucose, however, insulin secretion is attenuated by palmitoleate alone and when combined with palmitate (Figure 5.6B) causes a significant decrease in GSIS (Figure 5.6C). Furthermore, palmitate and palmitoleate (with or without palmitate) decrease the overall insulin content in islets (Figure 5.7), although the dampening effect of palmitoleate is not statistically significant.

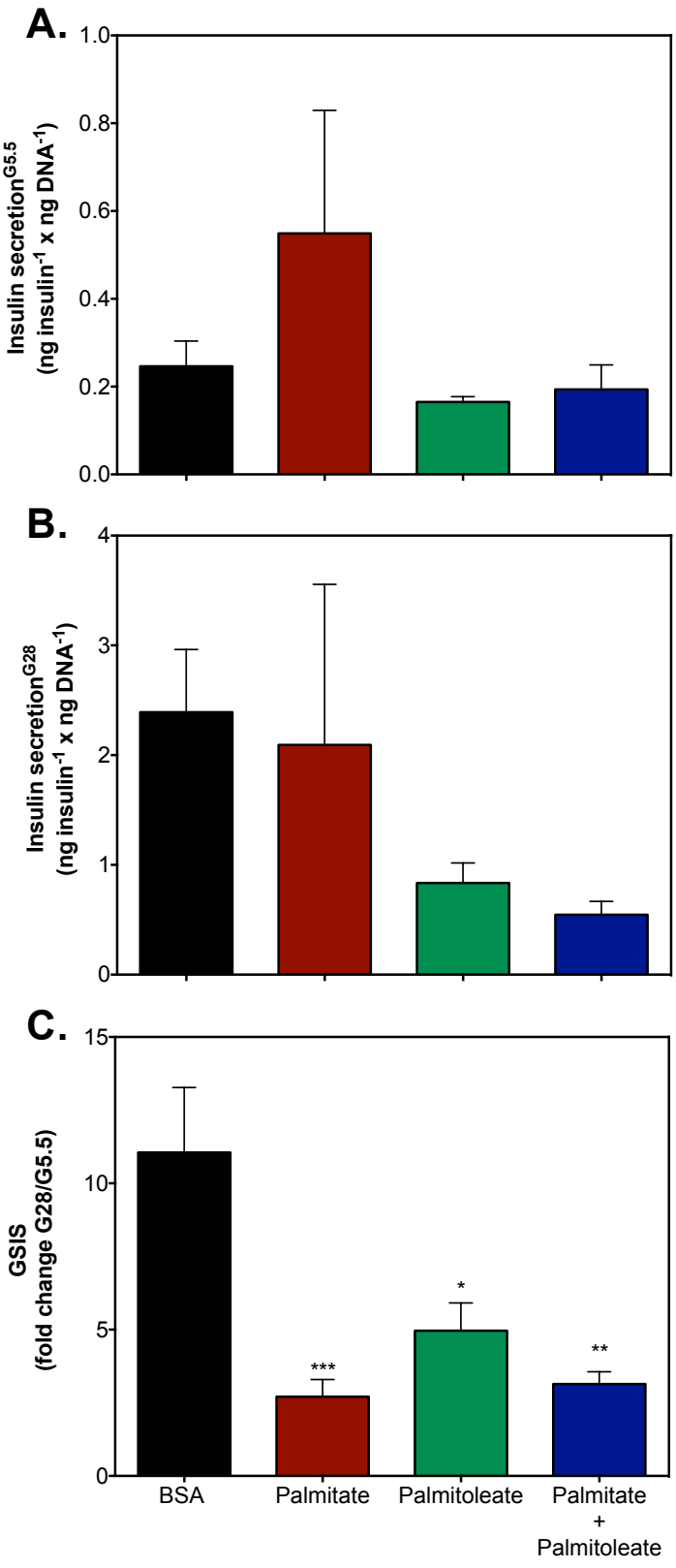

Figure 5.6 – NEFA exposure at high glucose attenuates glucose-stimulated insulin secretion of pancreatic islets

Basal insulin secretion measured in isolated pancreatic islets exposed for 48 hr to BSA-conjugated NEFAs or BSA alone in the presence of 11 mM glucose (**A**). Insulin secretion measured in isolated pancreatic islets exposed for 48 hr to BSA-conjugated NEFAs or BSA alone in the presence of high glucose stimulated with 28 mM glucose (**C**). GSIS expressed as the G28/G5.5 insulin secretion ratio (cf. **B** and **C**) (**A**). Data are means ± SEM of two independent experiments that involved 3-4 replicates per treatment. Statistical significance of mean differences was tested for by one-way ANOVA: * $P < 0.05$; ** $P < 0.01$; *** $P < 0.001$ differs from the BSA condition.

The GSIS defects caused by palmitate in islets (Figure 5.6C) agree with those found in INS-1E cells (Figure 3.6B). Moreover, these data confirm the lack of palmitoleate protection on palmitate-induced GSIS defects (Figure 3.6B). Discrepant with INS-1E cell studies (Figure 3.6B), exposure to palmitoleate alone also dampens islet GSIS (Figure 5.6C). Based on the internally normalised parameters shown in Figures 5.3B and 5.6C it appears that the NEFA effects on GSIS mirror the NEFA effects on glucose stimulated mitochondrial respiration (Figure 5.8A). It is important to note, however, that when these parameters are dissected into component rates, the effects of NEFAs on insulin secretion are

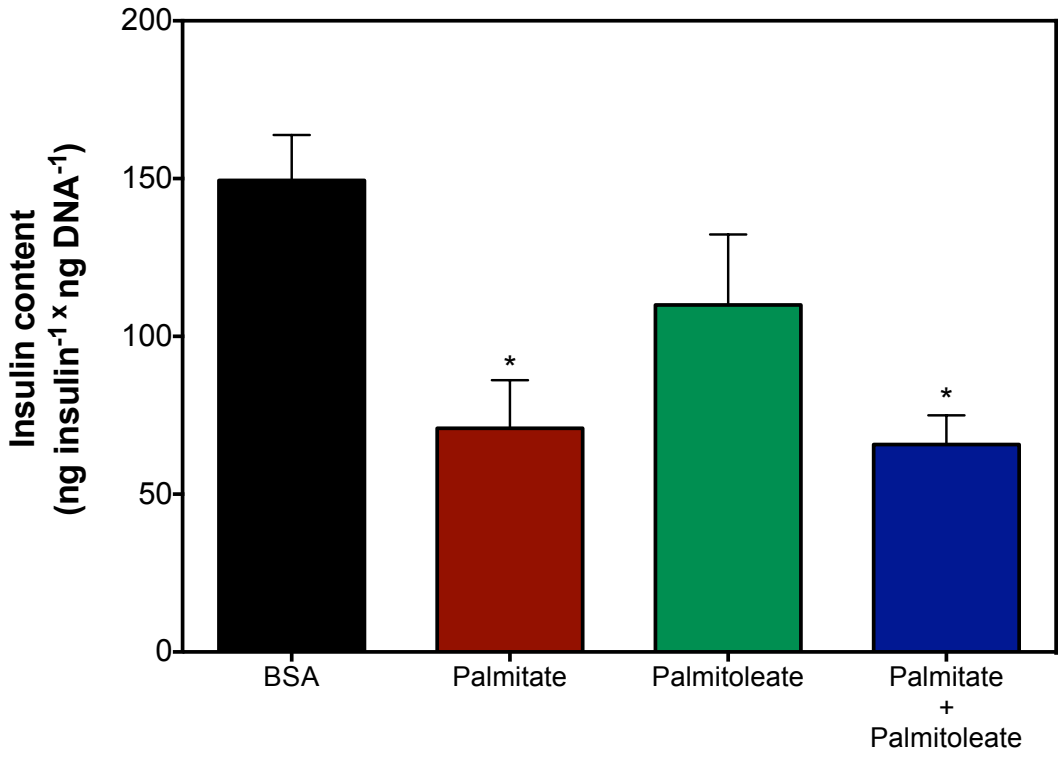

Figure 5.7 – Palmitate exposure at high glucose reduces insulin content in pancreatic islets

Total insulin content measured in homogenised pancreatic islets exposed for 48 hr to BSA-conjugated NEFAs or BSA alone at 11 mM glucose was normalised to DNA content. Data are means ± SEM of two independent experiments that involved 3-4 replicates per treatment. Statistical significance of mean differences was tested for by one-way ANOVA: * $P < 0.05$ differs from the BSA condition.

noticeably disconnected from the NEFA effects on absolute mitochondrial respiration (Figure 5.8B and 5.8C). The lack of NEFA effect on the coupling efficiency of oxidative phosphorylation (Figure 5.4) also supports the disconnection between GSIS and mitochondrial activity.

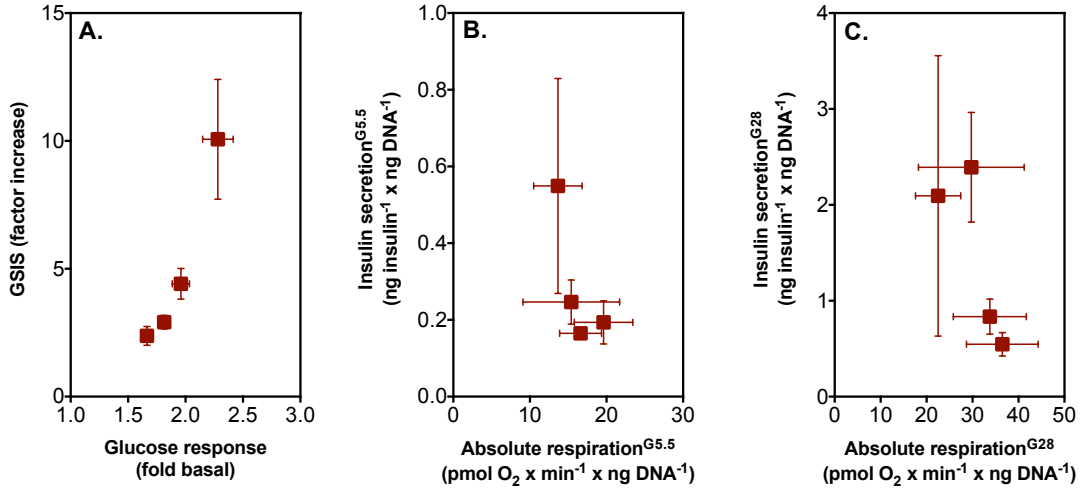

Figure 5.8 – Mitochondrial glucose-stimulated respiration as a predictor of glucose-stimulated insulin secretion

G28/G5.5 GSIS ratio (Figure 5.6C) plotted as a correlation with mitochondrial respiration stimulated with 28 mM glucose (Figure 5.3B) in pancreatic islets exposed for 48 hr to BSA-conjugated NEFAs or BSA alone at 11 mM glucose (**A**). Basal insulin secretion (Figure 5.6A) plotted as a correlation with absolute basal mitochondrial respiration (Figure 5.3A) in pancreatic islets exposed for 48 hr to BSA-conjugated NEFAs or BSA alone at 11 mM glucose (**B**). Insulin secreted after raising the glucose concentration to 28 mM (Figure 5.6B) plotted as a correlation with absolute respiration in the presence of 28 mM glucose (Figure 5.5) in pancreatic islets exposed for 48 hr to BSA-conjugated NEFAs or BSA alone at 11 mM glucose (**C**). Data are means ± SEM of two independent experiments that involved 3-4 replicates per treatment.

5.4 Discussion

5.4.1 Palmitate-induced mitochondrial dysfunction

The functional bioenergetic analysis in pancreatic islets confirms that palmitate impairs glucose-stimulated respiration (Figure 5.3B) as reported in INS-1E cells (Figure 3.2B). The effects of palmitate on islet respiration were observed after a longer exposure period of 48 h (Figure 5.3B), since after 24 h there was no clear deleterious effect of palmitate on mitochondrial respiration (Figure 5.1).

Interestingly and discrepant with INS-1E cells (Figure 3.3A), palmitate has no significant effect on the coupling efficiency of oxidative phosphorylation in pancreatic islets (Figure 5.4). The lack of effect on coupling efficiency by palmitate is explained by the amount of respiration that is used to drive ATP synthesis and proton leak (Figure 5.5). For example, in INS-1E cells the palmitate-induced impairment of absolute mitochondrial respiration in response to 28 mM glucose is entirely due to effects on ADP-phosphorylation (Figure 3.4), meaning that the percentage of respiration that is coupled to ATP synthesis (coupling efficiency) is lowered by palmitate exposure. In contrast, in pancreatic islets, the dampening effect caused by palmitate on absolute mitochondrial respiration in response to 28 mM glucose is linked to a decrease in both ADP phosphorylation and proton leak (Figure 5.5). This suggests that under conditions that alter the rate of glucose-stimulated mitochondrial respiration, for example in the presence of palmitate, islets are able to compensate for a lower energy supply by lowering proton leak in order to maintain their coupling efficiency.

On the internally normalised parameter for glucose-sensitivity, it appears that palmitoleate also tends to lower the sensitivity of islets to glucose and does not protect against the palmitate effects (Figure 5.3B). However, it is important to point out that this observation only occurs because palmitoleate, alone or plus palmitate, slightly increases basal mitochondrial respiration (Figure 5.3A). This

is further supported by the lack of effect of palmitoleate on absolute mitochondrial respiration in response to 28 mM glucose (Figure 5.5) and confirmed in previous findings using INS-1E cells (Figure 3.4). Therefore in the presence of palmitate, palmitoleate tends to prevent against the deleterious effect of palmitate on glucose-stimulated mitochondrial respiration. This suggests a protective role of palmitoleate against palmitate-induced impairment of mitochondrial respiration in pancreatic islets, which differs from the effects of palmitoleate on mitochondrial respiration in palmitate exposed INS-1E cells (Figure 3.4).

5.4.2 Fatty acid-induced insulin secretion defects

Insights into the effect of palmitate exposure on islet GSIS is considerable [65,86,95]. However, effects of other NEFAs, including mono-unsaturated fatty acids like palmitoleate, is scarce [99]. Consistent with findings in INS-1E cells (Figure 3.6B) and islets (Figure 5.6C), prolonged exposure of palmitate at high glucose significantly lowers GSIS. Importantly the dampening effect of palmitate on GSIS in islets is explained here by an amplifying effect of palmitate on basal insulin secretion (Figure 5.6A). This is demonstrated by the lack of palmitate effect on insulin secretion at high glucose (Figure 5.6B), but a clear increase in basal insulin secretion (Figure 5.6A). Therefore, GSIS is lower in palmitate treated islets as a consequence of amplified basal insulin secretion (Figure 5.6C).

Interestingly, palmitoleate, the mono-unsaturated equivalent of palmitate, also impairs GSIS (Figure 5.6C) and does not protect against the palmitate-induced GSIS defects (Figure 5.6C). Importantly, palmitoleate-induced impairment of GSIS cannot be explained by changes in basal insulin secretion, since basal insulin secretion is not affected by palmitoleate exposure (Figure 5.6A). Therefore the mechanisms leading to GSIS impairment in islets exposed to palmitoleate, alone or plus palmitate are unrelated to palmitate-induced GSIS defects. Interestingly, the GSIS defects in palmitoleate treated islets reported here disagree with previous findings in islets [99] and in INS-1E cells (Figure 3.6B). Furthermore, it has been reported that palmitoleate has a cytoprotective role in islets by ameliorating palmitate-induced impairment of GSIS [99]. To some extent palmitoleate does have a protective role against palmitate-induced GSIS defects in islets, since it prevents the potentiation of basal insulin secretion (Figure 5.6A). However in this study palmitoleate alone also dampens GSIS (Figure 5.6C). The discrepancies between data shown here and previously reported findings most likely arise due to experimental differences. In saying that, it is worth note that many publications investigating the long term effects of NEFAs on islet GSIS use islet number to normalise insulin secretion data. This normalisation assumes islet homogeneity, which is very unlikely due to the considerable variation of glucose responsiveness between islet preparations [193,194]. Furthermore, it is likely that chronic NEFA exposure promotes β-cell

death [118], thereby reducing the number of viable β-cells capable of secreting insulin. Some of these issues can be resolved by normalising to DNA content, however, even normalising to cellular DNA has limitations. For example, DNA is measured in every cell of the islet and despite the importance of paracrine signaling [195], only the β-cells contribute directly to insulin secretion. Additionally, DNA will also be measured in dead cells that do not contribute to islet function, presenting a further issue when investigating glucolipotoxic effects that likely result in the loss of β-cell viability [62,118]. Consequently, it is important to note that any parameter normalised to DNA will be somewhat underestimated under conditions that lead to a loss in cell viability.

5.4.3 Glucolipotoxic-induced defects in insulin secretion are disconnected from mitochondrial dysfunction

Until recently [84,176] it has not been possible to investigate the bioenergetics of intact pancreatic islets in real-time. Moreover, it has not been possible to measure basal respiration, glucose-stimulated respiration, coupling efficiency of oxidative phosphorylation and non-mitochondrial respiration in the same experiment using the same yield of islets. Indeed, measuring islet bioenergetics yields important insights into islet function but it must be noted that pancreatic islets are composed of many different cell types, which all contribute to the respiratory rate. Therefore when making inferences between islet mitochondrial respiration and GSIS, which is specific to β-cells this needs to be considered. In

saying that, pancreatic β-cells comprise about 60%-85% of the total islet cell yield [196]. Consequently, any lipotoxic effect on islet bioenergetics will likely be largely due to β-cell effects.

It has previously been reported that prolonged palmitate exposure significantly impairs GSIS in rodent [14,118] and human isolated islets [62,66]. Until now is was suggested that palmitate exposure leads to dampened GSIS due to impaired insulin secretion at high glucose [14,67]. Such defects in GSIS have also been linked with mitochondrial dysfunction [14,67](Figure 3.7). The findings in this chapter, however, provides new evidence that disconnects a causative role of mitochondria in palmitate-induced impairment of GSIS. It is shown here that palmitate lowers GSIS as a result of increased basal insulin secretion (Figure 5.6A). In line with short-term palmitate effects [13] it is revealed that prolonged palmitate exposure amplifies basal insulin secretion independently of mitochondrial activity, since palmitate has no effect on basal mitochondrial respiration (Figure 5.3). It must be noted that the potentiation of prolonged palmitate on basal insulin secretion is consistent with other studies in murine [14] and human islets [95] and in islets from mice fed on a high fat diet [86]. However, until now, these effects have not been discussed explicitly. It has also been reported that palmitate dampens insulin secretion at high glucose [14,95], however in this set of experiments no significant effect of palmitate was seen on islet insulin secretion when the glucose concentration was raised to 28

mM (Figure 5.6B). Such discrepancies are likely explained by experimental differences.

Importantly, palmitoleate, alone or with palmitate, also dampens GSIS in islets. However, it must be noted that this dampening effect is not due to increased basal insulin secretion (Figure 5.6A). Instead these effects occur due to the attenuation of insulin secretion at high glucose (Figure 5.6B). The GSIS defects caused by palmitoleate, alone or with palmitate are also disconnected from mitochondrial activity, since absolute glucose-stimulated mitochondrial respiration is unaffected in these islets (Figure 5.5). Indeed the data in Figure 5.8A reveal a distinct association between glucose-stimulated mitochondrial respiration and GSIS, however when these parameters are replotted with specific component rates this correlation is abolished (Figure 5.8B and 5.8C).

5.4.4 Glucolipotoxic-induced impairment of insulin content in pancreatic islets

In addition to effects on insulin secretion, palmitate also significantly lowers the total insulin content in pancreatic islets (Figure 5.7). These data provide evidence against using insulin content as a parameter to normalise islet data [82]. Palmitoleate dose not prevent against the palmitate effect and palmitoleate alone also tends to decrease islet insulin content (Figure 5.7). Unlike insulin secretion defects, the mechanism that leads to palmitate-induced effects on islet insulin content (Figure 5.7) might result from mitochondrial dysfunction. For

example, in palmitate treated islets, the rate of glucose-stimulated mitochondrial respiration which is linked to ADP-phosphorylation is attenuated (Figure 5.5), suggesting that the intracellular levels of ATP and thus energy supply could be lower in these islets. Under these conditions, it is possible that the rate of protein and/or DNA synthesis slows down, since these processes are most sensitive to changes in energy supply [197]. Therefore, in the presence of palmitate, when energy and ATP supply is compromised, islet β-cells might reallocate their energy demands to processes that are essential for the immediate needs of the cell and as a result shut down insulin biosynthesis. In support of this model, it has previously been reported that protein synthesis is down regulated by palmitate in pancreatic murine islets [14]. The effects of palmitoleate, alone or in the presence of palmitate, on islet insulin content, however, are unlikely related to mitochondrial effects, since glucose-stimulated mitochondrial respiration or ADP-phosphorylation is not affected under these conditions (Figure 5.5). Alternatively, it is possible that NEFAs lower islet insulin content through transcriptional effects, since it has been reported that prolonged exposure of NEFAs impairs insulin gene expression in the presence of high glucose [18]. This NEFA impairment arises due to inhibition of glucose-induced activation of the insulin promoter, which is mediated by *de novo* ceramide generation in β-cells [63]. Although the exact mechanisms whereby ceramide affects insulin gene transcription remain to be determined exclusively,

this evidence supports an involvement of ceramide in the mechanism by the way in which NEFAs mediate changes in islet insulin content.

5.4.5 Potential mechanisms of palmitate-induced mitochondrial dysfunction

It was reported previously that the negative impact of palmitate on glucose oxidation and GSIS in pancreatic islets is a result of increased fatty acid β oxidation, which was explained by the Randle cycle [68]. As a consequence of this, glucose metabolism is halted and by a negative feedback loop, the activity of pyruvate dehydrogenase is inhibited [67]. In the context of glucolipotoxicity, this is unlikely, in view of the fact that when glucose levels are high, the oxidation of long-chain fatty acids is limited due to the inhibition of CPT-1 via the accumulation of malonyl CoA [16]. Furthermore, under conditions that lead to enhanced fatty acid β oxidation, for example when glucose levels are low, palmitate no longer impairs β-cell function (Figures 3.6D and 3.9). Moreover, mitochondrial dysfunction can be promoted in β-cells by preventing fatty acid β oxidation (Figures 3.9A and 3.9B). Indeed, it is possible that pancreatic islets act differently in response to these glucolipotoxic conditions and therefore, to specifically exclude a role of fatty acid β oxidation in these phenotypes, experiments need to be performed on palmitate treated islets that have dampened and/or enhanced CPT-1 activity.

5.5 Conclusions

Cellular bioenergetics yield powerful insights into pancreatic islet function which is highlighted here by confirming some important glucolipotoxic phenotypes that have previously been discovered in model cell lines. Probing mitochondrial energy metabolism in pancreatic islets has also presented some distinct differences between different systems used for the study of pancreatic β-cell glucolipotoxicity. Importantly, data here provides new evidence to suggest that palmitate-induced impairment of GSIS is linked to a amplification effect on basal insulin secretion. Although the mechanisms of this apparent potentiation are unknown at present, data here likely suggest a possible disconnection between NEFA-induced GSIS defects and mitochondrial dysfunction. Despite these interesting findings it is important to note that the pancreatic islets used in this study were obtained from a rodent species and there are distinct differences between rodent and human islets. To make meaningful physiological inferences about human Type 2 diabetes from this data it is recommended that some of these observations are confirmed using isolated human islets.

Chapter 6

GENERAL DISCUSSION AND FUTURE WORK

The aim of this project was to explore the involvement of mitochondria in pancreatic β-cell glucolipotoxicity. By investigating mitochondrial metabolism in both INS-1E cells and pancreatic islets, this study has provided novel insights into the role of mitochondria in pancreatic β-cell dysfunction and destruction. In this study the exploitation of INS-1E cells and pancreatic islets have provided further understanding of the effects of NEFAs on mitochondrial bioenergetics. For example, it is revealed that prolonged exposure of exogenous palmitate in the presence of high glucose significantly impairs glucose sensitivity (Figure 3.2), ATP-coupled respiration (Figure 3.3) and GSIS (Figure 3.6B) in INS-1E cells. Importantly, the physiological relevance of INS-1E cells is confirmed, since glucose sensitivity (Figure 5.3B) and GSIS (Figure 5.6C) are also significantly dampened by prolonged palmitate exposure in pancreatic islets. By comparing palmitate-induced mitochondrial dysfunction (Figures 3.4 and 5.5) with GSIS defects (Figures 3.6 and 5.6) new light is shed on the mechanisms responsible for palmitate impairment of pancreatic β-cell function. Palmitate also significantly lowers INS-1E cell viability (Figure 4.6) which inversely correlates with the production of mitochondrial ROS (Figure 4.1). This inverse correlation suggests that NEFA-induced mitochondrial ROS are associated with pancreatic β-cell survival. Exploring the involvement of UCP2 in these glucolipotoxic phenotypes reveals that UCP2 neither regulates or protects against palmitate-induced production of mitochondrial ROS or loss in β-cell viability (Figures 4.3

and 4.5). New insights into the role of cytoprotection in pancreatic β-cells is also revealed, since palmitoleate, the mono-unsaturated counterpart of palmitate ameliorates the adverse effects of palmitate on β-cell viability (Figure 3.8 and 4.5), mitochondrial ROS production (Figures 3.5 and 4.4), glucose-stimulated mitochondrial oxidative phosphorylation (Figure 5.5) and basal insulin secretion (Figure 5.6). Although the mechanism of cytoprotection is unclear at present, it is shown here that UCP2 attenuates palmitoleate protection against palmitate-induced mitochondrial ROS production and loss in β-cell viability (Figures 4.4 and 4.5). Suggesting a possible role of UCP2 in the regulation of cytoprotection exerted by mono-unsaturated fatty acids against cytotoxic-induced stress.

6.1 Effects of fatty acids on mitochondrial function and glucose-stimulated insulin secretion

Although the concept of glucolipotoxicity in pancreatic β-cells was reported over a decade ago [198], the involvement of mitochondria in this phenomenon has not been explored in great detail. It is reported here that glucose-stimulated mitochondrial respiration (Figure 3.2 and 5.3) and ATP-coupled respiration (Figure 3.4) is dampened by prolonged palmitate exposure, demonstrating that mitochondrial dysfunction might contribute to NEFA-induced GSIS defects (Figures 3.6B and 5.6C). In agreement with the concept of glucolipotoxicity [18], mitochondrial defects only appear after cells are treated for prolonged periods

with both high levels of NEFAs and glucose (Figures 3.2 and 5.1). The glucose permissibility of palmitate toxicity is supported by the lack of mitochondrial impairment in cells treated with NEFAs at low glucose (Figure 3.9). Interestingly, mitochondrial defects can be induced under conditions of NEFA exposure at low glucose by restricting fatty acid β oxidation (Figure 3.9). Although the exact mechanisms responsible for NEFA-induced impairment of glucose-fueled oxidative phosphorylation and subsequent β-function are still unclear at present, these data exclude a role for mitochondrial β oxidation in NEFA-induced β-cell dysfunction.

In chapter 3 and 5 it was demonstrated that NEFA-induced defects in mitochondrial function positively correlate with NEFA-induced GSIS defects (Figure 3.7 and 5.8A). However, by separating out the GSIS components (Figure 5.6A and 5.6B) it is revealed that palmitate-induced GSIS defects arise due to a potentiation effect of palmitate on insulin secretion at low glucose (Figure 5.6A). In agreement with the literature [13] and unpublished data in INS-1E cells (Hirschberg Jensen and Affourtit, unpublished), the apparent palmitate potentiation is not related to mitochondrial activity (Figure 5.3A and 5.8B). In support of a disconnection between mitochondrial dysfunction and GSIS defects, treatment of pancreatic islets with palmitoleate alone, or with palmitate, significantly dampens GSIS without altering mitochondrial respiration (Figure 5.5). Moreover, when the absolute component rates of

insulin secretion and mitochondrial respiration at high glucose are plotted against each other (Figure 5.8B and 5.8C), the correlation between mitochondrial oxidative phosphorylation and insulin secretion is no longer evident. Although the exact mechanisms responsible for these NEFA-induced phenotypes are yet to be determined conclusively, the lack of palmitate effect on insulin secretion at high glucose (Figure 5.6B) provides evidence that disagrees with an effect on the exocytotic mechanisms of insulin secretion as suggested previously [93]. To firmly establish the effects of palmitate on GSIS, the mechanism responsible for the potentiation of insulin secretion at low glucose needs to be elucidated.

Unlike insulin secretion defects, the mechanism that leads to NEFA-induced effects on islet insulin content (Figure 5.7) might result from mitochondrial defects. For example, it is possible that under conditions that lower ATP supply, protein and/or DNA synthesis is halted, since these processes are most sensitive to changes in ATP [197]. Therefore, in the presence of NEFAs, islet β-cells might reallocate their energy demands to processes that are essential for the immediate needs of the cell and as a result shut down insulin biosynthesis. It is not clear, however, if the effects of palmitate on glucose-stimulated respiration (Figure 5.3) occur before or after the effects on insulin content. New findings using INS-1E cells suggests that the ATP/ADP ratio in β-cells controls both ATP demand and supply processes (Alberts and Affourtit, unpublished). With this

in mind, it is therefore possible that NEFAs lower ATP consuming processes, for example by impairing insulin biosynthesis. In consequence, the ATP/ADP ratio will increase and limit substrate oxidation. Therefore, the effects of palmitate on glucose-stimulated mitochondrial oxidative phosphorylation might be secondary to effects on protein synthesis. How exactly NEFAs impair insulin biosynthesis is not clear, but mechanisms involving transcriptional effects on insulin gene expression have been investigated [18]. More specifically, it has been reported that NEFAs prevent a glucose-induced activation of the insulin promoter [63]. Although the exact mechanisms of this impairment remain to be determined exclusively, evidence supports an involvement of ceramide in NEFA effects on insulin gene expression [63].

To confirm the physiological relevance of the reported NEFA-induced mitochondrial dysfunction and GSIS defects in INS-1E cells (Chapter 3), the exogenous exposure of NEFAs to mouse pancreatic islets was explored (Chapter 5). In contrast to INS-1E cells, palmitate only causes a dampening effect on the glucose sensitivity in islets (Figure 5.3), since coupling efficiency is unchanged (Figure 5.4). Moreover, in islets, palmitoleate alone, or in combination with palmitate, tend to increase basal mitochondrial respiration (Figure 5.3). Different from INS-1E cells palmitoleate prevents the deleterious effects of palmitate on mitochondrial dysfunction (Figure 5.5). Palmitoleate alone also significantly dampens GSIS in islets (Figure 5.6). Clearly, there are

important differences between using pancreatic islets and INS-1E cells as models for pancreatic β-cell glucolipotoxicity that need to be considered when making physiological inferences from data obtained using immortal cell lines.

It is not clear where the discrepancies between these two model systems arise, but it is possibly due to the differences in the time dependency of glucolipotoxicity in pancreatic islets (48 h) compared with INS-1E cells (24 h). It is likely, however, that pancreatic islets are better at coping with conditions that might otherwise be toxic to INS-1E cells. For example, when glucose oxidation is dampened by palmitate (Figure 5.3), it appears that islets respond by lowering mitochondrial uncoupling to ensure that ATP synthesis is maintained at a higher rate under conditions of decreased substrate oxidation (Figure 5.5). This would explain the differences in coupling efficiency between NEFA exposed INS-1E cells (Figure 3.3A) and islets (Figure 5.4). Although this is just speculation, it is supported by the slightly lower amount of respiration used to drive proton leak in palmitate treated islets (Figure 5.5). Glucolipotoxic effects on mitochondrial function in islets might also be confounded by the contribution of other islet cells [90]. However, until new methods are available to deconvolute islet cell bioenergetics it is not possible to normalise for such β-cell respiration specifically. Due to the abundance of β-cells in islets, it is plausible to assume that the rates of oxygen uptake measured in whole islets is predominantly associated with the β-cells [196], and thus any mitochondrial

phenotype is driven by this predominance. However, testing this experimentally is the desired approach. One possible way to differentiate between islet cell mitochondrial respiration would be to specifically inhibit β-cell mitochondrial respiration pharmacologically. This might be achieved in islets by using alloxan, a glucose analogue that is preferentially taken up into cells expressing GLUT-2, which is specifically expressed in islet β-cells [199]. Upon entry into the cell cytosol, alloxan rapidly (within 1 min) and selectively inhibits glucokinase activity, shutting down glucose oxidation and ATP synthesis [199]. Thereby, when probing mitochondrial respiration of islets in real-time, alloxan could be added to selectively inhibit mitochondrial β-cell respiration. This method does however, assume that glucose is the only substrate being used to drive mitochondrial oxidative phosphorylation and that the stability of alloxan is maintained prior to its addition.

6.2 Uncoupling protein-2 in pancreatic β-cells

The physiological function of UCP2 is heavily disputed and its activity in glucolipotoxicity is just as confusing. Since the discovery of UCP2 in pancreatic β-cells [87], UCP2 has been connected with the excessive proton leak that is observed in pancreatic β-cells [140]. However, not everyone is in agreement with an uncoupling function of UCP2 as its name implies and despite considerable efforts, the physiological and pathophysiological role of UCP2 in β-cells is still heavily debated [18]. The involvement of UCP2 in

glucolipotoxicity is also contentious [18] and several functional models have been proposed, including, roles in β-cell pathology and consequent development of Type 2 diabetes [85,86], and roles in protecting β-cells against oxidative stress [82]. Such fundamentally different functions suggest opposing roles for the involvement of UCP2 in glucolipotoxicity: a pathological model that predicts UCP2 is necessary for palmitate-provoked β-cell dysfunction, and a protective model that predicts UCP2 prevents such β-cell deterioration.

Although the activity of UCP2 in relation to cellular bioenergetics was not probed directly in these studies, it is plausible to speculate that UCP2 might be involved in palmitate toxicity [200]. Since the palmitate-induced impairment of glucose-stimulated respiration (Figures 3.2B and 5.3B) and GSIS (Figures 3.6B and 5.6C) shown here agree with a pathological role of UCP2 in β-cells [200]. That being said, if UCP2 contributes to proton leak in β-cells as suggested previously [91], the lack of palmitate effect on proton leak (Figures 3.4 and 5.5) appose such a pathological role of a β-cell UCP2. In agreement with these proton leak effects, NEFAs do not affect the expression level of UCP2 in INS-1E cells (Figure 4.2). Instead it might be argued that UCP2 has a protective function in β-cells by preventing the excessive build up of mitochondrial ROS [82, 179, 201]. However, the knockdown of UCP2 in INS-1E cells does not regulate or protect against NEFA-induced mitochondrial ROS (Figure 4.3). Alternatively, a new function of UCP2 has recently been reported [80], which suggests that

UCP2 regulates mitochondrial substrate oxidation by acting as a mitochondrial metabolite transporter of specific four-carbon (C4) dicarboxylate TCA cycle intermediates [80]. This suggests that UCP2 negatively controls the oxidation of acetyl-CoA–producing substrates via the TCA cycle and thus lowers the redox pressure on the mitochondrial respiratory chain and the ATP:ADP ratio [80]. With respect to this novel UCP2 function, in the face of elevated glucose and NEFA levels, UCP2 might have a protective role and transport C4 metabolites out of the mitochondria in order to decrease mitochondrial oxidative phosphorylation in response to glucose and increase fatty acid β oxidation. Consequently, this will prevent the build up of toxic intermediates that are believed to compromise pancreatic β-cell function [99, 18]. In this model, in the absence of UCP2, β-cell dysfunction is predicted to arise due to inhibited fatty acid β oxidation, which leads to mitochondrial dysfunction in INS-1E cells (Figure 3.9).

Despite the considerable efforts made over the past fifteen years, it is clear that the physiological and biochemical function of UCP2 is still under debate and its role in pancreatic β-cell glucolipotoxicity is still yet to be determined conclusively. The lack of NEFA effect on UCP2 expression levels in INS-1E cells and its controversial involvement in NEFA-induced β-cell dysfunction provoke a substantial reconsideration of the physiological and pathological roles ascribed to UCP2 in pancreatic β-cells. In order to provide insight into the role

of UCP2 in β-cell glucolipotoxicity, the activity of UCP2 needs to be explored in INS-1E cells exposed to NEFAs at high glucose. It is also important to measure the activity and expression levels of UCP2 protein in pancreatic islets, since there are clear differences between primary islets and pancreatic β-cell models. UCP2 has been explored previously in pancreatic islets [85, 86], however, it is hard to make substantial inferences to the direct function of UCP2 in β-cell glucolipotoxicity because such models are confounded by the expression of UCP2 in other islet cells [90]. Therefore, to completely understand the underlying role of UCP2 in glucolipotoxic-induced β-dysfunction, future investigation needs to focus on using isolated islets from β-cell specific Ucp2 knockout animals.

6.3 Mechanisms of palmitate-induced reactive oxygen species

In pancreatic β-cells, evidence suggests that acute and transient glucose-dependent ROS contribute to normal GSIS [50]. However, chronic and persistent formation of ROS, resulting from excessive metabolic fuels such as glucose and fatty acids, may lead to impaired pancreatic β-cell function [73]. Since $O_2^{\cdot -}$ production from the mitochondrial matrix is very sensitive to the pmf [51], mild uncoupling can substantially decrease mitochondria-derived ROS and is believed to aid in preventing oxidative damage. Therefore, accumulating evidence supports the idea that UCP2 participates in the control of mitochondria-derived ROS [77]. Given the mitochondrial origin of

glucolipotoxic-induced ROS (Figure 4.1), it is quite possible that UCP2 mediates these effects. Evidence provided here, however, disagrees with an involvement of UCP2 in glucolipotoxic-induced ROS, since UCP2 does not mediate or protect against palmitate-induced mitochondrial ROS in INS-1E cells (Figure 4.3). Alternatively, it is possible that UCP2 is related to the cytoprotection of long-chain monounsaturated fatty acids, since UCP2 knockdown amplifies the protection of palmitoleate against palmitate-induced mitochondrial ROS (Figure 4.4). Therefore, evidence in INS-1E cells suggests that (i) glucolipotoxic-induced ROS are not mediated by UCP2, and (ii) inactivation and/or downregulation of UCP2 may help to alleviate glucolipotoxic-induced oxidative stress in the presence of mono-unsaturated fatty acids.

Glucolipotoxic-induced mitochondrial ROS have been attributed to the loss of β-cell mass in Type 2 diabetes [183, 202]. Mechanisms of ROS-induced apoptosis have been explored in great detail (reviewed in [179]), however, the exact mechanism responsible for glucolipotoxic-induced pancreatic β-cell death remains to be determined. Indeed it is shown here that there is a strong inverse correlation between mitochondrial ROS production and cell viability (Figure 4.6). Nevertheless, it remains unclear if mitochondrial ROS cause pancreatic β-cell death or are a consequence of it. To confirm if glucolipotoxic-induced mitochondrial ROS cause the loss in β-cell viability, it would be beneficial to measure cell viability under glucolipotoxic conditions in the presence or

absence of ROS scavengers. Equally, it would also be useful to measure pancreatic β-cell viability in the presence of compounds that are known to stimulate mitochondrial ROS production. Moreover, to understand the mechanisms of glucolipotoxic-induced ROS, it might be worth investigating the level of mitochondrial β oxidation in cells exposed to palmitate, since mitochondrial β-oxidation is known to increase ROS production [203]. In saying that, based on the fact that basal mitochondrial respiration is not significantly altered in palmitate treated cells (Figure 3.2A) or islets (Figure 5.3A), it is unlikely that palmitate-induced mitochondrial ROS are related to mitochondrial β oxidation.

6.4 Cytoprotection of mono-unsaturated fatty acids

The cytoprotective ability of mono-unsaturated fatty acids was discovered over a decade ago [17]. It was initially shown that mono-unsaturated fatty acids were capable of protecting β-cells against apoptosis induced by saturated fatty acids, serum withdrawal or cytokine exposure [17]. Possible mechanisms of cytoprotection have been proposed, such as esterification into neutral lipids, inhibition of caspase activity, activation of G-protein coupled receptors and increased fatty acid beta oxidation [98]. Despite the efforts made over the past 5-10 years a molecular mechanism for cytoprotection still remains to be established. Until now, it was also unclear if mono-unsaturated fatty acids protected against other forms of glucolipotoxic-induced stresses, such as

mitochondrial dysfunction, GSIS and ROS production. By investigating the differential effects of fatty acids in INS-1E cells and pancreatic islets this study provides new information about the cytoprotective properties of mono-unsaturated fatty acids. For example, it is shown that palmitoleate is not harmful to INS-1E cells and in combination with palmitate, protects against palmitate-induced loss in cell viability (Figure 3.8) and production of mitochondrial ROS (Figure 3.5). Palmitoleate also tends to protect against aspects of palmitate-induced mitochondrial dysfunction (Figures 3.2A and 5.5). Interestingly, however, palmitoleate does not provide protection against GSIS, which is still significantly dampened in cells exposed to palmitate and palmitoleate (Figures 3.6B and 5.6). Therefore, although mono-unsaturated fatty acids are capable of promoting β-cell viability in the face of toxic intermediates, functional aspects of the remaining cells are still compromised. The differential protection by palmitoleate has also helped to delineate between the mechanisms responsible for glucolipotoxic-induced phenotypes. For example, it is suggested that the mechanisms responsible for palmitate-induced defects in GSIS and mitochondrial respiration are distinct from the mechanisms that lead to a loss in cell viability and the generation of mitochondrial ROS. Furthermore, the observation that UCP2 attenuates palmitoleate protection against glucolipotoxic-induced mitochondrial ROS and loss in cell viability (Figures 4.4 and 4.5) provides new insight that mitochondria might be involved in the

underlying mechanism of cytoprotection. How UCP2 mediates these effects is still to be determined conclusively and warrants further investigation.

In order to establish why palmitoleate protection is amplified in the absence of UCP2, requires a better understanding of how palmitoleate prevents the deleterious effects of saturated fatty acids in the first place. It is evident from this study that mitochondrial ROS are directly associated with palmitate-induced cell death (Figure 4.6), therefore experiments should be designed to explore this involvement in more detail. For example, measurements of ROS should be obtained in INS-1E cells exposed to NEFAs in the presence or absence of superoxide scavengers or mediators of mitochondrial ROS. Thereby measuring ROS and cell viability under such conditions will highlight if mitochondrial ROS are directly responsible for the loss in β-cell viability. If ROS appear to be causative in this response, the specific source of palmitate-induced production of ROS and the possible intermediates responsible for this effect should be explored. This will not only provide new information about how palmitate induces mitochondrial ROS, but also identify if protective effects of palmitoleate occur upstream or downstream of this response. Furthermore, it might be possible that cytoprotection is sensitive to metabolic effects, as under conditions when mitochondrial β oxidation is expected to be stimulated, for example when UCP2 is present [204, 205], the cytoprotection of palmitoleate is attenuated (Figure 4.4 and 4.5). To investigate this in more detail, mitochondrial

respiration and ROS production needs to be probed in UCP2 absent INS-1E cells oxidising different substrates in the presence and absence of mitochondrial β-oxidation inhibitors. It is important to note that ROS production was only assessed using INS-1E cells in this study, and therefore effects of NEFAs on mitochondrial ROS production in primary cells also requires investigation.

6.5 Clinical speculation

Due to the multifarious effects of palmitate on mitochondrial glucose oxidation alone, it seems difficult to believe that a specific target that can be used for the therapeutic intervention of Type 2 diabetes. Data in this study suggest a possible alternative, since glucolipotoxic-induced mitochondrial dysfunction and GSIS defects only occur when mitochondrial β oxidation is inhibited, for example when glucose levels are high or by pharmacological inhibition of CPT-1 (Figure 3.9). Therefore, exploring new ways to regulate mitochondrial β oxidation in cells might provide a novel way to improve or prevent glucolipotoxic-induced β-cell dysfunction. Importantly, the glucose permissibility of NEFA toxicity has not been firmly established in vivo, therefore it is important to investigate if i) NEFA impairment of islet β-cell function is dependent on the glucose concentration, and if ii) NEFA-induced mitochondrial dysfunction or GSIS defects can be regulated in primary islet β-cells by manipulating mitochondrial β oxidation. Such studies will not only provide significant insight into the mechanisms of glucolipotoxicity in primary

β-cells but also have the potential to provide a novel approach to eliminating β-cell dysfunction caused by glucolipotoxicity. It is also necessary to point out that the possible disconnection between mitochondrial respiration and GSIS questions the idea of using respirometry to assess islet health to predict transplantation outcome as a measure to reverse diabetes [176]. Clearly, a better understanding of pancreatic β-cell function is required to fully elucidate the connection between glucose-stimulated insulin secretion and mitochondrial bioenergetics. Furthermore, given the apparent paradoxical roles that exist for a function of UCP2 in the β-cell, a clearer understanding of the involvement of UCP2 in pancreatic β-cells and the pathogenesis of Type 2 diabetes is needed.

As a practical plan to address these issues, it is proposed that better *in vivo* animal models and methods are obtained to investigate the effects of NEFAs on β-cell function and survival in pancreatic islets. For example, to improve the understanding for a role of UCP2 involvement in β-cell glucolipotxicity, the expression levels and activity of UCP2 should be explored in pancreatic islets which lack Ucp2 specifically from the β-cells. Furthermore, the investigation of mitochondrial bioenergetics from islets and β-cells isolated from murine models fed different high fat diets should be explored in more detail. Insight into the underlying mechanisms of how glucolipotoxicity is linked with mitochondrial dysfunction in β-cells seems necessary in elucidating the pathogenesis of Type 2

diabetes and identifying potential targets for therapeutic interventions designed to retard or prevent these processes.

6.6 Overall conclusion

Mitochondrial dysfunction is important in the pathogenesis of Type 2 diabetes and it is therefore critical that ongoing research in this field focusses attention on this area. Investigating how different cells respond to pathological levels of NEFAs is key to the understanding of metabolic disease and provides a new approach for identifying novel targets in the development and treatment of Type 2 diabetes.

Publications

Posters

[1] Probing the involvement of fatty acid oxidation in pancreatic beta cell lipotoxicity - *(2012) Centre for research and translational biomedicine conference – UK, Plymouth University.*

[2] Probing the involvement of mitochondria in the cytotoxic and cytoprotective effects of fatty acids in INS-1 insulinoma cells – *(2012) Diabetes and Obesity Symposium – The European Molecular Biology Laboratory, Heidelberg, Germany.*

[3] Mitochondrial dysfunction is responsible for palmitate-impairment of glucose-stimulated insulin secretion in INS-1E insulinoma cells – *(2013) Diabetes and Obesity Symposium – UK, Warwick University.*

[4] UCP2 is not responsible for palmitate-induced mitochondrial ROS or loss of INS-1E insulinoma cells - *(2014) European Bioenergetics Conference (EBEC) - Lisbon, Portugal.*

Papers

[1] J. Barlow, V. Hirschburg, C. Affourtit, On the role of mitochondria in pancreatic beta cells, in: Research on Diabetes. ISBN: 978-14777555-01-9.

[2] Barlow, J., Hirschberg, V., Brand, M. D. and Affourtit, C. (2013) Measuring Mitochondrial Uncoupling Protein-2 Level and Activity in Insulinoma Cells. Methods in Enzymology. 528, 257–267.

[3] Barlow, J. and Affourtit, C. (2013) Novel insights into pancreatic β-cell glucolipotoxicity from real-time functional analysis of mitochondrial energy metabolism in INS-1E insulinoma cells. Biochemical Journal. 456, 417–426.

[4] Barlow, J., Jensen, V. H. and Affourtit, C. (2015) Uncoupling protein-2 attenuates palmitoleate protection against the cytotoxic production of mitochondrial reactive oxygen species in INS-1E insulinoma cells. Redox Biology. 4, 14–22.

References

1 Barlow, J., Hirschburg, V. and Affourtit, C. On the role of mitochondria in pancreatic beta cells. Research on Diabetes I. ISBN: 978-14777555-01-9.

2 Rutter, G. A. (2001) Nutrient-secretion coupling in the pancreatic islet beta-cell: recent advances. Molecular Aspects of Medicine **22**, 247–284.

3 DeFronzo, R. A., Bonadonna, R. C. and Ferrannini, E. (1992) Pathogenesis of NIDDM. A balanced overview. Diabetes Care **15**, 318–368.

4 Kahn, S. E., Hull, R. L. and Utzschneider, K. M. (2006) Mechanisms linking obesity to insulin resistance and type 2 diabetes. Nature **444**, 840–846.

5 Guilherme, A., Virbasius, J. V., Puri, V. and Czech, M. P. (2008) Adipocyte dysfunctions linking obesity to insulin resistance and type 2 diabetes. Nature Reviews Molecular Cell Biology **9**, 367–377.

6 Reaven, G. M., Hollenbeck, C., Jeng, C. Y., Wu, M. S. and Chen, Y. D. (1988) Measurement of plasma glucose, free fatty acid, lactate, and insulin for 24 h in patients with NIDDM. Diabetes **37**, 1020–1024.

7 Boden, G. (2008) Obesity and Free Fatty Acids. Endocrinology and Metabolism **37**, 635–646.

8 Kahn, S. E. S. (2003) The relative contributions of insulin resistance and beta-cell dysfunction to the pathophysiology of Type 2 diabetes. Diabetologia **46**, 3–19.

9 Leung, N., Sakaue, T., Carpentier, A., Uffelman, K., Giacca, A. and Lewis, G. F. (2004) Prolonged increase of plasma non-esterified fatty acids fully abolishes the stimulatory effect of 24 hours of moderate hyperglycaemia on insulin sensitivity and pancreatic beta-cell function in obese men. Diabetologia **47**, 204–213.

10 Carpentier, A., Mittelman, S. D., Bergman, R. N., Giacca, A. and Lewis, G. F. (2000) Prolonged elevation of plasma free fatty acids impairs pancreatic beta-cell function in obese nondiabetic humans but not in individuals with type 2 diabetes. Diabetes **49**, 399–408.

11 Poitout, V. (2003) The ins and outs of fatty acids on the pancreatic β cell. Trends in Endocrinology & Metabolism **14**, 201–203.

12 Poitout, V. and Robertson, R. P. (2007) Glucolipotoxicity: Fuel Excess and β-Cell Dysfunction. Endocrine reviews **29**, 351–366.

13 Schulz, N. (2013) Minor role of mitochondrial respiration for fatty-acid induced insulin secretion. International Journal of Molecular Sciences **14**, 18989–18998.

14 Zhou, Y. P. and al, E. (1994) Long-term exposure of rat pancreatic islets to fatty acids inhibits glucose-induced insulin secretion and biosynthesis through a glucose fatty acid cycle. Journal of Clinical Investigation **93**, 870-876.

15 Barlow, J. and Affourtit, C. (2013) Novel insights into pancreatic β-cell glucolipotoxicity from real-time functional analysis of mitochondrial energy metabolism in INS-1E insulinoma cells. Biochemical Journal **456**, 417–426.

16 Prentki, M., Joly, E., El-Assaad, W. and al, E. (2002) Malonyl-CoA signaling, lipid partitioning, and glucolipotoxicity. Diabetes **51**, 405-413.

17 Welters, H. J., Tadayyon, M., Scarpello, J. H. B., Smith, S. A. and Morgan, N. G. (2004) Mono-unsaturated fatty acids protect against β-cell apoptosis induced by saturated fatty acids, serum withdrawal or cytokine exposure. FEBS Letters **560**, 103–108.

18 Poitout, V., Amyot, J., Semache, M., Zarrouki, B., Hagman, D. and Fontés, G. (2010) Glucolipotoxicity of the pancreatic beta cell. Biochimica et Biophysica Acta (BBA) - Molecular and Cell Biology of Lipids **1801**, 289–298.

19 Chen, L., Magliano, D. J. and Zimmet, P. Z. (2011) The worldwide epidemiology of type 2 diabetes mellitus—present and future perspectives. Nature Reviews Endocrinology **8**, 228–236.

20 Jansson, S. P. O., Fall, K., Brus, O., Magnuson, A., Wändell, P., Östgren, C. J. and Rolandsson, O. (2015) Prevalence and incidence of diabetes mellitus: a nationwide population-based pharmaco-epidemiological study in Sweden. Diabetic Medicine **10**, 1-10.

21 Lin, Y. and Sun, Z. (2010) Current views on type 2 diabetes. Journal of Endocrinology **204**, 1–11.

22 Garber, A. J. (2011) Obesity and type 2 diabetes: which patients are at risk? Diabetes Obesity & Metabolism **14**, 399–408.

23 Eckel, R. H., Kahn, S. E., Ferrannini, E., Goldfine, A. B., Nathan, D. M., Schwartz, M. W., Smith, R. J. and Smith, S. R. (2011) Obesity and Type 2 Diabetes: What Can Be Unified and What Needs to Be Individualized? Diabetes Care **34**, 1424–1430.

24 Alberti, K. G. M. M., Zimmet, P. and Shaw, J. (2006) Metabolic syndrome—a new world-wide definition. A Consensus Statement from the International Diabetes Federation. Diabetic Medicine **23**, 469–480.

25 DeFronzo, R. A., Jacot, E., Jequier, E., Maeder, E., Wahren, J. and Felber, J. P. (1981) The effect of insulin on the disposal of intravenous glucose.

Results from indirect calorimetry and hepatic and femoral venous catheterization. Diabetes **30**, 1000–1007.

26 Patti, M.-E. and Kahn, B. B. (2004, October) Nutrient sensor links obesity with diabetes risk. Nature Medicine **10**, 1049-1050.

27 Muoio, D. M. and Newgard, C. B. (2008) Mechanisms of disease: molecular and metabolic mechanisms of insulin resistance and beta-cell failure in type 2 diabetes. Nature Reviews Molecular Cell Biology **9**, 193–205.

28 Prentki, M. and Madiraju, S. R. M. (2012) Glycerolipid/free fatty acid cycle and islet β-cell function in health, obesity and diabetes. Molecular and Cellular Endocrinology **353**, 88–100.

29 Lowell, B. B. and Shulman, G. I. (2005) Mitochondrial dysfunction and type 2 diabetes. Science, American Association for the Advancement of Science **307**, 384–387.

30 Maechler, P. and Wollheim, C. B. (2001) Mitochondrial function in normal and diabetic |[beta]|-cells. Nature **414**, 807–812.

31 Maechler, P., Carobbio, S. and Rubi, B. (2006) In beta-cells, mitochondria integrate and generate metabolic signals controlling insulin secretion. The International Journal of Biochemistry & Cell Biology **38**, 696–709.

32 Henquin, J. C. (2000) Triggering and amplifying pathways of regulation of insulin secretion by glucose. Diabetes **49**, 1751–1760.

33 Henquin, J.-C. (2011) The dual control of insulin secretion by glucose involves triggering and amplifying pathways in β-cells. Diabetes Research and Clinical Practice **93**, 27–31.

34 Straub, S. G. and Sharp, G. W. G. (2002) Glucose-stimulated signaling pathways in biphasic insulin secretion. Diabetes Metabolism Research Reviews **18**, 451–463.

35 MacDonald, M. J. (2004) Perspective: emerging evidence for signaling roles of mitochondrial anaplerotic products in insulin secretion. Endocrinology and Metabolism **288**, E1–E15.

36 MacDonald, M. J., Smith, A. D., Hasan, N. M., Sabat, G. and Fahien, L. A. (2007) Feasibility of pathways for transfer of acyl groups from mitochondria to the cytosol to form short chain acyl-CoAs in the pancreatic beta cell. Journal of Biological Chemistry **282**, 30596–30606.

37 MacDonald, M. J., Dobrzyn, A., Ntambi, J. and Stoker, S. W. (2008) The role of rapid lipogenesis in insulin secretion: Insulin secretagogues acutely alter lipid composition of INS-1 832/13 cells. Archives of Biochemistry and Biophysics **470**, 153–162.

38 Joseph, J. W., Odegaard, M. L., Ronnebaum, S. M., Burgess, S. C., Muehlbauer, J., Sherry, A. D. and Newgard, C. B. (2007) Normal flux through ATP-citrate lyase or fatty acid synthase is not required for glucose-stimulated insulin secretion. Journal of Biological Chemistry **282**, 31592–31600.

39 Detimary, P., Jonas, J. C. and Henquin, J. C. (1995) Possible links between glucose-induced changes in the energy state of pancreatic B cells and insulin release. Unmasking by decreasing a stable pool of adenine nucleotides in mouse islets. Journal of Clinical Investigation **96**, 1738–1745.

40 Detimary, P., Dejonghe, S., Ling, Z., Pipeleers, D., Schuit, F. and Henquin, J. C. (1998) The changes in adenine nucleotides measured in glucose-stimulated rodent islets occur in beta cells but not in alpha cells and are also observed in human islets. Journal of Biological Chemistry **273**, 33905–33908.

41 Ronner, P., Naumann, C. M. and Friel, E. (2001) Effects of glucose and amino acids on free ADP in betaHC9 insulin-secreting cells. Diabetes **50**, 291–300.

42 Sekine, N., Cirulli, V., Regazzi, R., Brown, L. J., Gine, E., Tamarit-Rodriguez, J., Girotti, M., Marie, S., MacDonald, M. J. and Wollheim, C.

B. (1994) Low lactate dehydrogenase and high mitochondrial glycerol phosphate dehydrogenase in pancreatic beta-cells. Potential role in nutrient sensing. Journal of Biological Chemistry **269**, 4895–4902.

43 Nicholls, D. G. and Ferguson, S. (2013) Bioenergetics4 4 ed., Academic Press.

44 Ainscow, E. K., Zhao, C. and Rutter, G. A. (2000) Acute overexpression of lactate dehydrogenase-A perturbs beta-cell mitochondrial metabolism and insulin secretion. Diabetes **49**, 1149–1155.

45 Lee, B., Miles, P. D., Vargas, L., Luan, P., Glasco, S., Kushnareva, Y., Kornbrust, E. S., Grako, K. A., Wollheim, C. B., Maechler, P., et al. (2003) Inhibition of Mitochondrial Na+-Ca2+ Exchanger Increases Mitochondrial Metabolism and Potentiates Glucose-Stimulated Insulin Secretion in Rat Pancreatic Islets. Diabetes **52**, 965–973.

46 MacDonald, M. J., Longacre, M. J., Stoker, S. W., Kendrick, M., Thonpho, A., Brown, L. J., Hasan, N. M., Jitrapakdee, S., Fukao, T., Hanson, M. S., et al. (2011) Differences between human and rodent pancreatic islets: low pyruvate carboxylase, atp citrate lyase, and pyruvate carboxylation and high glucose-stimulated acetoacetate in human pancreatic islets. Journal of Biological Chemistry **286**, 18383–18396.

47 Pi, J., Bai, Y., Zhang, Q., Wong, V., Floering, L. M., Daniel, K., Reece, J. M., Deeney, J. T., Andersen, M. E., Corkey, B. E., et al. (2007) Reactive Oxygen Species as a Signal in Glucose-Stimulated Insulin Secretion. Diabetes **56**, 1783–1791.

48 Leloup, C., Tourrel-Cuzin, C., Magnan, C., Karaca, M., Castel, J., Carneiro, L., Colombani, A.-L., Ktorza, A., Casteilla, L. and Pénicaud, L. (2009) Mitochondrial Reactive Oxygen Species Are Obligatory Signals for Glucose-Induced Insulin Secretion. Diabetes **58**, 673–681.

49 Newsholme, P., Morgan, D., Rebelato, E., Oliveira-Emilio, H. C., Procopio, J., Curi, R. and Carpinelli, A. (2009) Insights into the critical role of NADPH oxidase(s) in the normal and dysregulated pancreatic beta cell. Diabetologia **52**, 2489–2498.

50 Affourtit, C., Jastroch, M. and Brand, M. D. (2011) Uncoupling protein-2 attenuates glucose-stimulated insulin secretion in INS-1E insulinoma cells by lowering mitochondrial reactive oxygen species. Free Radical Biology and Medicine **50**, 609–616.

51 Murphy, M. P. (2009) How mitochondria produce reactive oxygen species. Biochemical Journal **417**, 1-13.

52 Quinlan, C. L., Perevoschikova, I. V., Goncalves, R. L. S., Hey-Mogensen, M. and Brand, M. D. (2013) The determination and analysis of site-

specific rates of mitochondrial reactive oxygen species production. Methods in Enzymology **526**, 189–217.

53 Hey-Mogensen, M., Goncalves, R. L. S., Orr, A. L. and Brand, M. D. (2014) Production of superoxide/H2O2 by dihydroorotate dehydrogenase in rat skeletal muscle mitochondria. Free Radical Biology and Medicine **72**, 149–155.

54 Goncalves, R. L. S., Quinlan, C. L., Perevoshchikova, I. V., Hey-Mogensen, M. and Brand, M. D. (2015) Sites of Superoxide and Hydrogen Peroxide Production by Muscle Mitochondria Assessed ex vivo Under Conditions Mimicking Rest and Exercise. Journal of Biological Chemistry **1**, 209-227.

55 Morgan, N. G. (2009) Fatty acids and β-cell toxicity. Current Opinion in Clinical Nutrition and Metabolic Care **12**, 117–122.

56 El-Assaad, W. (2003) Saturated Fatty Acids Synergize with Elevated Glucose to Cause Pancreatic β-Cell Death. Endocrinology **144**, 4154–4163.

57 Brun, T., Roche, E., Assimacopoulos-Jeannet, F., Corkey, B. E., Kim, K.-H. and Prentki, M. (1996) Evidence for an Anaplerotic/Malonyl-CoA Pathway in Pancreatic β-Cell Nutrient Signaling. Diabetes **45**, 190–198.

58 Poitout, V. and Robertson, R. P. (2002) Minireview: Secondary beta-cell failure in type 2 diabetes--a convergence of glucotoxicity and lipotoxicity. Endocrinology **143**, 339–342.

59 Newsholme, P., Keane, D., Welters, H. J. and Morgan, N. G. (2007) Life and death decisions of the pancreatic β-cell: the role of fatty acids. Clinical Science **112**, 27.

60 Listenberger, L. L., Han, X., Lewis, S. E. and al, E. (2003) Triglyceride accumulation protects against fatty acid-induced lipotoxicity. PNAS **100**, 3077-3082.

61 Moore, P. C., Ugas, M. A., Hagman, D. K., Parazzoli, S. D. and Poitout, V. (2004) Evidence Against the Involvement of Oxidative Stress in Fatty Acid Inhibition of Insulin Secretion. Diabetes **53**, 2610–2616.

62 Lupi, R., Dotta, F., Marselli, L., Del Guerra, S., Masini, M., Santangelo, C., Patane, G., Boggi, U., Piro, S., Anello, M., et al. (2002) Prolonged Exposure to Free Fatty Acids Has Cytostatic and Pro-Apoptotic Effects on Human Pancreatic Islets: Evidence that β-Cell Death Is Caspase Mediated, Partially Dependent on Ceramide Pathway, and Bcl-2 Regulated. Diabetes **51**, 1437–1442.

63 Kelpe, C. L. (2003) Palmitate Inhibition of Insulin Gene Expression Is Mediated at the Transcriptional Level via Ceramide Synthesis. Journal of Biological Chemistry **278**, 30015–30021.

64 Malmgren, S., Spegel, P., Danielsson, A. P. H., Nagorny, C. L., Andersson, L. E., Nitert, M. D., Ridderstrale, M., Mulder, H. and Ling, C. (2013) Coordinate Changes in Histone Modifications, mRNA Levels, and Metabolite Profiles in Clonal INS-1 832/13 β-Cells Accompany Functional Adaptations to Lipotoxicity. Journal of Biological Chemistry **288**, 11973–11987.

65 Somesh, B. P., Verma, M. K., Sadasivuni, M. K., Mammen-Oommen, A., Biswas, S., Shilpa, P. C., Reddy, A. K., Yateesh, A. N., Pallavi, P. M., Nethra, S., et al. (2013) Chronic glucolipotoxic conditions in pancreatic islets impair insulin secretion due to dysregulated calcium dynamics, glucose responsiveness and mitochondrial activity. Cell Biology **14**, 31.

66 Zhou, Y. P. and Grill, V. (1995) Long term exposure to fatty acids and ketones inhibits B-cell functions in human pancreatic islets of Langerhans. Journal of Clinical Endocrinology & Metabolism **80**, 1584–1590.

67 Zhou, Y. P. and Grill, V. E. (1995) Palmitate-induced β-cell insensitivity to glucose is coupled to decreased pyruvate dehydrogenase activity and enhanced kinase activity in rat pancreatic islets. Diabetes **80**, 1584-1590.

68 Hue, L. and Taegtmeyer, H. (2009) The Randle cycle revisited: a new head for an old hat. Endocrinology and Metabolism **297**, E578–91.

69 Hong, Y., Fink, B. D., Dillon, J. S. and Sivitz, W. I. (2001) Effects of adenoviral overexpression of uncoupling protein-2 and -3 on mitochondrial respiration in insulinoma cells. Endocrinology **142**, 249–256.

70 Chan, C. B., Saleh, M. C., Koshkin, V. and Wheeler, M. B. (2004) Uncoupling Protein 2 and Islet Function. Diabetes **53**, S136–S142.

71 De Souza, C. T., Araujo, E. P., Stoppiglia, L. F., Pauli, J. R., Ropelle, E., Rocco, S. A., Marin, R. M., Franchini, K. G., Carvalheira, J. B., Saad, M. J., et al. (2007) Inhibition of UCP2 expression reverses diet-induced diabetes mellitus by effects on both insulin secretion and action. The FASEB Journal **21**, 1153–1163.

72 Affourtit, C. and Brand, M. D. (2008) On the role of uncoupling protein-2 in pancreatic beta cells. Biochimica et Biophysica Acta (BBA) - Bioenergetics **1777**, 973–979.

73 Pi, J. and Collins, S. (2010) Reactive oxygen species and uncoupling protein 2 in pancreatic β-cell function. Diabetes Obesity & Metabolism **12**, 141–148.

74 Ma, Z. A., Zhao, Z. and Turk, J. (2012) Mitochondrial Dysfunction and *β*-Cell Failure in Type 2 Diabetes Mellitus. Journal of Diabetes Research **2012**, 1-11.

75 Couplan, E., del Mar Gonzalez-Barroso, M., Alves-Guerra, M. C., Ricquier, D., Goubern, M. and Bouillaud, F. (2002) No evidence for a basal, retinoic, or superoxide-induced uncoupling activity of the uncoupling protein 2 present in spleen or lung mitochondria. Journal of Biological Chemistry **277**, 26268–26275.

76 Nedergaard, J. and Cannon, B. (2003) The 'novel'"uncoupling"proteins UCP2 and UCP3: what do they really do? Pros and cons for suggested functions. Experimental physiology **88**, 65-84.

77 Brand, M. D. and Esteves, T. C. (2005) Physiological functions of the mitochondrial uncoupling proteins UCP2 and UCP3. Cell Metabolism **2**, 85–93.

78 Schrauwen, P., Hoeks, J. and Hesselink, M. K. C. (2006) Putative function and physiological relevance of the mitochondrial uncoupling protein-3:

involvement in fatty acid metabolism? Progress in lipid research **45**, 17–41.

79 Bouillaud, F. (2009) UCP2, not a physiologically relevant uncoupler but a glucose sparing switch impacting ROS production and glucose sensing. Biochimica et Biophysica Acta (BBA) - Bioenergetics **1787**, 377-383.

80 Vozza, A., Parisi, G., De Leonardis, F., Lasorsa, F. M., Castegna, A., Amorese, D., Marmo, R., Calcagnile, V. M., Palmieri, L., Ricquier, D., et al. (2014) UCP2 transports C4 metabolites out of mitochondria, regulating glucose and glutamine oxidation. PNAS **111**, 960–965.

81 Zhang, C. Y., Baffy, G., Perret, P., Krauss, S., Peroni, O. and al, E. (2001) Uncoupling protein-2 negatively regulates insulin secretion and is a major link between obesity, β cell dysfunction, and type 2 diabetes. Cell **105**, 745-755.

82 Pi, J., Bai, Y., Daniel, K. W., Liu, D., Lyght, O., Edelstein, D., Brownlee, M., Corkey, B. E. and Collins, S. (2009) Persistent oxidative stress due to absence of uncoupling protein 2 associated with impaired pancreatic beta-cell function. Endocrinology **150**, 3040–3048.

83 Parker, N., Vidal-Puig, A. J., Azzu, V. and Brand, M. D. (2009) Dysregulation of glucose homeostasis in nicotinamide nucleotide

transhydrogenase knockout mice is independent of uncoupling protein 2. Biochimica et Biophysica Acta (BBA) - Bioenergetics **1787**, 1451–1457.

84 Robson-Doucette, C. A., Sultan, S., Allister, E. M., Wikstrom, J. D., Koshkin, V., Bhattacharjee, A., Prentice, K. J., Sereda, S. B., Shirihai, O. S. and Wheeler, M. B. (2011) β-Cell Uncoupling Protein 2 Regulates Reactive Oxygen Species Production, Which Influences Both Insulin and Glucagon Secretion. Diabetes **60**, 2710–2719.

85 Joseph, J. W., Koshkin, V., Zhang, C.-Y., Wang, J., Lowell, B. B., Chan, C. B. and Wheeler, M. B. (2002) Uncoupling protein 2 knockout mice have enhanced insulin secretory capacity after a high-fat diet. Diabetes **51**, 3211–3219.

86 Joseph, J. W. (2004) Free Fatty Acid-induced β-Cell Defects Are Dependent on Uncoupling Protein 2 Expression. Journal of Biological Chemistry **279**, 51049–51056.

87 Fleury, C., Neverova, M., Collins, S., Raimbault, S., Champigny, O., Levi-Meyrueis, C., Bouillaud, F., Seldin, M. F., Surwit, R. S., Ricquier, D., et al. (1997) Uncoupling protein-2: a novel gene linked to obesity and hyperinsulinemia. Nature Genetics **15**, 269–272.

88 Chan, C. B., MacDonald, P. E., Saleh, M. C., Johns, D. C., Marbàn, E. and Wheeler, M. B. (1999) Overexpression of uncoupling protein 2 inhibits

glucose-stimulated insulin secretion from rat islets. Diabetes **48**, 1482–1486.

89 Xiong, S., Mu, T., Wang, G. and Jiang, X. (2014) Mitochondria-mediated apoptosis in mammals. Protein Cell **5**, 737–749.

90 Diao, J., Allister, E. M., Koshkin, V., Lee, S. C., Bhattacharjee, A., Tang, C., Giacca, A., Chan, C. B. and Wheeler, M. B. (2008) UCP2 is highly expressed in pancreatic α-cells and influences secretion and survival. PNAS **105**, 12057–12062.

91 Affourtit, C. and Brand, M. D. (2008) Uncoupling protein-2 contributes significantly to high mitochondrial proton leak in INS-1E insulinoma cells and attenuates glucose-stimulated insulin secretion. Biochemical Journal **409**, 199.

92 Lameloise, N., Muzzin, P., Prentki, M. and Assimacopoulos-Jeannet, F. (2001) Uncoupling Protein 2: A Possible Link Between Fatty Acid Excess and Impaired Glucose-Induced Insulin Secretion? Diabetes **50**, 803–809.

93 Kato, T., Shimano, H., Yamamoto, T., Yokoo, T., Endo, Y., Ishikawa, M., Matsuzaka, T., Nakagawa, Y., Kumadaki, S., Yahagi, N., et al. (2006) Granuphilin is activated by SREBP-1c and involved in impaired insulin secretion in diabetic mice. Cell Metabolism **4**, 143–154.

94 Olofsson, C. S., Collins, S., Bengtsson, M., Eliasson, L. and al, E. (2007) Long-term exposure to glucose and lipids inhibits glucose-induced insulin secretion downstream of granule fusion with plasma membrane. Diabetes **56**, 1888-1897.

95 Hoppa, M. B., Collins, S., Ramracheya, R., Hodson, L., Amisten, S., Zhang, Q., Johnson, P., Ashcroft, F. M. and Rorsman, P. (2009) Chronic Palmitate Exposure Inhibits Insulin Secretion by Dissociation of Ca2+ Channels from Secretory Granules. Cell Metabolism **10**, 455–465.

96 Diakogiannaki, E., Dhayal, S., Childs, C. E., Calder, P. C., Welters, H. J. and Morgan, N. G. (2007) Mechanisms involved in the cytotoxic and cytoprotective actions of saturated versus monounsaturated long-chain fatty acids in pancreatic β-cells. Journal of Endocrinology **194**, 283–291.

97 Dhayal, S. and Morgan, N. G. (2011) Pharmacological characterization of the cytoprotective effects of polyunsaturated fatty acids in insulin-secreting BRIN-BD11 cells. British Journal of Pharmacology **162**, 1340–1350.

98 Morgan, N. G., Dhayal, S., Diakogiannaki, E. and Welters, H. J. (2008) The cytoprotective actions of long-chain mono-unsaturated fatty acids in pancreatic β-cells. Biochemical Society Transactions **36**, 905.

99 Maedler, K., Oberholzer, J., Bucher, P., Spinas, G. A. and Donath, M. Y. (2003) Monounsaturated Fatty Acids Prevent the Deleterious Effects of Palmitate and High Glucose on Human Pancreatic β-Cell Turnover and Function. Diabetes **52**, 726–733.

100 Morgan, N. G. and Dhayal, S. (2010) Unsaturated fatty acids as cytoprotective agents in the pancreatic β-cell. Prostaglandins, Leukotrienes and Essential Fatty Acids **82**, 231–236.

101 Gravena, C., Mathias, P. C. and Ashcroft, S. J. (2002) Acute effects of fatty acids on insulin secretion from rat and human islets of Langerhans. Journal of Endocrinology **173**, 73–80.

102 Shimabukuro, M., Higa, M., Zhou, Y. T., Wang, M. Y., Newgard, C. B. and Unger, R. H. (1998) Lipoapoptosis in beta-cells of obese prediabetic fa/fa rats. Role of serine palmitoyltransferase overexpression. Journal of Biological Chemistry **273**, 32487–32490.

103 Veluthakal, R., Palanivel, R., Zhao, Y., McDonald, P., Gruber, S. and Kowluru, A. (2005) Ceramide induces mitochondrial abnormalities in insulin-secreting INS-1 cells: Potential mechanisms underlying ceramide-mediated metabolic dysfunction of the β cell. Apoptosis **10**, 841–850.

104 Maedler, K., Spinas, G. A., Dyntar, D., Moritz, W. and Kaiser, N. (2001) Distinct effects of saturated and monounsaturated fatty acids on β-cell turnover and function. Diabetes **50**, 69-76.

105 Beeharry, N., Chambers, J. A. and Green, I. C. (2004) Fatty acid protection from palmitic acid-induced apoptosis is lost following PI3-kinase inhibition. Apoptosis **9**, 599–607.

106 Xu, C., Bailly-Maitre, B. and Reed, J. C. (2005) Endoplasmic reticulum stress: cell life and death decisions. Journal of Clinical Investigation **115**, 2656–2664.

107 Karaskov, E., Scott, C., Zhang, L., Teodoro, T., Ravazzola, M. and Volchuk, A. (2006) Chronic palmitate but not oleate exposure induces endoplasmic reticulum stress, which may contribute to INS-1 pancreatic beta-cell apoptosis. Endocrinology **147**, 3398–3407.

108 Laybutt, D. R., Preston, A. M., Akerfeldt, M. C., Kench, J. G., Busch, A. K., Biankin, A. V. and Biden, T. J. (2007) Endoplasmic reticulum stress contributes to beta cell apoptosis in type 2 diabetes. Diabetologia **50**, 752–763.

109 Wei, Y., Wang, D., Topczewski, F. and Pagliassotti, M. J. (2006) Saturated fatty acids induce endoplasmic reticulum stress and apoptosis

independently of ceramide in liver cells. American Journal of Physiology, Endocrinology and Metabolism **291**, E275–81.

110 Borradaile, N. M., Buhman, K. K., Listenberger, L. L., Magee, C. J., Morimoto, E. T. A., Ory, D. S. and Schaffer, J. E. (2006) A critical role for eukaryotic elongation factor 1A-1 in lipotoxic cell death. Molecular Biology Of The Cell **17**, 770–778.

111 Wang, H., Kouri, G. and Wollheim, C. B. (2005) ER stress and SREBP-1 activation are implicated in beta-cell glucolipotoxicity. Journal of Cell Science **118**, 3905–3915.

112 Takahashi, A., Motomura, K., Kato, T., Yoshikawa, T., Nakagawa, Y., Yahagi, N., Sone, H., Suzuki, H., Toyoshima, H., Yamada, N., et al. (2005) Transgenic Mice Overexpressing Nuclear SREBP-1c in Pancreatic β-Cells. Diabetes **54**, 492–499.

113 Yamashita, T. (2004) Role of Uncoupling Protein-2 Up-Regulation and Triglyceride Accumulation in Impaired Glucose-Stimulated Insulin Secretion in a β-Cell Lipotoxicity Model Overexpressing Sterol Regulatory Element-Binding Protein-1c. Endocrinology **145**, 3566–3577.

114 Lingohr, M. K., Dickson, L. M., Wrede, C. E., Briaud, I., McCuaig, J. F., Myers, M. G. and Rhodes, C. J. (2003) Decreasing IRS-2 expression in pancreatic beta-cells (INS-1) promotes apoptosis, which can be

compensated for by introduction of IRS-4 expression. Molecular and Cellular Endocrinology **209**, 17–31.

115 Maestre, I. (2003) Mitochondrial Dysfunction Is Involved in Apoptosis Induced by Serum Withdrawal and Fatty Acids in the beta-Cell Line Ins-1. Endocrinology **144**, 335–345.

116 Iverson, S. L. and Orrenius, S. (2004) The cardiolipin–cytochrome c interaction and the mitochondrial regulation of apoptosis. Archives of Biochemistry and Biophysics **423**, 37–46.

117 Ott, M., Gogvadze, V., Orrenius, S. and Zhivotovsky, B. (2007) Mitochondria, oxidative stress and cell death. Apoptosis **12**, 913–922.

118 Piro, S., Anello, M., Di Pietro, C., Lizzio, M. N., Patan egrave, G., Rabuazzo, A. M., Vigneri, R., Purrello, M. and Purrello, F. (2002) Chronic exposure to free fatty acids or high glucose induces apoptosis in rat pancreatic islets: Possible role of oxidative stress. Metabolism **51**, 1340–1347.

119 Diakogiannaki, E., Welters, H. J. and Morgan, N. G. (2008) Differential regulation of the endoplasmic reticulum stress response in pancreatic - cells exposed to long-chain saturated and monounsaturated fatty acids. Journal of Endocrinology **197**, 553–563.

120 Dhayal, S., Welters, H. J. and Morgan, N. G. (2008) Structural requirements for the cytoprotective actions of mono-unsaturated fatty acids in the pancreatic beta-cell line, BRIN-BD11. British Journal of Pharmacology **153**, 1718–1727.

121 Covington, D. K., Briscoe, C. A., Brown, A. J. and Jayawickreme, C. K. (2006) The G-protein-coupled receptor 40 family (GPR40-GPR43) and its role in nutrient sensing. Biochemical Society Transactions **34**, 770–773.

122 Zhang, Y., Xu, M., Zhang, S., Yan, L., Yang, C., Lu, W., Li, Y. and Cheng, H. (2007) The role of G protein-coupled receptor 40 in lipoapoptosis in mouse beta-cell line NIT-1. Journal of Molecular Endocrinology **38**, 651–661.

123 Sum, C. S., Tikhonova, I. G., Neumann, S., Engel, S., Raaka, B. M., Costanzi, S. and Gershengorn, M. C. (2007) Identification of residues important for agonist recognition and activation in GPR40. Journal of Biological Chemistry **282**, 29248–29255.

124 Hirasawa, A., Tsumaya, K., Awaji, T., Katsuma, S., Adachi, T., Yamada, M., Sugimoto, Y., Miyazaki, S. and Tsujimoto, G. (2005) Free fatty acids regulate gut incretin glucagon-like peptide-1 secretion through GPR120. Nature Medicine **11**, 90–94.

125 Evans, J. L., Goldfine, I. D., Maddux, B. A. and Grodsky, G. M. (2002) Oxidative stress and stress-activated signaling pathways: a unifying hypothesis of type 2 diabetes. Endocrine reviews **23**, 599–622.

126 Tanaka, Y., Tran, P. O. T., Harmon, J. and Robertson, R. P. (2002) A role for glutathione peroxidase in protecting pancreatic beta cells against oxidative stress in a model of glucose toxicity. PNAS **99**, 12363–12368.

127 Robertson, R. P., Harmon, J., Tran, P. O. and Tanaka, Y. (2003) Glucose toxicity in β-cells: type 2 diabetes, good radicals gone bad, and the glutathione connection. Diabetes **52**, 581-587.

128 Newsholme, P., Haber, E. P., Hirabara, S. M., Rebelato, E. L. O., Procopio, J., Morgan, D., Oliveira-Emilio, H. C., Carpinelli, A. R. and Curi, R. (2007) Diabetes associated cell stress and dysfunction: role of mitochondrial and non-mitochondrial ROS production and activity. The Journal of Physiology **583**, 9–24.

129 Turrens, J. F. (2003) Mitochondrial formation of reactive oxygen species. The Journal of Physiology **552**, 335–344.

130 Balaban, R. S., Nemoto, S. and Finkel, T. (2005) Mitochondria, Oxidants, and Aging. Cell **120**, 483–495.

131 Chance, B., Sies, H. and Boveris, A. (1979) Hydroperoxide metabolism in mammalian organs. Physiology Reviews **59**, 527-605.

132 Cadenas, E. and Davies, K. J. A. (2000) Mitochondrial free radical generation, oxidative stress, and aging. Free Radical Biology and Medicine **29**, 222–230.

133 Raha, S. and Robinson, B. H. (2000) Mitochondria, oxygen free radicals, disease and ageing. Trends in Biochemical Sciences **25**, 502–508.

134 Adam-Vizi, V. and Chinopoulos, C. (2006) Bioenergetics and the formation of mitochondrial reactive oxygen species. Trends in Pharmacological Sciences **27**, 639–645.

135 Muller, F. (2000) The nature and mechanism of superoxide production by the electron transport chain: Its relevance to aging. Journal of American Aging Association **23**, 227–253.

136 Lenzen, S., Drinkgern, J. and Tiedge, M. (1996) Low antioxidant enzyme gene expression in pancreatic islets compared with various other mouse tissues. Free Radical Biology and Medicine **20**, 463–466.

137 Tiedge, M., Lortz, S., Drinkgern, J. and Lenzen, S. (1997) Relation between antioxidant enzyme gene expression and antioxidative defense status of insulin-producing cells. Diabetes **46**, 1733–1742.

138 Maechler, P., Jornot, L. and Wollheim, C. B. (1999) Hydrogen peroxide alters mitochondrial activation and insulin secretion in pancreatic beta cells. Journal of Biological Chemistry **274**, 27905–27913.

139 Tanaka, Y., Gleason, C. E., Tran, P. O., Harmon, J. S. and Robertson, R. P. (1999) Prevention of glucose toxicity in HIT-T15 cells and Zucker diabetic fatty rats by antioxidants. PNAS **96**, 10857–10862.

140 Brand, M. D., Parker, N., Affourtit, C., Mookerjee, S. A. and Azzu, V. (2010) Mitochondrial uncoupling protein 2 in pancreatic β-cells. Diabetes Obesity and Metabolism **12**, 134–140.

141 Brand, M. D. and Nicholls, D. G. (2011) Assessing mitochondrial dysfunction in cells. Biochemical Journal **435**, 297–312.

142 Leahy, J. L., Bonner-Weir, S. and Weir, G. C. (1992) Beta-cell dysfunction induced by chronic hyperglycemia. Current ideas on mechanism of impaired glucose-induced insulin secretion. Diabetes Care **15**, 442–455.

143 Hribal, M. L., Perego, L., Lovari, S., Andreozzi, F., Menghini, R., Perego, C., Finzi, G., Usellini, L., Placidi, C., Capella, C., et al. (2003) Chronic hyperglycemia impairs insulin secretion by affecting insulin receptor expression, splicing, and signaling in RIN beta cell line and human islets of Langerhans. The FASEB Journal **17**, 1340–1342.

144 McQuaid, T. S., Saleh, M. C., Joseph, J. W., Gyulkhandanyan, A., Manning-Fox, J. E., MacLellan, J. D., Wheeler, M. B. and Chan, C. B. (2006) cAMP-mediated signaling normalizes glucose-stimulated insulin

secretion in uncoupling protein-2 overexpressing beta-cells. Journal of Endocrinology **190**, 669–680.

145 Oliveira, H. R., Verlengia, R., Carvalho, C. R. O., Britto, L. R. G., Curi, R. and Carpinelli, A. R. (2003) Pancreatic β-Cells Express Phagocyte-Like NAD(P)H Oxidase. Diabetes **52**, 1457–1463.

146 Morgan, D., Oliveira-Emilio, H. R., Keane, D., Hirata, A. E., Santos da Rocha, M., Bordin, S., Curi, R., Newsholme, P. and Carpinelli, A. R. (2006) Glucose, palmitate and pro-inflammatory cytokines modulate production and activity of a phagocyte-like NADPH oxidase in rat pancreatic islets and a clonal beta cell line. Diabetologia **50**, 359–369.

147 Merglen, A. (2003) Glucose Sensitivity and Metabolism-Secretion Coupling Studied during Two-Year Continuous Culture in INS-1E Insulinoma Cells. Endocrinology **145**, 667–678.

148 Ozturk, S. S. and Palsson, B. O. (1990) Chemical decomposition of glutamine in cell culture media: effect of media type, pH, and serum concentration. Biotechnology Progression **6**, 121–128.

149 Hurtaud, C., Gelly, C., Chen, Z., Lévi-Meyrueis, C. and Bouillaud, F. (2007) Glutamine stimulates translation of uncoupling protein 2mRNA. Cellular and Molecular Life Sciences **64**, 1853–1860.

150 Spector, A. A. (1975) Fatty acid binding to plasma albumin. The Journal of Lipid Research **16**, 165–179.

151 Huber, A. H., Kampf, J. P., Kwan, T., Zhu, B. and Kleinfeld, A. M. (2006) Fatty acid-specific fluorescent probes and their use in resolving mixtures of unbound free fatty acids in equilibrium with albumin. Biochemistry **45**, 14263–14274.

152 Maris, M., Waelkens, E., Cnop, M., D'Hertog, W., Cunha, D. A., Korf, H., Koike, T., Overbergh, L. and Mathieu, C. (2011) Oleate-Induced Beta Cell Dysfunction and Apoptosis: A Proteomic Approach to Glucolipotoxicity by an Unsaturated Fatty Acid. Journal of Proteome Research **10**, 3372–3385.

153 Mott, D. M., Stone, K., Gessel, M. C., Bunt, J. C. and Bogardus, C. (2007) Palmitate action to inhibit glycogen synthase and stimulate protein phosphatase 2A increases with risk factors for type 2 diabetes. AJP: Endocrinology and Metabolism **294**, E444–E450.

154 Haber, E. P., Hirabara, S. M., Gomes, A. D., Curi, R., Carpinelli, A. R. and Carvalho, C. R. O. (2003) Palmitate modulates the early steps of insulin signalling pathway in pancreatic islets. FEBS Letters **544**, 185–188.

155 Coll, T., Eyre, E., Rodriguez-Calvo, R., Palomer, X., Sanchez, R. M., Merlos, M., Laguna, J. C. and Vazquez-Carrera, M. (2008) Oleate

Reverses Palmitate-induced Insulin Resistance and Inflammation in Skeletal Muscle Cells. Journal of Biological Chemistry **283**, 11107–11116.

156 Affourtit, C. and Brand, M. D. (2009) Chapter 23 Measuring Mitochondrial Bioenergetics in INS-1E Insulinoma Cells. Methods in Enzymology **45723**, 405–424.

157 Barlow, J., Hirschberg, V., Brand, M. D. and Affourtit, C. (2013) Measuring Mitochondrial Uncoupling Protein-2 Level and Activity in Insulinoma Cells. Methods in Enzymology **528**, 257–267.

158 Atale, N., Gupta, S., Yadav, U. C. S. and Rani, V. (2014) Cell-death assessment by fluorescent and nonfluorescent cytosolic and nuclear staining techniques. Journal of Microscopy **255**, 7–19.

159 Josephy, P. D., Eling, T. and Mason, R. P. (1982) The horseradish peroxidase-catalyzed oxidation of 3,5,3“,5-”tetramethylbenzidine. Free radical and charge-transfer complex intermediates. Journal of Biological Chemistry **257**, 3669–3675.

160 Robinson, K. M., Janes, M. S., Pehar, M., Monette, J. S., Ross, M. F., Hagen, T. M., Murphy, M. P. and Beckman, J. S. (2006) Selective fluorescent imaging of superoxide in vivo using ethidium-based probes. PNAS **103**, 15038–15043.

161 Björntorp, P., Bergman, H. and Varnauskas, E. (1969) PLASMA FREE FATTY ACID TURNOVER RATE IN OBESITY. Acta Medica Scandinavica **185**, 351–356.

162 Unger, R. H. (1995) Lipotoxicity in the Pathogenesis of Obesity-Dependent NIDDM: Genetic and Clinical Implications. Diabetes **44**, 863–870.

163 Prentki, M. (2006) Islet cell failure in type 2 diabetes. Journal of Clinical Investigation **116**, 1802–1812.

164 Lee, M.-S., Kim, K.-A. and Kim, H. S. (2012) Role of pancreatic β-cell death and cell death-associated inflammation in diabetes. Current Molecular Medicine **12**, 1297–1310.

165 Elks, M. L. (1993) Chronic perifusion of rat islets with palmitate suppresses glucose-stimulated insulin release. Endocrinology **133**, 208–214.

166 Lovis, P., Roggli, E., Laybutt, D. R., Gattesco, S., Yang, J.-Y., Widmann, C., Abderrahmani, A. and Regazzi, R. (2008) Alterations in microRNA expression contribute to fatty acid-induced pancreatic beta-cell dysfunction. Diabetes **57**, 2728–2736.

167 Akash, M. S. H., Rehman, K. and Chen, S. (2013) Role of inflammatory mechanisms in pathogenesis of type 2 diabetes mellitus. Journal of Cellular Biochemistry **114**, 525–531.

168 Cnop, M., Foufelle, F. and Velloso, L. A. (2012) Endoplasmic reticulum stress, obesity and diabetes. Trends in Molecular Medicine **18**, 59–68.

169 Nolan, C. J. and Larter, C. Z. (2009) Lipotoxicity: Why do saturated fatty acids cause and monounsaturates protect against it? Journal of Gastroenterology and Hepatology **24**, 703–706.

170 Mulder, H. and Ling, C. (2009) Mitochondrial dysfunction in pancreatic β-cells in Type 2 Diabetes. Molecular and Cellular Endocrinology **297**, 34–40.

171 Malmgren, S., Nicholls, D. G., Taneera, J., Bacos, K., Koeck, T., Tamaddon, A., Wibom, R., Groop, L., Ling, C., Mulder, H., et al. (2009) Tight Coupling between Glucose and Mitochondrial Metabolism in Clonal -Cells Is Required for Robust Insulin Secretion. Journal of Biological Chemistry **284**, 32395–32404.

172 Affourtit, C. and Brand, M. D. (2006) Stronger control of ATP/ADP by proton leak in pancreatic β-cells than skeletal muscle mitochondria. Biochemical Journal **393**, 151.

173 Luiken, J. J. F. P., Niessen, H. E. C., Coort, S. L. M., Hoebers, N., Coumans, W. A., Schwenk, R. W., Bonen, A. and Glatz, J. F. C. (2009) Etomoxir-induced partial carnitine palmitoyltransferase-I (CPT-I) inhibition in vivo does not alter cardiac long-chain fatty acid uptake and oxidation rates. Biochemical Journal **419**, 447.

174 Larsson, O., Deeney, J. T., Bränström, R., Berggren, P. O. and Corkey, B. E. (1996) Activation of the ATP-sensitive K+ channel by long chain acyl-CoA. A role in modulation of pancreatic beta-cell glucose sensitivity. Journal of Biological Chemistry **271**, 10623–10626.

175 Zhao, Y., Sharp, G. W. G. and Straub, S. G. (2007) The inhibitors of protein acylation, cerulenin and tunicamycin, increase voltage-dependent Ca2+ currents in the insulin-secreting INS 832/13 cell. Biochemical Pharmacology **74**, 273–280.

176 Wikstrom, J. D., Sereda, S. B., Stiles, L., Elorza, A., Allister, E. M., Neilson, A., Ferrick, D. A., Wheeler, M. B. and Shirihai, O. S. (2012) A Novel High-Throughput Assay for Islet Respiration Reveals Uncoupling of Rodent and Human Islets. PLoS One **7**, 1-7.

177 Joseph, J. W., Chan, C. B. and Wheeler, M. B. (2005) UCP2 knockout mouse islets have lower consumption and faster oscillations of beta cell oxygen. Canadian Journal of Diabetes **29**, 19-26.

178 Hovsepyan, M., Sargsyan, E. and Bergsten, P. (2010) Palmitate-induced changes in protein expression of insulin secreting INS-1E cells. Journal of Proteomics **73**, 1148–1155.

179 Circu, M. L. and Aw, T. Y. (2010) Reactive oxygen species, cellular redox systems, and apoptosis. Free Radical Biology and Medicine **48**, 749–762.

180 Mehmeti, I., Gurgul-Convey, E., Lenzen, S. and Lortz, S. (2011) Induction of the intrinsic apoptosis pathway in insulin-secreting cells is dependent on oxidative damage of mitochondria but independent of caspase-12 activation. Biochimica Biophysica Acta (BBA) Bioenergetics **1813**, 1827–1835.

181 Pi, J., Zhang, Q., Fu, J., Woods, C. G., Hou, Y., Corkey, B. E., Collins, S. and Andersen, M. E. (2010) ROS signaling, oxidative stress and Nrf2 in pancreatic beta-cell function. Toxicology and Applied Pharmacology **244**, 77–83.

182 Lim, S., Rashid, M. A., Jang, M., Kim, Y., Won, H., Lee, J., Woo, J.-T., Kim, Y. S., Murphy, M. P., Ali, L., et al. (2011) Mitochondria-targeted Antioxidants Protect Pancreatic β-cells against Oxidative Stress and Improve Insulin Secretion in Glucotoxicity and Glucolipotoxicity. Cellular and Physiological Biochemistry **28**, 873–886.

183 Lin, N., Chen, H., Zhang, H., Wan, X. and Su, Q. (2012) Mitochondrial reactive oxygen species (ROS) inhibition ameliorates palmitate-induced INS-1 beta cell death. Endocrine **42**, 107–117.

184 Schönfeld, P. and Wojtczak, L. (2008) Fatty acids as modulators of the cellular production of reactive oxygen species. Free Radical Biology and Medicine **45**, 231–241.

185 Graciano, M., Valle, M., Kowluru, A. and Curi, R. (2011) Regulation of insulin secretion and production of reactive oxygen species by free fatty acids in pancreatic islets. Islets **3**, 213-223.

186 Kessel, D., Beck, W. T., Kukuruga, D. and Schulz, V. (1991) Characterization of multidrug resistance by fluorescent dyes. Cancer Research **51**, 4665–4670.

187 Esteves, T. C. and Brand, M. D. (2005) The reactions catalysed by the mitochondrial uncoupling proteins UCP2 and UCP3. Biochimica Biophysica Acta (BBA) Bioenergetics **1709**, 35–44.

188 Anello, M., Lupi, R., Spampinato, D., Piro, S., Masini, M., Boggi, U., Del Prato, S., Rabuazzo, A. M., Purrello, F. and Marchetti, P. (2005) Functional and morphological alterations of mitochondria in pancreatic beta cells from type 2 diabetic patients. Diabetologia **48**, 282–289.

189 Sol, E., Sargsyan, E., Akusjärvi, G. and al, E. (2008) Glucolipotoxicity in INS-1E cells is counteracted by carnitine palmitoyltransferase 1 over-expression. Biochemical and Biophysical Research Communications **375**, 517-521.

190 Lupi, R., Del Guerra, S., Fierabracci, V., Marselli, L., Novelli, M., Patanè, G., Boggi, U., Mosca, F., Piro, S., Del Prato, S., et al. (2002) Lipotoxicity in Human Pancreatic Islets and the Protective Effect of Metformin. Diabetes **51**, 134–S137.

191 Sweet, I. R., Gilbert, M., Scott, S., Todorov, I., Jensen, R., Nair, I., Al-Abdullah, I., Rawson, J., Kandeel, F. and Ferreri, K. (2008) Glucose-stimulated increment in oxygen consumption rate as a standardized test of human islet quality. American Journal of Transplantation **8**, 183–192.

192 Ravier, M. A. and Rutter, G. A. (2005) Glucose or Insulin, but not Zinc Ions, Inhibit Glucagon Secretion From Mouse Pancreatic α-Cells. Diabetes **54**, 1789–1797.

193 Pipeleers, D. G. (1992) Heterogeneity in pancreatic β-cell population. Diabetes **41**, 777-781.

194 Karaca, M. (2010) In vivo functional heterogeneity among β-cells. Islets **2**, 124-126.

195 Walker, J. N., Ramracheya, R., Zhang, Q. and al, E. (2011) Regulation of glucagon secretion by glucose: paracrine, intrinsic or both? Diabetes, Obesity and Metabolism **13**, 95-105.

196 Carter, J. D., Dula, S. B., Corbin, K. L., Wu, R. and al, E. (2009) A practical guide to rodent islet isolation and assessment. Biological Procedures Online **11**, 3-13.

197 Buttgereit, F. and Brand, M. D. (1995) A hierarchy of ATP-consuming processes in mammalian cells. Biochemical Journal **312**, 163–167.

198 Briaud, I., Harmon, J. S., Kelpe, C. L., Segu, V. B. G. and Poitout, V. (2001) Lipotoxicity of the Pancreatic β-Cell Is Associated With Glucose-Dependent Esterification of Fatty Acids Into Neutral Lipids. Diabetes **50**, 315–321.

199 Lenzen, S. (2007) The mechanisms of alloxan- and streptozotocin-induced diabetes. Diabetologia **51**, 216–226.

200 Chan, C. B., De Leo, D., Joseph, J. W., McQuaid, T. S., Ha, X. F., Xu, F., Tsushima, R. G., Pennefather, P. S., Salapatek, A. M. and Wheeler, M. B. (2001) Increased uncoupling protein-2 levels in beta-cells are associated with impaired glucose-stimulated insulin secretion: mechanism of action. Diabetes **50**, 1302–1310.

201 Chang, Y.-C. and Chuang, L.-M. (2010) The role of oxidative stress in the pathogenesis of type 2 diabetes: from molecular mechanism to clinical implication. American Journal of Translational Research **2**, 316–331.

202 Sato, Y., Fujimoto, S., Mukai, E., Sato, H., Tahara, Y., Ogura, K., Yamano, G., Ogura, M., Nagashima, K. and Inagaki, N. (2014) Palmitate induces reactive oxygen species production and β-cell dysfunction by activating nicotinamide adenine dinucleotide phosphate oxidase through Src signaling. Journal of Diabetes Investigation **5**, 19–26.

203 Rosca, M. G., Vazquez, E. J., Chen, Q., Kerner, J., Kern, T. S. and al, E. (2012) Oxidation of Fatty acids is the source of increased mitochondrial reactive oxygen species production in kidney cortical tubules in early diabetes. Diabetes **61**, 2074-2083.

204 Boss, O., Hagen, T. and Lowell, B. B. (2000) Uncoupling proteins 2 and 3: potential regulators of mitochondrial energy metabolism. Diabetes **49**, 143–156.

205 Pecqueur, C., Bui, T., Gelly, C., Hauchard, J., Barbot, C., Bouillaud, F., Ricquier, D., Miroux, B. and Thompson, C. B. (2008) Uncoupling protein-2 controls proliferation by promoting fatty acid oxidation and limiting glycolysis-derived pyruvate utilization. The FASEB Journal **22**, 9–18.